

The representation of cloudiness over southern West Africa in global climate models

Die Darstellung der Bewölkung über dem südlichen Westafrika in globalen Klimamodellen

Masterarbeit im Fach Meteorologie
von

Lisa Hannak

Juli 2015



INSTITUT FÜR METEOROLOGIE UND KLIMAFORSCHUNG
KARLSRUHER INSTITUT FÜR TECHNOLOGIE (KIT)

Referent:

Prof. Dr. Peter Knippertz

Koreferent:

Prof. Dr. Andreas Fink

Zusammenfassung

Der westafrikanische Monsun (WAM) gehört zu den bedeutendsten Monsungegenden weltweit. Die dortige, ständig wachsende Bevölkerung ist stark abhängig von den Niederschlägen während des Sommermonsuns. Doch der westafrikanische Monsun zeichnet sich durch starke Schwankungen in seiner Entwicklung und Stärke aus, was zu katastrophalen Auswirkungen in der Bevölkerung führen kann, da diese hauptsächlich von der Agrarwirtschaft lebt. Zudem zeigen globale Klimamodelle Schwierigkeiten bei der Simulation des Monsuns in West Afrika. Damit verbunden ist die Problematik, Wolkenbildung und Niederschlag realistisch zu simulieren, was zu großen Unterschieden in der solaren Strahlung am Boden und Temperatur führt. Aus diesen Gründen ist das Verständnis von Modellfehlern wichtig um Klimamodelle und die Wettervorhersage zu verbessern.

Der Schwerpunkt dieser Arbeit liegt auf der niedrigen Bewölkung über dem südlichen Teil von Westafrika zwischen Juli und September, der Zeit des niederschlagsreichen Monsuns. Als Datengrundlage dienen zwei Datensätze, einer vom Coupled Model Intercomparison Project Phase 5 (CMIP5) und der zweite vom GEWEX Atmosphere System Study (GASS) and Year of Tropical Convection (YoTC) Vertical Structure and Physical Processes Multi-Model Experiment welches von Mai 2008 bis April 2010 stattfand. Für die Analyse wurden ausschließlich atmosphärische Modelle verwendet, bei denen die Meeresoberflächentemperatur auf Beobachtungen basiert. Darunter befinden sich 18 Modelle vom CMIP5-Datensatz und acht vom YoTC-Datensatz. Um die Modellergebnisse mit einem beobachtungsbasierten Datensatz zu vergleichen, wurden ReAnalysis-Interim (ERA-Interim) Daten vom European Centre for Medium-Range Weather Forecasts (ECMWF) hinzugezogen.

Das Ziel dieser Arbeit liegt darin, die Gründe für die Unterschiede zwischen ERA-Interim und den globalen Klimamodellen zu finden und zu verstehen. Wie schon in einigen Arbeiten zuvor, zeigen auch die hier verwendeten globalen Klimamodellen große Unterschiede in der Simulation der niedrigen Bewölkung über der Guineaküste. Auch bei der Analyse anderer Variablen, wie zum Beispiel Windgeschwindigkeit, Temperatur- und Feuchteadvektion lassen sich große Unterschiede finden, die stark von den Ergebnissen der Reanalyse abweichen. Die Ergebnisse der Reanalyse spiegeln gut das zugrunde liegende Verständnis der Wolkenbildung wieder. Verglichen dazu simulieren die Klimamodelle die niedrige Bewölkung meist zu hoch und überschätzen größtenteils die maximale Windgeschwindigkeit in Bodennähe. Die wenigen Modelle, die die Höhe der niedrigen Bewölkung gut darstellen, zeigen die maximalen Werte der Temperatur- und Feuchte tendenzen in niedrigeren Höhen als die Klimamodelle mit zu hoher Bewölkung, die meist kaum einen Tagesgang aufweisen.

Abstract

The West-African monsoon is one of the world's major monsoon regions. The local population, which is continuously increasing, depends on the precipitation during the West-African summer monsoon, which is characterized by strong inter-annual variations in development and strength. This leads to potentially catastrophic results for the population which subsist on agriculture. Moreover global climate models show difficulties in simulating the monsoon in West Africa correctly. Linked with this, the climate models show large problems to simulate the formation of clouds and precipitation correctly which leads to large differences in surface solar radiation and temperature. Therefore understanding the causes of model errors is important to improve climate models and weather forecast.

In this work, the focus is on ultra-low stratus clouds over southern West Africa during the wet monsoon season between July and September. Two data sets were used - one from the Coupled Model Intercomparison Project Phase 5 (CMIP5) and one from the GEWEX Atmosphere System Study (GASS) and Year of Tropical Convection (YoTC) Vertical Structure and Physical Processes Multi-Model Experiment, which took place from May 2008 to April 2010. For analysis, only models that use observed sea surface temperature (so called AMIP-type experiments) were chosen: 18 models from the CMIP5-data set and eight models from the YoTC-data set. The model results were compared with an observational data set, the ReAnalysis-Interim (ERA-Interim) data of the European Centre for Medium-Range Weather Forecasts (ECMWF).

The aim of this work is to find and understand the differences between ERA-Interim and the global climate models. Like in previous studies, the global climate models show large differences in the simulation of low-level cloudiness at the Guinea Coast. Furthermore by analyzing other variables like wind speed, advection of temperature and moisture, there are large deviations from ERA-Interim. The fields of ERA-Interim match very well with the understanding of cloud formation. Compared with this, the climate models simulate the cloudiness too high and overestimate the maximum wind speed near the ground. The few models that simulate the height of the low-level cloudiness correctly show the maximum values in the tendencies of temperature and moisture at lower levels compared to the climate models with cloudiness in higher levels and less diurnal variations.

Contents

1	Introduction	4
2	Current State of Research	6
2.1	West African Summer Monsoon	6
2.1.1	Nocturnal Low-Level Jet	7
2.1.2	Formation of Low-Level Clouds	7
2.2	Research Questions and Objectives	10
3	Data and Methods	12
3.1	Coupled Model Intercomparison Project Phase 5	12
3.2	GASS-YoTC Vertical Structure and Physical Processes Multi-Model Experiment	13
3.3	ECMWF ReAnalysis-Interim	15
3.4	Maximum-Random Overlap Assumption for Total Cloud Cover	17
3.5	Rank Correlation	18
3.6	Calculation of Vertical Profiles	18
3.7	Calculation of Advection and Wind Speed	19
4	Results for the Global Climate Models in CMIP5	22
4.1	Representation of Low-Level Clouds and Wind Speed	22
4.2	Representation of the Advection of Moisture and Temperature	24
4.3	Rank Correlation	26
4.4	Short Summary of the Results for CMIP5 Models	28
5	Results for the Global Climate Models in GASS YoTC	30
5.1	Representation of Low-Level Clouds and Wind Speed: Diurnal Variations	30
5.2	Representation of Low-Level Clouds and Wind Speed: Monthly Variations	32
5.3	Case Examples	33
5.4	Representation of the Advection of Moisture and Temperature	35
5.5	Representation of Surface Solar Radiation	38
5.6	Representation of the Tendency of Specific Humidity	41
5.7	Representation of the Tendency of Temperature	43
5.8	Rank Correlation	46
5.9	Summary of the Processes in the Models	52

Contents	3
----------	---

6 Discussion, Summary and Outlook	60
--	-----------

A Appendix	64
-------------------	-----------

Bibliography	82
---------------------	-----------

1. Introduction

One of the world's major monsoon region is West Africa. The inter-annual variations in characteristics of the monsoon development and precipitation are remarkable with potentially catastrophic results for the growing population. Agriculture is the main part of the gross national product (Fink, 2006) in West Africa, therefore the population depends on a reliable weather and seasonal forecast for their farming. Up to now, global climate models have problems to simulate the monsoon correctly. The simulation of low-level clouds over the Guinea Coast is one part of model errors (Knippertz et al., 2011; Nam et al., 2012). The problems involved are large differences in surface radiation and temperature.

This work is embedded in the EU-funded project Dynamics-Aerosol-Chemistry-Cloud Interactions in West Africa (DACCIWA), which runs from 2015-2018. Included are several observation sites, airplanes, satellites, and models to better understand the dynamics, variations, and development during the wet monsoon in this area (Knippertz et al., 2015). In this part of the world, a strong increase in the population and, linked with this, large air pollution are major problems. These are some of the reasons why this campaign is organized. In DACCIWA seven scientific workpackages are formulated and this study can be included in the research area monsoon processes with the focus on the stratiform cloudiness during the wet monsoon. Global climate models have problems to simulate the low-level stratiform cloudiness, so for improving climate models regarding this issue, it is important to find the causes of model errors in cloudiness and to have a better understanding of the physical processes behind the formation of these low-level clouds.

The focus of this work is on low-level cloudiness over southern West Africa during the wet monsoon from July to September. The main emphasis is to look at the condition of low-level cloud formation over southern West Africa to gain a better understanding of the dynamical processes behind it and therefore contribute to the improvement of weather and seasonal forecasts in this region. This work is a preparative study for active modelling in DACCIWA and uses several models out of CMIP5, which mostly have a temporal resolution of daily or even monthly data. This temporal resolution is not enough to analyze the diurnal variations of low-level cloud formation. That is the reason why this work also includes global climate models of the YoTC data set with a temporal resolution of six hours. Six of these models are contained in both data sets. An overview over the current state of research is given in chapter 2, followed by a description of the data and methods used in this work in chapter 3. The results of the representation of low-level cloudiness

and several other variables like the nocturnal low-level jet (NLLJ) or the advection of moisture and temperature are presented in chapters 4 and 5. The discussion and the summary of the work can be found at the end with an outlook and open questions for future work.

2. Current State of Research

2.1 West African Summer Monsoon

The yearly variations of the rainfall and other features of the wet monsoon in West Africa are immense but the population depends on the wet season for their farming. Therefore doing research in this part of the world is important to help the population with a reliable weather, seasonal and climate forecast that the agriculture can be planned better to enhance yields. The focus of this work is the southern part of West Africa during the wet monsoon season. The wet monsoon is triggered by differential heating of land and ocean. In the summer, the Sahara heats up faster and stronger than the ocean and generates ascending air masses above the desert (Hall and Peyrillé, 2006). The ascending warm air causes high pressure at upper levels over land. The horizontal pressure gradient generates a flow towards the ocean in the upper troposphere. Contrary to the upper level, an opposed flow arises near the ground from the ocean to the heat-low in the Sahara. In Figure 2.1 the described circulation is shown with the southern flow near the ground, ascending over the Sahara and descending over the Atlantic. Also an important factor in this circulation is the

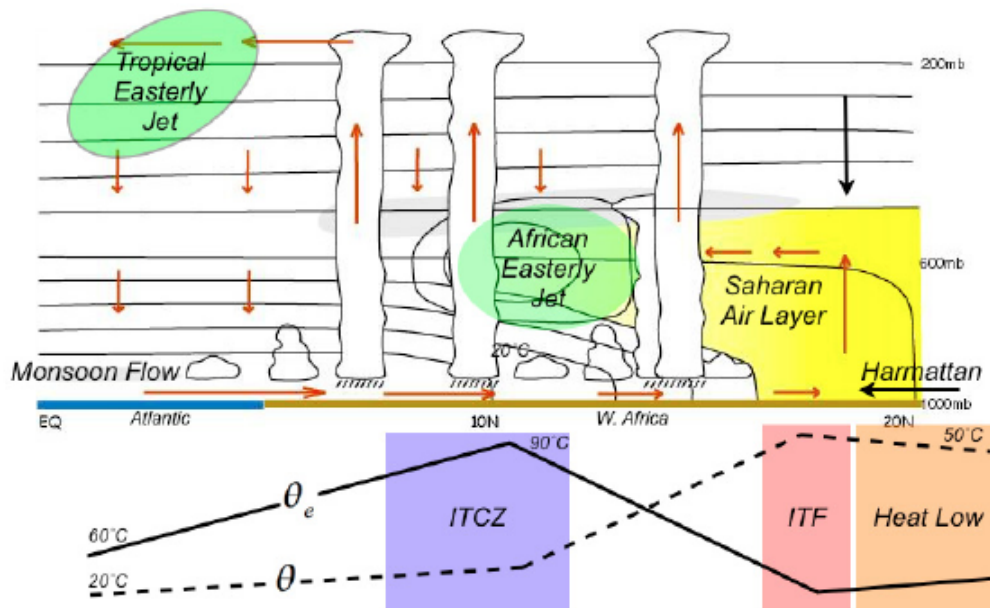


Figure 2.1: Schematic illustration of the West African monsoon by Mohr and Thorncroft (2006) and adapted by Hall and Peyrillé (2006).

shift of the InterTropical ConvergenceZone (ITCZ) from 5° N to 10° N (Sultan and Janicot, 2003). The convergence effect in this zone together with the change of the sign of the Coriolis force at the equator induces a wind which turns from a south-easterly to a south-westerly direction while crossing the equator. During the wet monsoon season almost the complete annual precipitation occurs along the Guinea Coast. Hence the conditions at the coast of southern West Africa during the wet monsoon are affected by a south-westerly flow and strong precipitation. Further north, the moist and cold air from the monsoonal flow is confronted with hot and dry air from the Sahara which forms a border, the Inter-Tropical Front (ITF) (Hall and Peyrillé, 2006). The positions of the ITF, the ITCZ and the heat-low over the Sahara are illustrated in Figure 2.1.

2.1.1 Nocturnal Low-Level Jet

Representative for the rainy phase of the monsoon is the formation of a Nocturnal Low-Level Jet (NLLJ). The NLLJ is formed due to large temperature and pressure gradients from the heat-low over the Sahara to the Atlantic. In the afternoon, the heat-low reaches its minimum of the day (Parker et al., 2005). In spite of the strong pressure gradient during the day, the wind speed near the ground is low because of the turbulent boundary layer. At night the turbulence decreases due to missing solar radiation but the pressure gradient is still substantial, so the NLLJ can form (Abdou et al., 2010). The wind speed of the NLLJ reaches its maximum in the early morning before sunrise just a few hundred meters above the ground (Gounou et al., 2012). In the morning, when the convective boundary layer develops, momentum from the jet can mix down and strengthens the surface winds, which show their maximum at the morning (Abdou et al., 2010; Parker et al., 2005). A similar diurnal cycle of the NLLJ is also visible over Australia during the Australian monsoon (Rácz and Smith, 1999).

2.1.2 Formation of Low-Level Clouds

In most of the nights during the summer monsoon, low-level clouds are formed along the Guinea Coast in southern West Africa after sunset. During the course of the night, the extension of these clouds grows farther inland and shows the maximum in the early morning (Schuster et al., 2013). An example for low-level clouds in a satellite image of SEVIRI is illustrated in Figure 2.2 taken from Linden et al. (2015). In this example, the low-level clouds cover the whole area along the Guinea Coast over southern West Africa in August. The cloud level during the night and early morning is very low, that is the reason why these clouds are called ultra-low clouds (Knippertz et al., 2011). The formation of low-level stratiform clouds during the night at the Guinea Coast is connected with the NLLJ. The NLLJ produces wind shear which lets turbulent eddies arise. This turbulence mixes moist air from the ground to higher levels which form the basis for cloud formation (Schrage and Fink, 2012). An other important factor is the stability at night. In case the stable nocturnal boundary layer is developed too early due to outgoing longwave radiation and is fully decoupled from the atmosphere above, the wind shear underneath the jet can not influence the conditions inside the boundary layer and there is no mixing of moisture. So the stability in the boundary layer at night is important for cloud formation and, linked with that, the advection

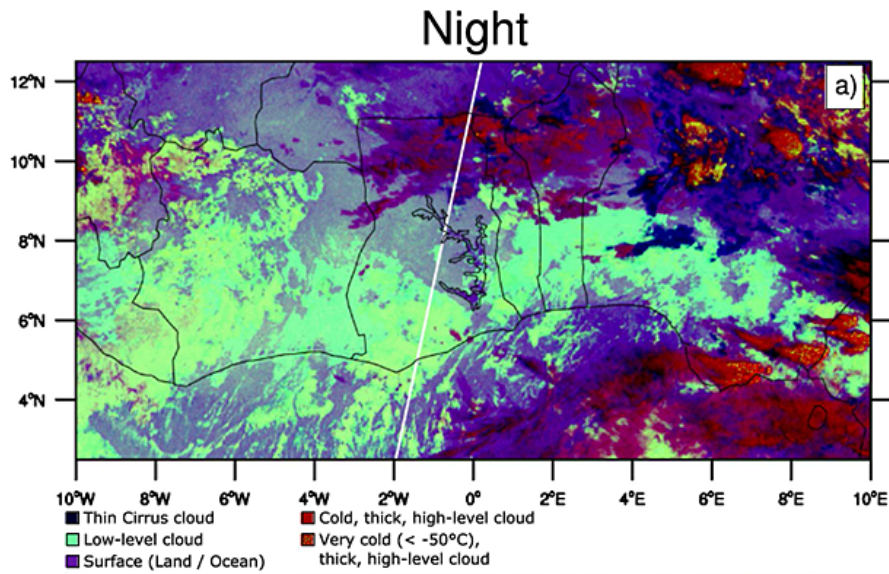


Figure 2.2: Satellite image of MSG SEVIRI (used product: red-green-blue composite 'night microphysical scheme') on 19 August 2007 about 0130 UTC by Linden et al. (2015).

of cold air from the Atlantic (Schuster et al., 2013). The differential cold air advection destabilize the static stability in the boundary layer and turbulence can develop easier. Vertical mixing is affected by static stability and wind shear underneath the NLLJ (Schuster et al., 2013) and this vertical mixing of moisture is needed for cloud formation. Clouds influence the energy budget, especially the surface radiation (Gounou et al., 2012), so the existence of clouds have wide-ranging effects. The processes of low-level cloud formation are summarized in Schuster et al. (2013), in which several model configurations were tested in six experiments. In these experiments different skill scores were calculated to find the best model which represent the low-level clouds realistic compared to observations of the African Monsoon Multidisciplinary Analyses (AMMA) project. Like represented in Figure 2.3 on the left, the low-level cloud formation is affected by the NLLJ, latent and sensible heat fluxes, and dry and cold air advection. The NLLJ has its maximum a few hundred meters above ground and drives the turbulence underneath. Just as important as the NLLJ are the energy fluxes from the ground to the cloud level and the advection which is greatest in the figure at the level of the jet maximum. At first, dry air advection from the Atlantic is unexpected. The reason can be the monsoonal Shallow Meridional Circulation (SMC) which requires a strong meridional surface pressure gradient (Zhang et al., 2008). The pressure gradient appears over West Africa due to strong heating over the Sahara during the early summer. Near the ground the air masses move from the Atlantic into the heat-low where the air masses ascent. The position of the ascending of low-level air is not the same as the position of the ITCZ which is represent in Figure 2.3 on the right. The shallow return flow (approx. at 700 hPa) interfuses the zone of the heavy monsoonal rainfalls by moving southwards towards the Atlantic which is the reason of moist advection in this height. Over the ocean the air descends, meanwhile dryer air from above can mixes into the descending air masses, which is the reason of dry advection near the

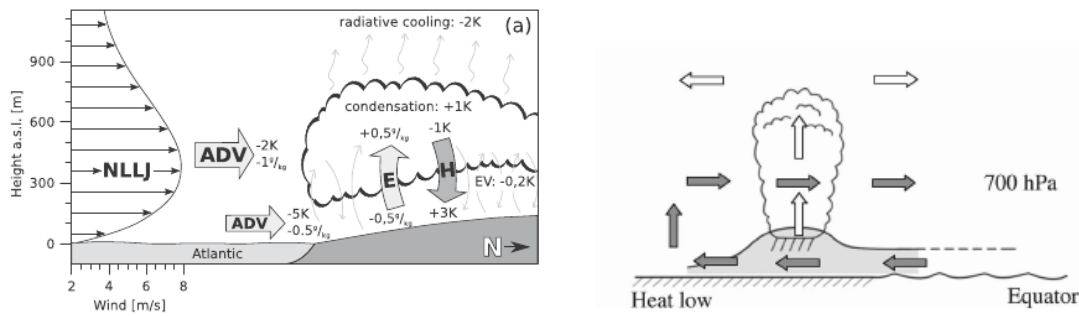


Figure 2.3: Left: schematic illustration of the formation of low clouds near the Atlantic coast in southern West Africa. Used abbreviations in this figure are ADV: advection, E: latent heat flux, H: sensible heat flux, EV: evaporation, NLLJ: nighttime low-level jet. Figure and description are by Schuster et al. (2013). Right: schematic illustration of the monsoonal SMC by Zhang et al. (2008).

ground. During the day the NLLJ slows down due to the turbulent boundary layer and the cloud level raises to 850 hPa. These low-level clouds during the day are triggered by different physical processes which are involved by the turbulent boundary layer and buoyancy. The boundary layer during the day is less stable than at night and is characterized by more turbulence and convection.

So the question is, can global climate models simulate the low-level cloud formation correctly? An example for research with climate models of the Coupled Model Intercomparison Project Phase 3 (CMIP3) over southern West Africa is Knippertz et al. (2011), in which several variables like the low-level cloudiness, wind speed, and surface solar radiation in the models are compared to short-term ECMWF forecasts. The ECMWF forecasts match to observations, but the models of CMIP3 have problems in simulating the wind speed and the cloud cover. The wind speed near the ground is overestimated in the models and the ultra-low cloudiness is underestimated. The conclusions are that the climate models represent the wind speed and the low-level clouds badly and this has an immense effect on the surface solar radiation. An assumption is that the vertical mixing is underestimated and the boundary layer is too stable. Hence the formation of low-level clouds is blocked by too little moisture transport from the ground. A better temporal resolution and a more detailed vertical resolution in the models will be of use to look at the diurnal variations of the process in more detail. A study with climate models of the project CMIP5 is Nam et al. (2012) in which COSP-products are compared to observational satellite data. COSP stands for Cloud Feedback Model Intercomparison Project (CFMIP) Observation Simulator Package. The goal of these products is to directly compare the model-output with the observational data. Therefore, the model simulates the signal that a satellite sensor would receive. With this simulated model-product the comparison with observation is simplified. The conclusions in this study are that the low-level clouds are too few and too bright. The radiation budget at the top of the atmosphere has to be balanced in coupled ocean-atmospheric models compared to observations, that is the reason for compensation errors in coupled models. An example is that models with too few low-level clouds may overestimate the feedback of low-level clouds on shortwave radiation.

So global climate models of CMIP3 and CMIP5 have problems by simulating the low-level cloudiness correctly and linked with that show large differences in the representation of the radiation. There are still problems in CMIP5 models which are not improved since CMIP3. The spread of model projections is still large in CMIP5, for example in the variables temperature or precipitation (Roehrig et al., 2013). Furthermore, as in the study of Couvreux et al. (2014), models still have problems by simulating the diurnal cycle of the boundary layer correctly which have an effect on the physical parametrizations in the models.

2.2 Research Questions and Objectives

The main question of this study is why global climate models have problems to simulate low-level clouds during the West African summer monsoon in southern West Africa. With the understanding of the causes of model errors the knowledge of the simulated monsoon in the models can be improved. Conclusions of previous works are that the formation of low-level clouds is very sensitive, so that little biases have a large effect (Schuster et al., 2013). The objectives of this work are

- to document differences between the models and compare the results to ERA-Interim,
- to identify relationships between different variables, like presence and strength of the NLLJ, the advection of cold air and the advection of moisture, and the tendencies of moisture and temperature,
- to analyze the diurnal cycle of the low-level cloudiness, wind speed, tendencies, and advection, and
- to find out which model simulate the physically processes behind the formation of the low-level clouds most realistic.

3. Data and Methods

To analyze the cloudiness, wind speed, and diabatic processes in southern West Africa, two different data sets were used, one from the Coupled Model Intercomparison Project Phase 5 (CMIP5) and the second one from the GASS-YoTC Vertical Structure and Physical Processes Multi-Model Experiment. In this analysis, only atmospheric models which use observed Sea Surface Temperatures (SST) (so called AMIP-type experiments) were chosen. Coupled models still show biases in simulating the SSTs correctly compared to AMIP runs and, linked with this, show a southward shift of the ITCZ (Roehrig et al., 2013). In the first part, the data set of CMIP5 is described, followed by an overview of the second data set and a description of ECMWF ReAnalysis-Interim, which is used to compare the model-output with an observation based reanalysis. The section closes with an overview over the used methods in this work.

3.1 Coupled Model Intercomparison Project Phase 5

The models from CMIP5 were used in the Intergovernmental Panel on Climate Change (IPCC) report although the models have problems by predicting the effects of climate change, especially the rainfall, correctly (Roehrig et al., 2013). CMIP5 includes coupled and atmosphere-only models from different institutions and countries, but the focus of the analysis is on atmosphere-only models. The SSTs in these models are based on a data set which is described by Hurrell et al. (2008). There are two versions, the HadISST1 and one of the National Oceanic and Atmospheric Administration (NOAA) which use mean values of observational data. For a daily resolution, the monthly mean values are linearly interpolated. The vertical coordinate differs between the models, so some model-outputs (HADGEM2-A, ACCESS1.0, ACCESS1.3) are based on the unit 'meter' but the analysis concentrates on models which use the pressure unit 'pascal'. CMIP5 includes some different versions of models for example with different horizontal resolutions (IPSL, GFDL HIRAM, MPI). In this case only the model version with the higher resolution is chosen. The models from CMIP5 used here are documented in Table 3.1. Further models are CanAM4, GFDL-HIRAM-C180, IPSL-CM5A-LR, IPSL-CM5B-LR, MPI-ESM-LR, HADGEM2-A, ACCESS1.0, and ACCESS1.3 which are not used in this study because of the reasons described before. A disadvantage of this data set is the time resolution. Most of the variables have a time resolution of monthly or daily mean values. This time resolution is sub-optimal and does not allow analyzing diurnal variations.

Table 3.1: List of chosen atmospheric models, their simulated period of time and the available resolution for the variable cloud fraction of the CMIP5 data set.

Institute	Model	Periode of time	lat x lon	Levels	Levels \geq 700 hPa
BCC	BCC-CSM1.1	1979-2008	2.8125 x 2.8125	26	5
BNU	BNU-ESM	1979-2008	2.8125 x 2.8125	26	4
CMCC	CMCC-CM	1979-2008	0.75 x 0.75	31	4
CNRM	CNRM-CM5	1979-2008	1.40625 x 1.40625	31	9
CSIRO	CSIRO-Mk3.6.0	1979-2009	0.875 x 0.875	18	4
ICHEC	EC-EARTH	1978-2008	1.125 x 1.125	62	4
INM	INMcm4	1979-2008	1.5 x 2	21	4
IPSL	IPSL-CM5A-MR	1950-2009	1.27 x 2.5	39	9
MIROC	MIROC5	1979-2008	1.4 x 1.4	40	13
MPI-M	MPI-ESM-MR	1979-2008	1.875 x 1.875	95	4
MRI	CGCM3	1979-2010	1.125 x 1.125	35	10
NASA-GISS	GISS-E2-R	1950-2010	2 x 2.5	29	4
NCAR	CCSM4	1979-2010	1.25 x 1.25	26	4
NCC	NorESM1-M	1979-2008	1.8947 x 2.5	26	4
NOAA-GFDL	CM3	1979-2008	2 x 2.5	48	12
NOAA-GFDL	HIRAM-C360	1979-2008	0.25 x 0.3125	32	4
LASG	FGOALS S2, G2	1979-2009	1.67 x 2.8125	26	4

3.2 GASS-YoTC Vertical Structure and Physical Processes Multi-Model Experiment

The 'GASS-YoTC Vertical Structure and Physical Processes Multi-Model Experiment' was launched by the World Climate Research Program (WCRP) and the Observing System Research and Predictability Experiment (THORPEX) of the World Weather Research Program (WWRP) (Waliser et al., 2012) from May 2008 to April 2010. It was initiated for global model evaluation with the focus on vertical structure. The program includes three different experiments - firstly, twenty-year climate simulations, secondly, 2-day hindcasts, and thirdly, 20-day hindcasts. The twenty-year simulations with a time resolution of 6 hours were made with coupled and atmosphere-only models, but like before atmosphere-only models were chosen for the analysis. In these models the SSTs are based on a weekly data set of the National Oceanic and Atmospheric Administration (NOAA), the Optimum Interpolation V2 (Reynolds et al., 2002). The majority of the atmospheric models use the parametrizations of the National Center for Atmospheric Research Community Atmosphere Model (NCAR CAM), except five atmospheric models, UCSD CAM, ISUGCM, NCAR CAM5, TAMU Modified Cam4 and LLNL CAM5ZMMicro which use a different version of NCAR CAM (Jiang et al., 2014). An example of a modified parametrization is the model TAMU Modified Cam4 which includes the observed vertical latent heating. The latent heating is based on the tropical rainfall measuring mission Precipitation Radar (TRMM) (Lappen and Schumacher, 2012). A special component of the YoTC project is the model CNRM which has

three model versions, one is a coupled ocean-atmosphere model (CNRM-CM), the second is an atmospheric-only version (CNRM-AM) and the third one is an atmospheric model in which the SSTs are based on monthly mean data of the coupled version of CNRM-CM (Jiang et al., 2014).

Some models have a unrealistic unit description, for example in the variable stratiform cloud fraction (cls). The unit is declared to be in 'per cent' but the values were much too small (more than 10^{-4}) in these models. One model has negative values in the variable cls, which is physically unrealistic. Although the responsible persons of these models were contacted, the problem could not be solved and the models were excluded from in this study. The eight models used in this study are documented in Table 3.2. The models have a horizontal resolution of $2.5^\circ \times 2.5^\circ$ and 22

Table 3.2: List of chosen atmospheric models of GASS YoTC (Jiang et al., 2014).

Model	Institute
GEOS5 AGCM	Global Modeling and Assimilation Office, NASA
GISS ModelE	Goddard Institute for Space Studies, NASA
MIROC5	AORI/NIES/JAMSREC, Japan
MRI AGCM	Meteorological Research Institute, Japan
NCAR CAM5	National Center for Atmospheric Research
NRL NAVGEMv1.0	US Naval Research Laboratory
CNRM AM	Centre National de la Recherche Scientifique, Météo-France
FGOALS s2	Institute of Atmospheric Physics, Chinese Academy of Sciences
LLNL CAM5ZMMicro	Lawrence Livermore National Laboratory

vertical levels (nine of them below 700 hPa). The models GISS, MIROC5, MRI, NCAR, CNRM, and FGOALS S2 are integrated in CMIP5 and included in the YoTC data set as well.

Additional model-outputs are the physical tendencies of heat, moisture and momentum which are not available in the CMIP5 models. Like described in Xiaopeng et al. (2009) the tendency of specific humidity can be written with the equation

$$\frac{\delta q}{\delta t} + v \cdot \Delta q = S_q, \quad (3.1)$$

in which S_q stands for the sources and sinks of specific humidity. The tendency of temperature can be expressed similar to that equation. So what are the sources and sinks of specific humidity and temperature? Equation 3.2 shows the different sinks and sources of specific humidity and equation 3.3 the different sinks and sources of temperature.

$$S_q = \underbrace{S_{con}}_{convection} + \underbrace{S_{pbl}}_{boundary\ layer\ physics} + \underbrace{S_{lscp}}_{processes\ in\ grid-scale\ clouds\ and\ precipitation} + \underbrace{S_{diff}}_{diffusion} \quad (3.2)$$

$$S_T = \underbrace{S_{con}}_{convection} + \underbrace{S_{pbl}}_{boundary\ layer\ physics} + \underbrace{S_{lscp}}_{processes\ in\ grid-scale\ clouds\ and\ precipitation} + \underbrace{S_{diff}}_{diffusion} + \underbrace{S_{rad}}_{radiation} \quad (3.3)$$

The processes in grid-scale clouds and precipitation can be included to micro-physics. In grid-scale clouds, water vapor can make a phase change to precipitation. This precipitation can evaporate and increase the humidity underneath the clouds. Convection leads to a drying-out near the ground because the moisture is transported to higher levels. Also an important term is the boundary layer physic where the stability plays an important role. Changes in the temperature can be caused by for example shortwave and longwave radiation.

In the following, several abbreviations are used for the tendencies of moisture (Table 3.3). In

Table 3.3: Used abbreviations for the tendencies of moisture.

Tendency of moisture (specific humidity)	tnq
Tendency of moisture due to advection	tnqadv
Tendency of moisture due to convection	tnqcon
Tendency of moisture due to boundary layer processes	tnqpbl
Tendency of moisture due to large scale clouds and precipitation	tnqlscp
Tendency of moisture due to diffusion	tnqdiff

Table 3.4 the used abbreviations for the tendencies of temperature are documented.

Table 3.4: Used abbreviations for the tendencies of temperature.

Tendency of temperature	tnT
Tendency of temperature due to advection	tnTadv
Tendency of temperature due to convection	tnTcon
Tendency of temperature due to boundary layer processes	tnTpbl
Tendency of temperature due to large scale clouds and precipitation	tnTlscp
Tendency of temperature due to diffusion	tnTdiff
Tendency of temperature due to shortwave radiative heating	tnTsrاد
Tendency of temperature due to shortwave radiative heating clear sky	tnTsrادcs
Tendency of temperature due to longwave radiative heating	tnTlrad
Tendency of temperature due to longwave radiative heating clear sky	tnTlradcs
Tendency of temperature due to due to orographic gravity wave drag	tnTgravwave

3.3 ECMWF ReAnalysis-Interim

The period of time which is covered by the ECMWF ReAnalysis-Interim (ERA-Interim) is from 1979 up to now. Some details of the ERA-Interim data set is given in Dee et al. (2011).

The ERA-Interim data are an improvement of the earlier ERA-40 data. Several data assimilation problems of ERA-40 were corrected in the new reanalysis. The data assimilation is the main part of a reanalysis. Before including observations in the data assimilation process, the data are tested in a quality control. The data assimilation is a combined system of a forecast model and observational data. The basic features of the data assimilation are 12-hourly analysis cycles. In these cycles the simulated fields of the model were corrected with observations. These fields build the basis of the next cycle. The method which is used in the data assimilation is 4D-Var. As shown in Figure 3.1, the function of the previous forecast of the model (blue line) is corrected with observations, so the new function of the forecast (red line) adapts to the observations.

The time resolution of ERA-Interim is six hours for 3-D variables and three hours for some 2-D fields at the surface. The advantages over ERA-40 are

- the hydrological cycle, which is improved in ERA-Interim compared to ERA-40,
- an enhanced stratospheric circulation,
- and the improved correction of satellite data, so that more observations can be included in the data assimilation process. In 2010, up to 10^7 observations were used in the data assimilation, mostly because of satellite observations.

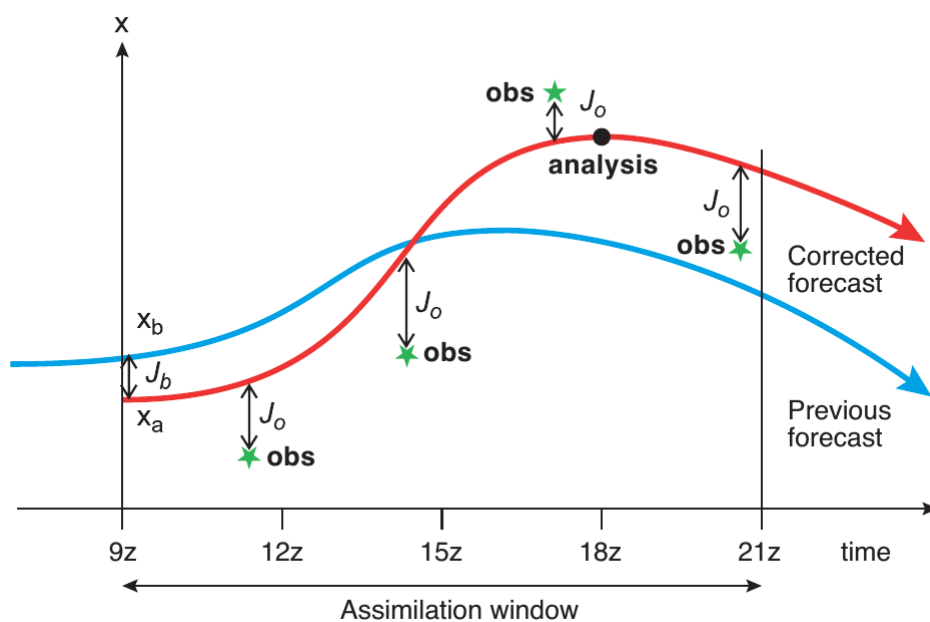


Figure 3.1: Schematic illustration of the 4Dvar analysis by Persson and Grazzini (2007).

3.4 Maximum-Random Overlap Assumption for Total Cloud Cover

The variable cloud fraction is usually given on pressure levels in per cent. To calculate the total cloud fraction, an assumption on overlap was used. A schematic illustration of the overlap assumption is shown in Figure 3.2 where the horizontal lines represent the different layers. In case there are clouds in two adjacent layers, the maximum of these two cloud fractions

$$C_{total} = \max(C_{lower}, C_{upper}) \quad (3.4)$$

was used. This case is demonstrated at model layer one-two and four-five in Figure 3.2. If two clouds are separated by a cloud-free layer, the random-overlap assumption

$$C_{total} = C_{lower} + C_{upper} - (C_{lower} \cdot C_{upper}) \quad (3.5)$$

was chosen. In the example of Figure 3.2, the cloud fraction in the layer three is zero. Therefore the total cloud fraction of the whole area is calculated in the cloud with the maximum assumption, in this case $C_{lower} = 25\%$ applies for the lower cloud and $C_{upper} = 30\%$ for the upper cloud. In the layer three no cloud is simulated, so the result of the whole example is $C_{total} = 0.25 + 0.30 - (0.25 \cdot 0.30) = 0.475 = 47.5\%$. The idea behind this method is that clouds on adjacent layers are physically connected and because of this connection the overlap is expected to be maximal. In case the clouds are disconnected in two separate clouds the physical link is not as strong and the overlap of these two clouds can be smaller, such that the total cloud fraction calculated from these two clouds becomes larger.

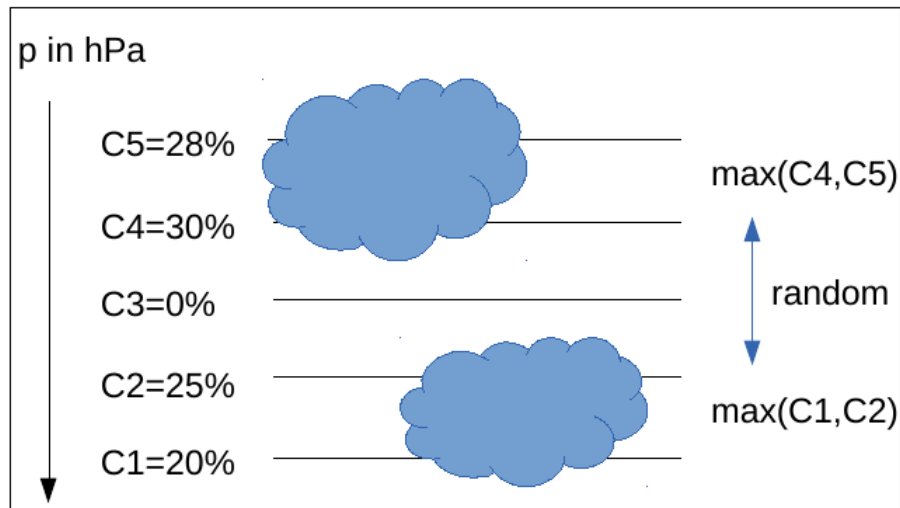


Figure 3.2: Used overlap assumption to calculate the total cloud fraction out of several model layers.

3.5 Rank Correlation

To get an idea, whether two variables have a connection, calculating the rank correlation coefficient can be useful. Instead of comparing the values of the two variables (ordered in two vectors) in a normal correlation, the rank correlation compares the ranks of the values. After allocating the values of the two variables to their rank position number, the rank correlation r can be calculated with

$$r = \frac{cov(x, y)}{std(x) * std(y)}, \quad (3.6)$$

in which $cov(x, y)$ represents the covariance of x and y and $std(x)$ is the standard deviation of x . The advantage of using the rank correlation instead of a normal correlation coefficient is that the connection between x and y do not have to be linear, only monotonic. The rank correlation is a statistical method to find a connection but this connection can be theoretically random, so the connection do not have to be necessarily physically explainable. To identify whether the calculated rank correlation is significant, the t-test was used. The null hypothesis assumes that x and y are independent, such that the calculated rank correlation is zero. The approach of a t-test is to calculate

$$t = r * \sqrt{\frac{n - 2}{1 - r^2}}, \quad (3.7)$$

with the rank correlation coefficient r and the numbers of elements n . The second step is to compare the calculated value of t with a tabular value, in which each value is ordered with its particular numbers of degrees of freedom and the p-quantile. In case the calculated t is greater than the tabular value, the rank correlation coefficient r is significant to the chosen p-quantile (e.g. 0.9) and the null hypothesis is rejected.

3.6 Calculation of Vertical Profiles

To represent a vertical profile in the area of the southern part of West Africa, a horizontal box was defined from -8° E to 8° E and from 5° N to 10° N (Figure 3.3). The values of the chosen variable were horizontally averaged over the defined box, such that the result is one mean vertical profile for this area. For a climatological mean the values of the profiles were averaged over thirty years (1979-2008) for the models of CMIP5 and over twenty years (1991-2010) for the models of the YoTC data set. The focus of this study is on July, August and September during the wet phase of the monsoon. To note is that the horizontal resolution in the models of CMIP5 differs, so that different numbers of grid-points are integrated in this horizontal box in the different models. Two examples are the model BCC with ten included grid-points and the model GFDL HIRAM C360 with 1040 included grid-points, so the range of included grid-points is large.

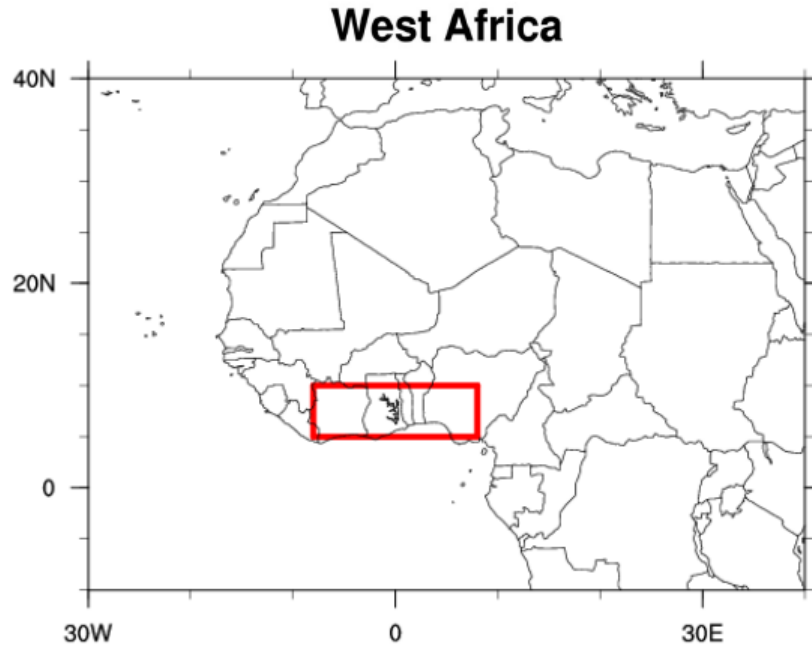


Figure 3.3: Defined horizontal box (red) for mean vertical profiles of this area.

3.7 Calculation of Advection and Wind Speed

In Schuster et al. (2013) it is shown, that the advection of temperature and moisture plays an important role in the formation of low-level clouds. For calculating the advection in the models of CMIP5, all global climate models were linearly regridded to the same horizontal grid ($1.4^\circ \times 1.4^\circ$) by using a function of the climate data operators (cdo). The different operators in cdo give the opportunity to manipulate data easily. To get temperature differences, the mathematical method central differences was chosen. The first position is at 5.4° N at a zonal line from -8° E to 8° E, the second position is from an identical line at 8.2° N (position 3). These two lines represent the area around the southern part of the defined box near the Guinea Coast in southern West Africa (Figure 3.3). The meridional wind component is based on a line from -8° E to 8° E at the position 6.8° N (position 2). The three lines are illustrated in Figure 3.4 on the left. On the right, the positions in the models of the YoTC data set are represented. The two positions for the calculation of the temperature difference are at 2.5° N (position 1) and at 7.5° N (position 2). The position for the meridional wind component is at 5° N. Like in the models of CMIP5, all positions reach from -8° E to 8° E. The models in the YoTC data set are based on the same horizontal grid, so that these models do not have to be regridded. The advection of temperature can then be calculated with the equation

$$adv(T) = v_2 * \frac{T_1 - T_3}{2\Delta y} \quad (3.8)$$

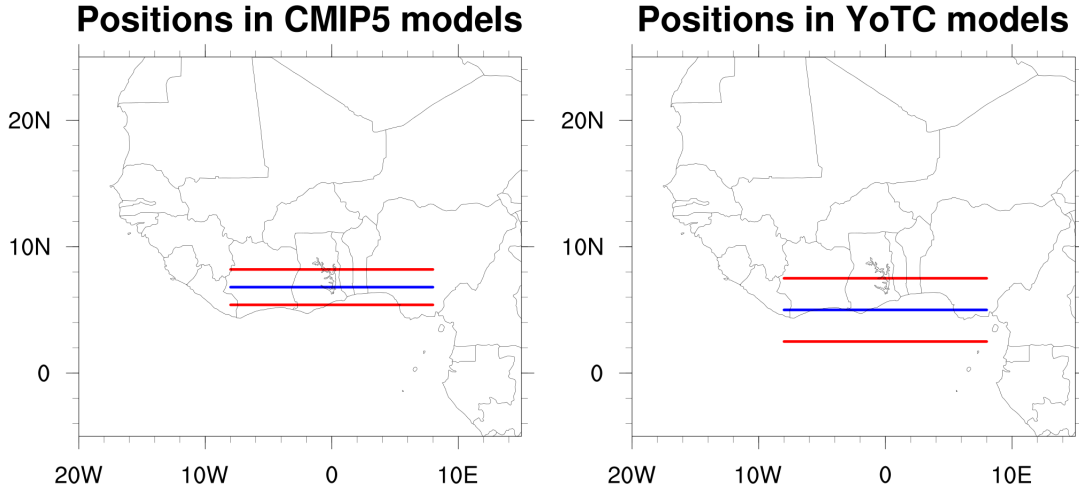


Figure 3.4: Left: zonal lines for the calculation of the advection in the models of CMIP5. Right: zonal lines for the calculation of the advection in the models of the YoTC data set.

and the advection of moisture with

$$adv(q) = v_2 * \frac{q_1 - q_3}{2\Delta y}. \quad (3.9)$$

After calculating, the values were averaged over these lines to get one vertical profile of this area. To get a climatology, the values were also averaged over thirty years for CMIP5 models and over twenty years for YoTC models in the months July, August, and September. The positions in ERA-Interim are 1.5° N (position 1), 4.5° N (position 3) and 3° N (position 2) (not shown).

To note is that the calculation of the advection should be done ideally before averaging because

$$\overline{v \cdot \Delta T} \neq \bar{v} \cdot \overline{\Delta T}. \quad (3.10)$$

This is important for the calculation of the average in space and time. The data of the models in CMIP5 are monthly mean values. So here we have the problem that the averaging is made before calculating the advection. The result is that the calculated advection is underestimated. To better compare ERA-Interim to these models, the data of ERA-Interim was averaged over every month before calculating the advection but only for the comparison with the CMIP5 models. The values in the models of the YoTC data set are instantaneous data, so here the calculation of the advection can be done before averaging and compared directly with ERA-Interim. The differences of the left part of equation 3.10 and the right part are represented in Figure 3.5 on the left. For this illustration ERA-Interim data were used from 1979-2008. The blue line represent the results of the calculation of the advection of moisture with instantaneous data before averaging, for the red line monthly mean values of specific humidity and the meridional wind component were used for the calculation of the advection of moisture. The differences and the errors are small.

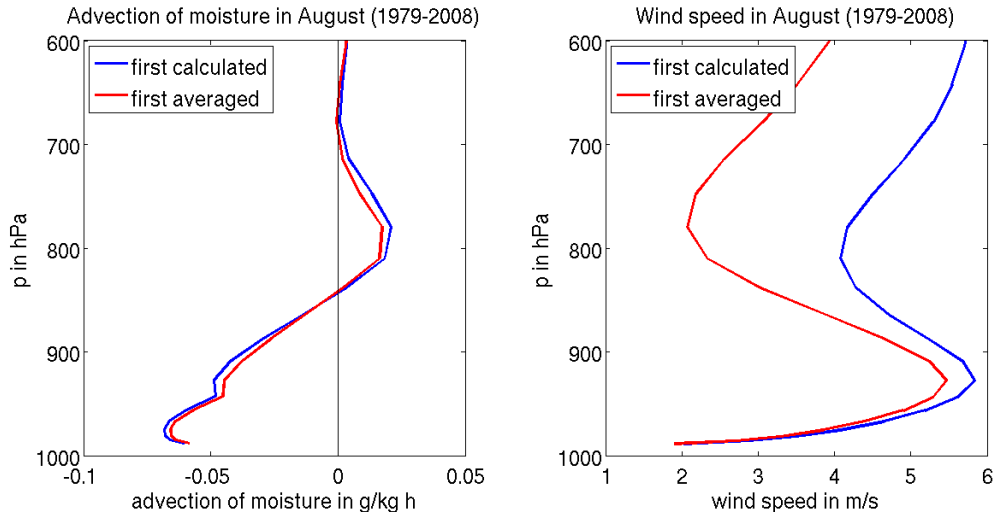


Figure 3.5: Differences of different calculated advection of moisture (left) and wind speed (right) in ERA-Interim from 1979-2008.

The variable wind speed is computed from the horizontal wind components

$$v_{speed} = \sqrt{u^2 + v^2}. \quad (3.11)$$

Like before in the calculation of the advection, the CMIP5 models are based on monthly or daily mean values. That is the reason why the data of ERA-Interim was monthly averaged before calculating the wind speed to better compare the results of ERA-Interim with the models of CMIP5. By calculating a mean, the values become smaller than the instantaneous data, such that

$$\sqrt{\overline{u^2 + v^2}} \geq \sqrt{\overline{u}^2 + \overline{v}^2}. \quad (3.12)$$

By comparing mean values to instantaneous data this has to keep in mind. To illustrate that fact, the wind speed was first calculated like on the left part of the equation (Figure 3.5, on the right in blue) and a second time like on the right part (Figure 3.5, on the right in red) with ERA-Interim data from 1979-2008 in August. Near the ground the differences are small but increase to higher levels.

4. Results for the Global Climate Models in CMIP5

4.1 Representation of Low-Level Clouds and Wind Speed

At the beginning of the analysis the focus is on the vertical structure into southern West Africa. As described in Schuster et al. (2013), the formation of low-level clouds is connected to the wind speed. The mean vertical profiles of the cloudiness and wind speed below 650 hPa near the Guinea Coast in the southern part of West Africa averaged over thirty years are shown in Figure 4.1.

The vertical profile of ERA-Interim in July (Panel a) is split in two local maxima, the low-level clouds at 850 hPa and the ultra-low clouds, as described in Knippertz et al. (2011), at 950 hPa. This cloud structure remains stable in August and September (Panel b and c). The low-level clouds show maximal values in August and September with values of more than 27 %, the ultra-low clouds show their maximal extension in July and August with values of about 24 %. Comparing the reanalysis to the different global climate models, it is remarkable that no global climate model has the low-level clouds split like the reanalysis. Also the large spread between the different global climate models with variations of 35 % in the cloud area fraction is striking. In addition the models show large differences in the height of the cloud maximum. Some models show the maximum of cloudiness too high for example the models EC EARTH and CSIRO at around 800 hPa. Others simulate no or less low-level clouds below 650 hPa like the model BNU and CNRM. The monthly variations are generally small between July to September.

The local maxima in ERA-Interim and those of the different models are simulated at nearly the same level around 950 hPa for the variable wind speed in July (Panel d). This maximum indicates the NLLJ. As described before, the height of the NLLJ should be placed higher than the maximum of cloudiness because the wind shear below the jet produces turbulence, which mixes moisture upwards and the cloudiness develops. In ERA-Interim the NLLJ is analyzed higher than the ultra-low clouds with values up to $5.5 \frac{\text{m}}{\text{s}}$. That can be the reason why ERA-Interim produces the ultra-low clouds. The spread between the maximal values in the wind speed of the climate models in July is large with variations up to $5 \frac{\text{m}}{\text{s}}$. Moreover nearly all models overestimate the wind speed compared to ERA-Interim. The models CNRM, BCC, and FGOALS S2 simulate the strongest NLLJ with more than $8 \frac{\text{m}}{\text{s}}$ but it is to note, that the models BCC and CNRM are based

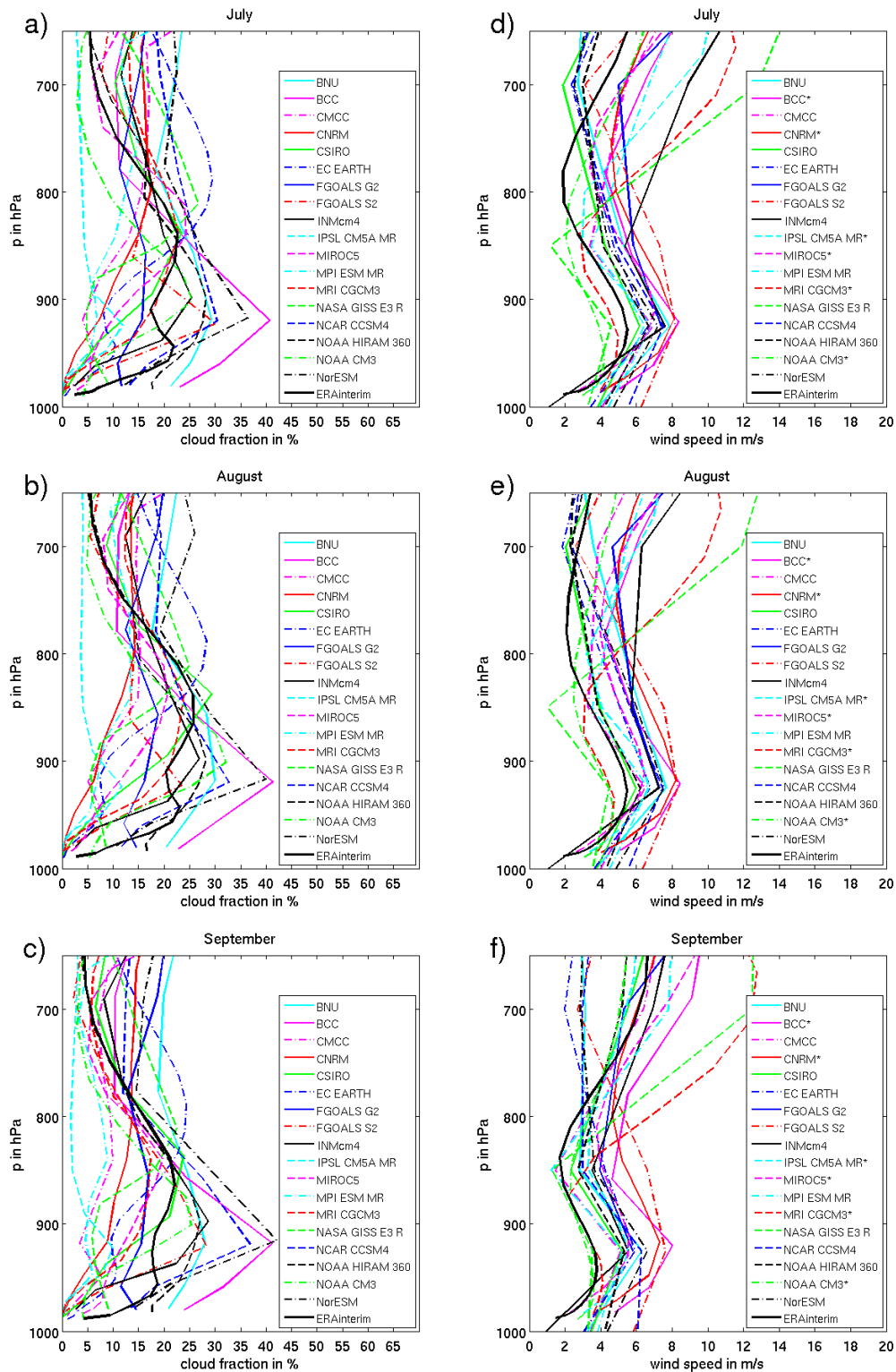


Figure 4.1: Mean vertical profiles in southern West Africa averaged over 79-08 of cloud area fraction in % below 650 hPa (left column) and wind speed in $\frac{m}{s}$ (right column) in the months July (top row), August (second row) and September (bottom row). The thick black line represents the results of ERA-Interim. Models which are marked with stars are based on daily mean data.

on daily mean data. The model NOAA CM3 simulate a weaker NLLJ than ERA-Interim (less than $5 \frac{\text{m}}{\text{s}}$) although the data of NOAA CM3 is based on daily data as well. ERA-Interim shows larger wind speed in the months July and August (Panel d and e) with values up to $5.5 \frac{\text{m}}{\text{s}}$, in September (Panel f) the wind slows down (less than $5 \frac{\text{m}}{\text{s}}$). The monthly variations in the climate models are less but generally show lower values in September.

4.2 Representation of the Advection of Moisture and Temperature

As described in Schuster et al. (2013) the advection of temperature and moisture is connected with the formation of low-level clouds. In Figure 4.2, the mean vertical profiles of the advection of temperature (on the left) and moisture (on the right) near the coast in southern West Africa are represented. The values of the temperature advection in July (Panel a) are negative below 800 hPa. That result is in accordance with the study of Schuster et al. (2013). The turbulent mixing in the boundary layer, which is important for the mixing of moisture during the night, depends on wind shear underneath the jet and static stability. The cold air advection destabilize the lower layers, such that turbulent eddies can develop easier. In ERA-Interim the minimum is analyzed at 930 hPa with $-0.05 \frac{\text{K}}{\text{h}}$ in July, $-0.04 \frac{\text{K}}{\text{h}}$ in August and $-0.025 \frac{\text{K}}{\text{h}}$ in September. The values are smaller than in the study of Schuster et al. (2013). In this study the values are around eight times larger than the values presented here for ERA-Interim. One reason can be that the monthly mean causes smaller values, but like shown in section 3.7 the differences of the calculation with monthly mean data and instantaneous data are small. The spread between the different global climate models is large like in the variables before. Furthermore the global climate models tend to produce stronger cold air advection compared to ERA-Interim by up to $-0.01 \frac{\text{K}}{\text{h}}$. The strongest cold air advection in July is produced by the models MIROC5 and FGOALS S2 with values of more than $-0.1 \frac{\text{K}}{\text{h}}$. The model BCC simulates the cold air advection similar to ERA-Interim below 900 hPa but show problems aloft. Nearly all models show too warm air advection above 900 hPa compared to ERA-Interim. The monthly variations are small but the values are larger in July and show a decrease to September.

In ERA-Interim the advection of moisture in July (Figure 4.2, Panel d) is minimal with negative values near the ground and maximal with positive values at 800 hPa. The advection of moisture can be explained with the monsoonal SMC (Zhang et al., 2008). The strong pressure gradient from the Sahara to the Atlantic generates a flow from the Atlantic towards the heat-low, where low-level air ascends. The shallow return flow above from the Sahara to the Atlantic crosses the zone of the strongest monsoonal rainfalls. That is the reason why the air masses absorb moisture and cause moist air advection at around 700 to 800 hPa. Near the ground the advection in ERA-Interim is dry. The reason can be the descending branch of the SMC over the Atlantic which carries dry air from higher levels downwards and generates dry advection. The dry advection near the ground is strongest in July with up to $-0.08 \frac{\text{g}}{\text{kg h}}$ and decreases in September. In the global climate models the dry advection near the ground is too weak but better represented at around 900 hPa. The val-

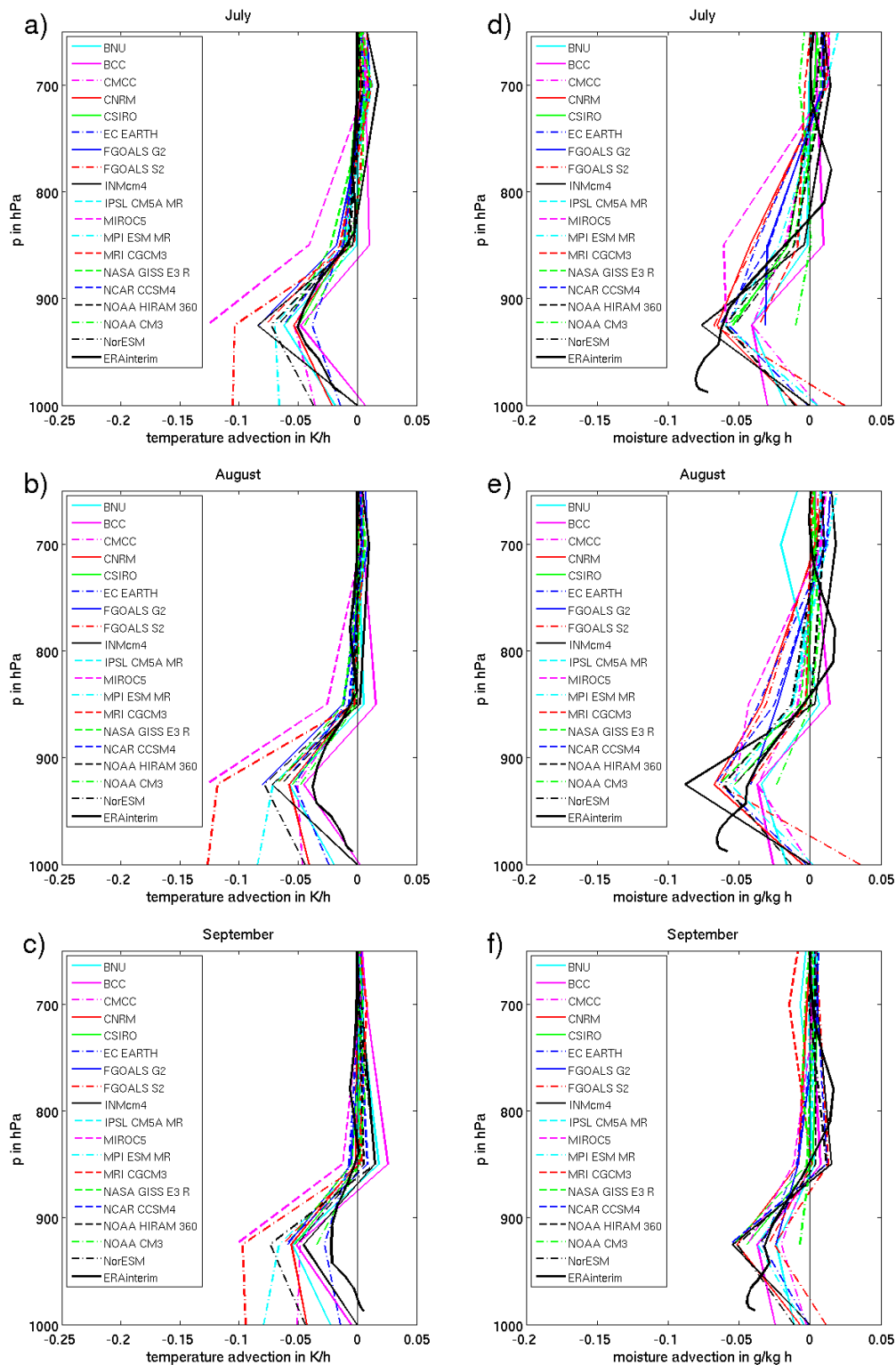


Figure 4.2: Mean vertical profiles in southern West Africa averaged over 79-08 of the advection of temperature in $\frac{\text{K}}{\text{h}}$ below 650 hPa (left column) and the advection of moisture in $\frac{\text{g}}{\text{kg h}}$ (right column) in the months July (top row), August (second row) and September (bottom row). The thick black line represents the results of ERA-Interim.

ues get smaller towards September which is comparable to ERA-Interim. The moist advection is visible at 800 hPa in ERA-Interim where the shallow return flow of the SMC is placed. This return flow is badly represented in most of the global climate models. In July and August (Panel d and e) the height of the return flow is mostly simulated too high at around 700 hPa and too weak in the models, in September (Panel f) the height is underestimated compared to ERA-Interim (around 850 hPa).

4.3 Rank Correlation

In this section, a rank correlation was calculated between low-level cloudiness and several variables. The two vectors for the calculation were created out of the mean vertical profiles of each model. The values of these profiles were averaged over thirty years in the defined horizontal box near the Atlantic coast (Figure 3.3). For each model the maximal value below 900 hPa was chosen and the results were ordered in the vector. Afterward each values were allocated to their rank position numbers. The analysis contains 18 different models, such that the vectors consist of rank numbers from 1 to 18. In Table 4.1 the first column represents the rank correlation between the

Table 4.1: Rank correlation between different models of mean maximal values below 900 hPa of the variables cloud fraction (cl) with wind speed, advection of temperature (advT) and advection of moisture (advq); italics and bold value: value is significant to the level 0.95.

months	cl/wind speed	cl/advT	cl/advq
July	<i>0.41</i>	0.08	-0.16
August	0.25	0.12	-0.27
September	<i>0.55</i>	0.22	-0.09

variables cloud fraction and wind speed. The second column shows the rank correlation between cloud fraction and advection of temperature and the last column contains the rank correlation between the cloud fraction and the advection of moisture. Values which are in italics and bold are significant to the level 0.95 (calculated with a t-test, described in section 3.5). It would be expected that the correlation between the cloud fraction and the wind speed is positive during the night. The wind shear underneath the jet produces turbulence at night and mixes moisture from the ground in higher levels where clouds can form. During the day, the cloud formation is driven by buoyancy in the turbulent boundary layer, so the correlation should be smaller. The differences in the processes at night and day can not be illustrated and analyzed with this data set. The temporal resolution of monthly mean values is not enough to analyze the diurnal variations. Furthermore it would be expected that cold air advection favors cloud formation. The cold advection changes the stability in lower layers, such that turbulence can develop easier. Dry air advection has an negative effect for cloud formation, such that a positive correlation would be expected. The rank correlation coefficient of the cloud fraction and the wind speed near the ground are positive. The correlation is highest in September (0.55) and lowest in August (0.25). In July and September the

values are reliable to the 95 % level of significance. So there is a statistical connection between these two variables. The turbulent eddies underneath the NLLJ mix moisture from the ground in higher levels, so clouds can form. But the turbulent eddies also transport momentum from the jet level to the ground which weakens the jet. So if the rank correlation was negative, the transport of momentum would be dominant. As the rank correlation is positive, the mixing of moisture probably plays a more important role. The values of the rank correlation between the cloud fraction and the advection of temperature and moisture are very small. Warmer and drier air advection leads to more clouds. That result is surprising, but the values are small, such that the statistical connection is weak. Although the rank correlation is small, there can be a physical connection between the variables. All variables are connected to each other, that is the reason why regarding one alone can not show whole processes.

So far, the rank correlation was calculated out of climatological mean values and compared for the different models. A future question is, how the connection between the low-level cloudiness and the wind speed changes when the rank correlation is calculated for each model alone. In this case the values of the two vectors which are important for the calculation of a rank correlation coefficient consist of maximal values below 900 hPa and vary with time. In Figure 4.3 the rank correlation of ERA-Interim, GFDL CM3, and FGOALS S2 between the low-level cloudiness and the maximal windspeed below 900 hPa are represented in a horizontal view over West Africa. Insignificant values (to the level 0.9, calculated with the t-test) are hatched in the Figure. All global climate models in this analysis have a monthly resolution, so to compare the results of the models to ERA-Interim in a fair way, the values of ERA-Interim are monthly mean values too.

The results of ERA-Interim show positive correlations over land and negative correlations over the ocean along the Guinea Coast. The positive correlation in the southern part of West Africa becomes greater from July to September, especially over the region Liberia, Nigeria, and Cameroon. Also the negative correlation over the ocean along the coast gets stronger. That means that over land the stronger wind speed is associated with more low-level cloudiness, so the mixing of moisture is more intensive than the dissipation of momentum which weakens the jet. Over the Atlantic it is the other way around. Also the regions of Angola and Congo show negative correlation coefficients which increase from July to September. So stronger wind speeds are associated with less low-level cloudiness. The model GFDL CM3 shows positive rank correlation coefficients in a zonal band with a width from 0° N to 20° N and higher values along the Guinea Coast. So like before in ERA-Interim the mixing of moisture appears to dominate. Over the Sahara the values become negative from July to September, like over the ocean in the south-western part of the Figure. So stronger winds seem to have a negative influence on low-level clouds. In the model FGOALS S2 the rank correlation coefficients are insignificant along the Guinea Coast. Positive values are located in a zonal band along 20° N. In this area the ITF is located, so perhaps this has an effect on the correlation. Further examples of calculated rank correlations of the other models are included in the appendix (Figure A.1 to A.4). Most of the models show positive or insignificant rank correlations at the coast in southern West Africa. Especially the models BNU ESM and

IPSL CM5A MR show high rank correlations in southern West Africa.

4.4 Short Summary of the Results for CMIP5 Models

The global climate models of the CMIP5 data set have large problems to simulate the low, precisely the ultra-low cloudiness. Most of the models represent the low-level cloudiness too high and not extensive enough. Also in the variables wind speed, advection of temperature and moisture the differences are large between the models and compared to ERA-Interim. These deviations existed in the models of CMIP3 too (Knippertz et al., 2011). Processes such as the cold advection near the ground are overestimated in the global climate models and the circulation of the SMC is located in other levels and too weak against ERA-Interim. The calculation of the rank correlation between the models shows a connection between low-level cloudiness and the maximal wind speed below 900 hPa. So the assumption is, that higher wind speed in the NLLJ is associated with more turbulent eddies, which mix moisture from the ground to higher levels and favor cloud formation as described in Schuster et al. (2013). The rank correlation between the low-level cloudiness and the maximal advection of temperature and moisture below 900 hPa are very small, such that the statistical conclusion is that the connection is insignificant. So perhaps the advection plays a smaller role in the formation of low-level clouds than described in the study of Schuster et al. (2013) or the models are inconsistent. But like said before, the rank correlation of one variable can not resolve whole processes, such that the advection can be important in collaboration with other variables even though the correlation is small. The rank correlation between the low-level cloudiness and the wind speed calculated separately for each model shows positive values along the Guinea Coast in ERA-Interim and the model GFDL CM3 but insignificant values in the model FGOALS S2, so there are differences between the models. The problem of using this data set is the temporal resolution. The analysis of the diurnal cycle can be useful to understand the causes of differences between the models.

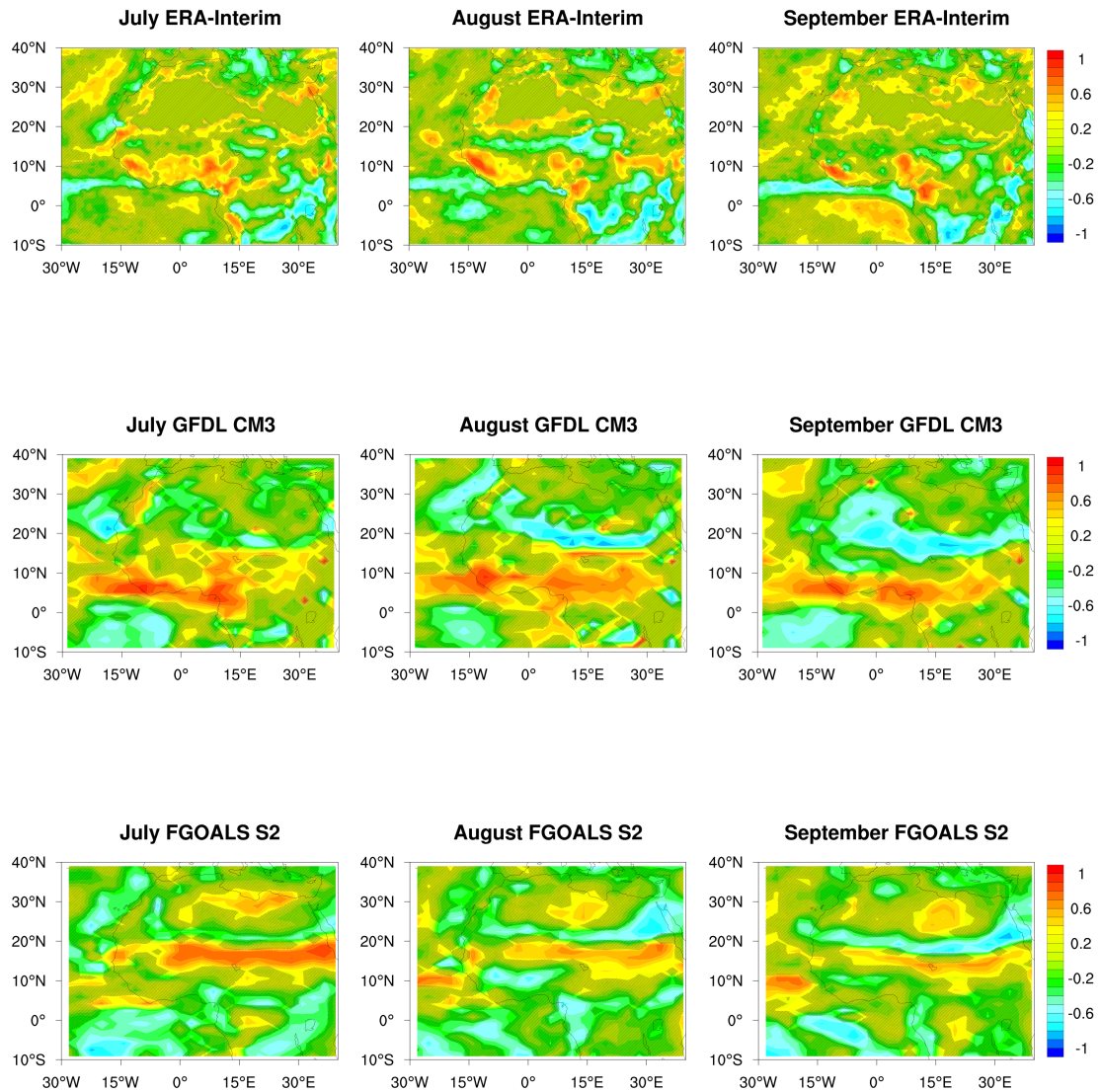


Figure 4.3: Rank correlation between the maximal value of cloud fraction and wind speed below 900 hPa in the months July (first column), August (second column), and September (third column) of ERA-Interim (top row), GFDL CM3 (second row), and FGOALS S2 (bottom row); Insignificant values to the level 0.9 are hatched.

5. Results for the Global Climate Models in GASS YoTC

5.1 Representation of Low-Level Clouds and Wind Speed: Diurnal Variations

The data set of GASS YoTC covers twenty years (1991-2010) with a temporal resolution of six hours. The mean vertical profiles were calculated as before (section 3.6). The values were averaged over the defined box from -8° E to 8° E and from 5° N to 10° N (Figure 3.3) and for a climatological mean profile the values were averaged over twenty years for the months July, August and September. In the model FGOALSs the data of the year 1991 are missing.

At first, the focus is on the diurnal cycle of stratiform cloudiness in ERA-Interim (Figure 5.1, left). The diurnal cycle is very typical for the wet phase of the monsoon as described in Knippertz et al. (2011) and Schuster et al. (2013). At midnight (Panel a) the maximal cloudiness is located below 900 hPa, which is very low. That is the reason why these clouds are described as ultra-low clouds (Knippertz et al., 2011). In the early morning (Panel b), the cloudiness reaches the maximal value of 40 %, then raises up to 825 hPa at midday (Panel c) and in the afternoon the cloudiness decreases to less than 16 % (Panel d). The diurnal cycle explains the two maxima in the vertical profile of ERA-Interim in Figure 4.1 (section 4.1), in which monthly mean values were used. The vertical structure of the wind speed is presented in Figure 5.1 (right column). The NLLJ in ERA-Interim is simulated at 930 hPa with slightly less than $6 \frac{\text{m}}{\text{s}}$ at midnight (Panel e). In the early morning (Panel f) the wind strengthens and reaches its maximum at the same height. During the course of the day the maximal value drops to $4 \frac{\text{m}}{\text{s}}$ (Panel g and h). This behavior is consistent with the theory described in Gounou et al. (2012). The NLLJ evolves at night because of the strong horizontal pressure gradient from the Sahara to the coast. During the day the pressure gradient is confronted with turbulent mixing in the boundary layer, which weakens the jet. At night the turbulence relaxes because of a lack of solar radiation but the strong pressure gradient from the heat-low at the Sahara to the Atlantic generates the NLLJ. The height of the NLLJ in ERA-Interim at night is a bit higher than the low-level cloudiness which is consistent with the theory because the wind shear is an important factor for low-level cloud formation.

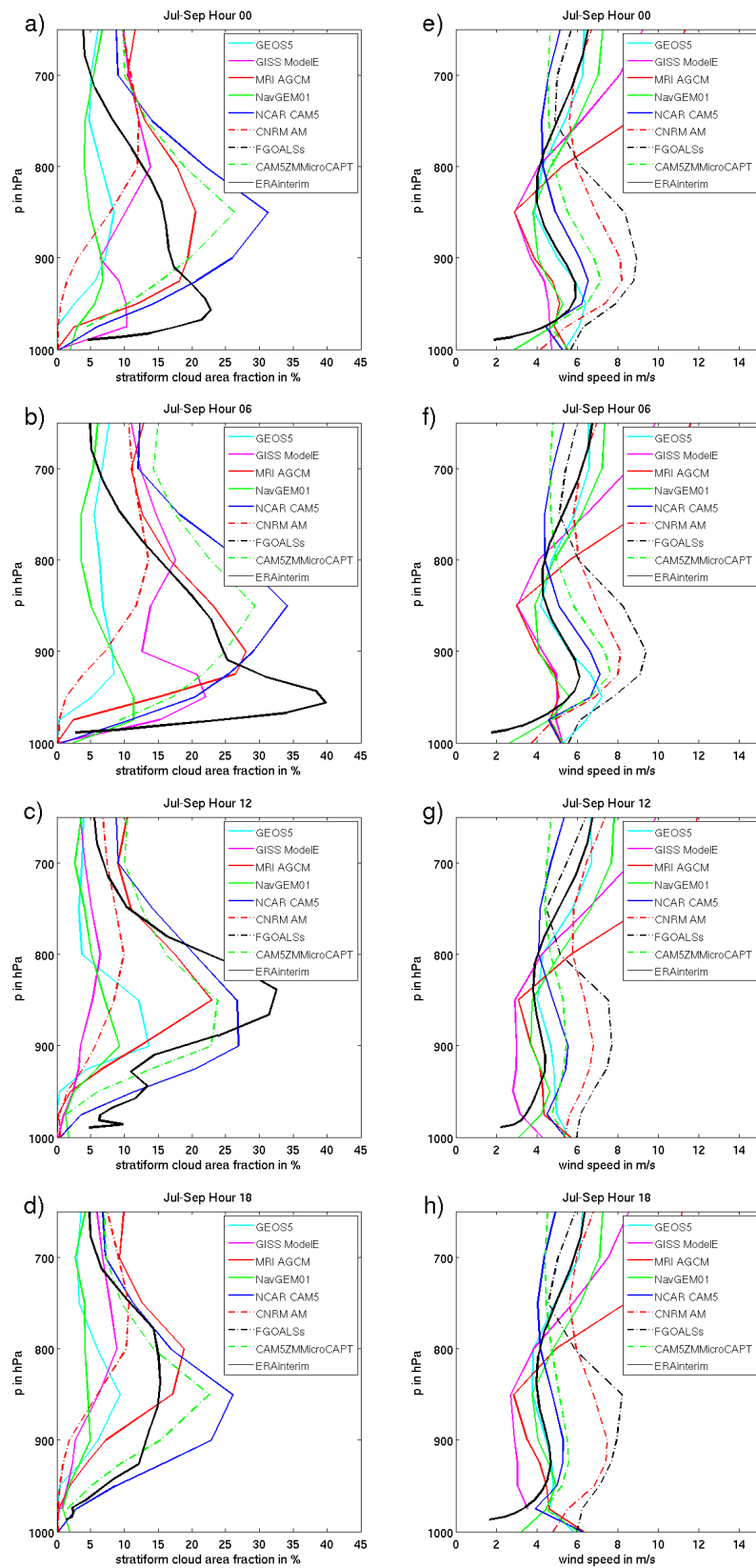


Figure 5.1: Mean vertical profiles over 'red box' (Figure 3.3) near the Guinea Coast in southern West Africa of stratiform cloud fraction (first column) in % and wind speed (second column) in $\frac{m}{s}$ from 1991-2010 below 650 hPa at midnight (top row), at 06 UTC (second row), at midday (third row) and 18 UTC (bottom row) in the months July to September. The thick black line represents the results of ERA-Interim.

When looking at the global climate models the large spread between the models catches the eye. The model FGOALSs simulates no stratiform cloudiness below 650 hPa. At midnight (Panel a) the models MRI AGCM, CAM5ZMMicroCAPT, and NCAR CAM5 do not reproduce the ultra-low clouds. These models simulate the low-level clouds too high at 850 hPa. Furthermore the simulated clouds in CAM5ZMMicroCAPT and NCAR CAM5 show less diurnal variations. There are other physical processes causing this kind of clouds. The model MRI AGCM has a weak diurnal cycle. In the early morning (Panel b) the model simulates the low-level cloudiness in 900 hPa with more than 27 %. Afterward the cloud cover raises up to 850 hPa at midday (Panel c) and decreases in the afternoon and night (Panel d and a) with values around 20 %. So the behavior is similar to ERA-Interim but the height is located too high. NAVGEM01 and GISS ModelE also simulate a similar behavior, like shown in the diurnal cycle of the reanalysis, even in the same height but the values are too small with maximal values at 06 UTC less than 12 % in NAVGEM01 and 23 % in GISS ModelE. Just as in the cloudiness, the global climate models show large differences between each other in the vertical profiles of the wind speed. CNRM AM and FGOALSs simulate the maximum at 900 hPa which is a little higher than in ERA-Interim. Furthermore the maximal value reaches more than $8 \frac{\text{m}}{\text{s}}$ at night and the early morning (Panel e and f) which is much stronger than in ERA-Interim. NAVGEM01 and GEOS5 AGCM represent the maximal wind speed in a lower height than in ERA-Interim. MRI AGCM and GISS ModelE show the weakest NLLJ of all models. These two are the only ones which have a weaker NLLJ than ERA-Interim. All other models overestimate the wind speed. MRI AGCM, GISS ModelE, CAM5ZMMicroCAPT, and NCAR CAM5 show a strong wind speed at the bottom. That is strange because normally the wind speed lessens with lower height. This could be an extrapolation problem. Normally the model layers are not based on a pressure unit, such that errors can accrue by inter- or extrapolating the model layers to pressure levels.

5.2 Representation of Low-Level Clouds and Wind Speed: Monthly Variations

The variations from July to September in the variables stratiform cloud fraction and wind speed are small. An example for the monthly variations in these months at 06 UTC is shown in Figure 5.2. A slight variation is observable in ERA-Interim from August to September (Panel b to c) in which the stratiform cloudiness decreases from 44 % to less than 35 %. Also the wind speed weakens about $2 \frac{\text{m}}{\text{s}}$ from August to September (Panel e to f). The model MRI AGCM shows the greatest monthly variations. In July (Panel a) the maximal cloudiness reaches values around 28 %, in August (Panel b) the cloudiness grows to 32 % and in September (Panel c) the cloudiness reduces to less than 24 %. Less variations are observable in NCAR CAM5 and CAM5ZMMicroCAPT, in which only a slight increase is visible from July to August. The wind speed variations from August to September are greatest in GEOS5 AGCM. The decrease is about $3 \frac{\text{m}}{\text{s}}$.

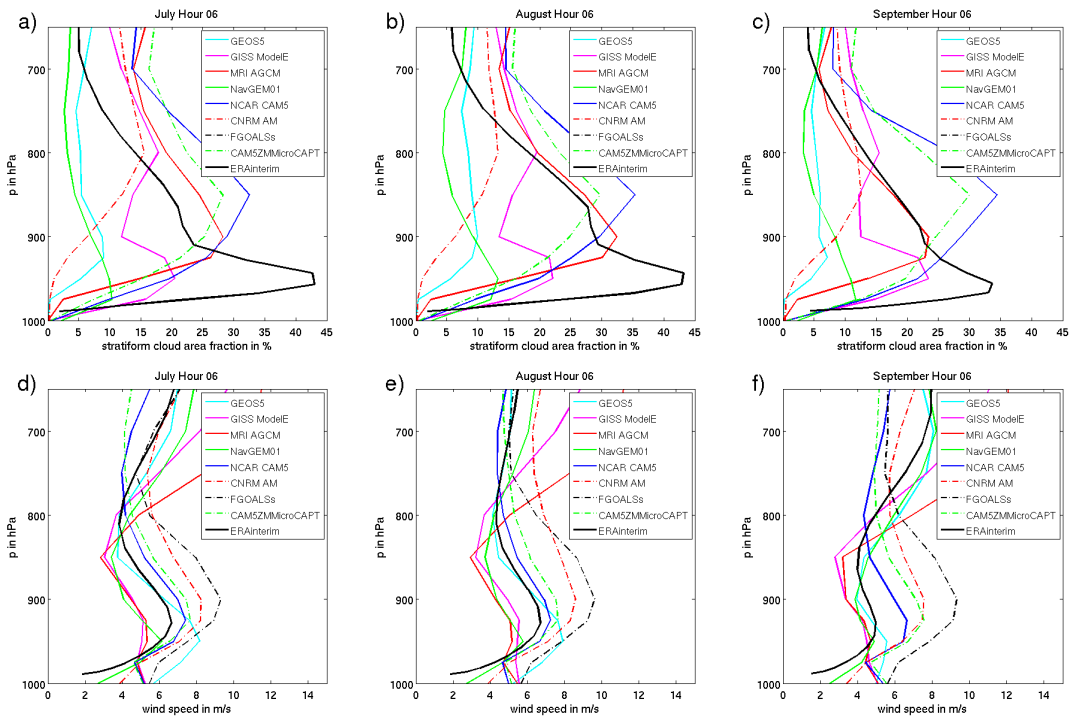


Figure 5.2: Mean vertical profiles over 'red box' near the Guinea Coast in southern West Africa of stratiform cloud fraction (first row) in % and wind speed (second row) in $\frac{m}{s}$ from 1991-2010 below 650 hPa at July (first column), August (second column) and September (third column) at 06 UTC. The thick black line represents the results of ERA-Interim.

5.3 Case Examples

So far, the vertical structure in a defined area of southern West Africa was investigated in this analysis. At this point the question appears, how the diurnal cycles of low-level cloudiness and wind speed are represented in a horizontal view over West Africa. Therefore a new variable, total low-level stratiform cloud fraction, was built out of the variable stratiform cloud area fraction, which originally depends on time, latitude, longitude, and vertical. To calculate the total cloud fraction below 900 hPa with only a temporal and a horizontal dimension, the maximum-random overlap assumption was used (described in section 3.4). The total cloud fraction to a given level was calculated with the maximum assumption, in case a cloud fraction is existent in two adjacent layers. If there is a cloud-free layer between two clouds, the random-overlap assumption was used.

As demonstrated before in the vertical profiles of the variable stratiform cloud fraction, GISS ModelE showed a similar behavior like ERA-Interim but the values were smaller. That is the reason why this model is chosen for taking a closer look at the diurnal variations of the total low-level stratiform cloudiness. The model MRI AGCM also showed a similar behavior like ERA-Interim in the vertical profiles of the stratiform cloud fraction but the height was simulated too high. In Figure 5.3, the total low-level stratiform cloudiness below 900 hPa is given in contours, the vectors represent the wind speed and direction in 900 hPa. Both variables were averaged over 20

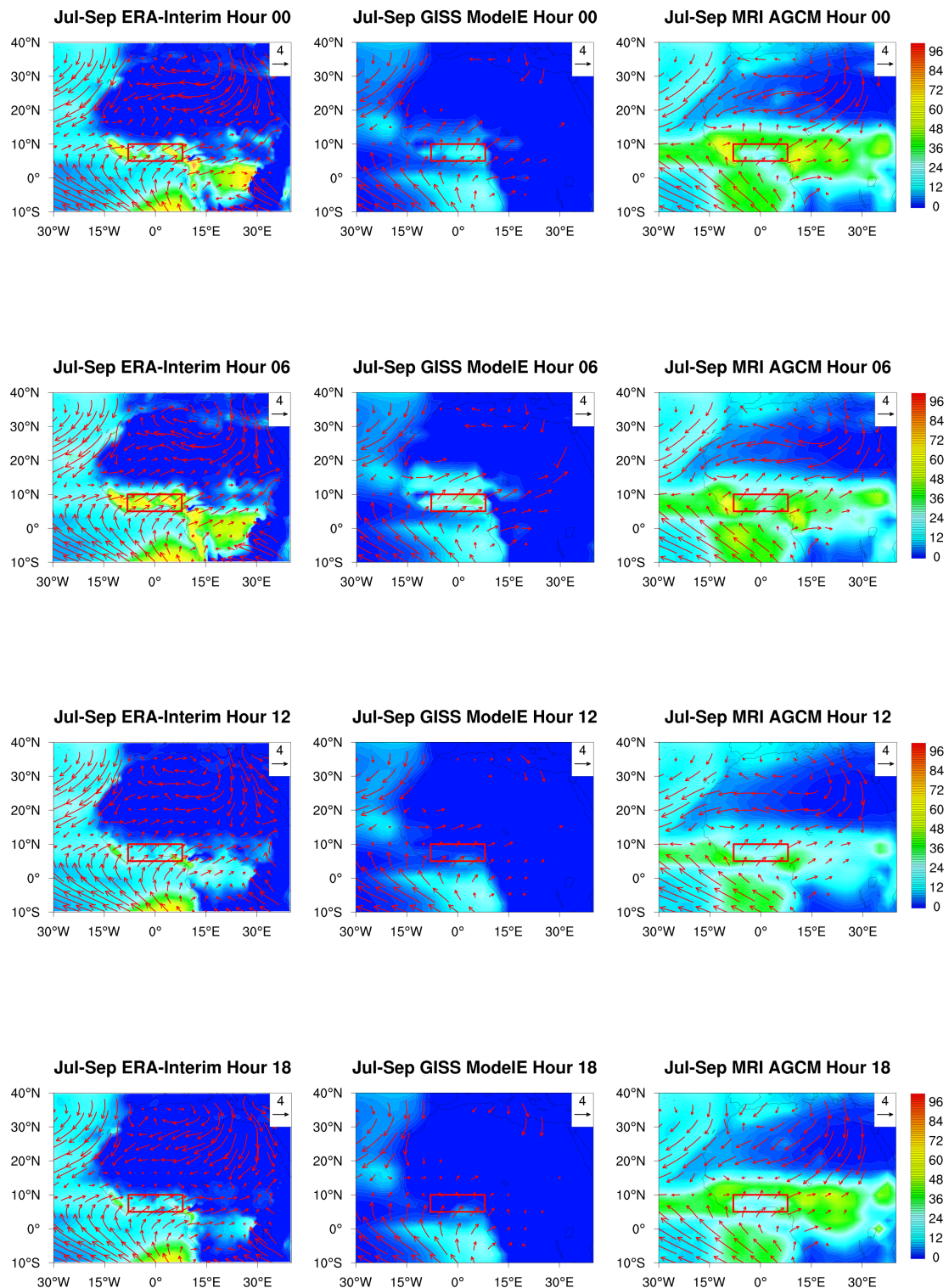


Figure 5.3: Horizontal view of total stratiform cloudiness below 900 hPa in % (contours) and wind vectors in $\frac{\text{m}}{\text{s}}$ (arrows) at 900 hPa of ERA-Interim (first column), GISS ModelE (second column), and MRI AGCM (third column) at midnight (top row), at 06 UTC (second row), at midday (third row) and 18 UTC (bottom row) in the months July to September from 1991-2010. The red box, which was used for the vertical profiles, is integrated in these Figures.

years for the months July to September. There are some missing wind vectors because of missing data at this height and place. At first the results of the diurnal cycle in ERA-Interim are described.

Some low-level cloudiness is located over the Guinea Coast in southern West Africa and in the south over the Atlantic. At night, the low-level cloudiness over the Guinea Coast develops with a maximal increase in the early morning. At 06 UTC, the wind speed at the coast in southern West Africa is maximal and the direction is south-west. In the course of the day the low-level stratiform cloudiness decreases and reaches its minimum in the afternoon. GISS ModelE simulates the cloudiness at the same positions like ERA-Interim but the values are smaller. The maximal cloudiness at the Guinea Coast is observable at 06 UTC and the wind direction there is South-West. In MRI AGCM the cloudiness is arranged in a zonal band with a width from 5° N to 10° N and included maxima, one around Liberia at the south-westerly coast and one over Cameroon. The cloudiness develops at night and reaches its maximum at the early morning. Afterward the cloudiness decreases at midday. The results of the other models are included in the appendix (Figure A.5 and A.6). The models CNRM AM and GEOS5 AGCM show no or less low-level cloudiness over the whole domain. NAVGEM01 underestimates the low-level cloudiness along the Guinea Coast over land.

5.4 Representation of the Advection of Moisture and Temperature

As described in Schuster et al. (2013), the advection of moisture and temperature plays a significant role in the formation of low-level clouds. The cold air advection at low levels has an effect on the static stability in the boundary layer. The advection of temperature was calculated with equation 3.8 and the advection of moisture with equation 3.9. The positions for the calculation are described in section 3.7.

In ERA-Interim the diurnal variations of the temperature advection are small (Figure 5.4, left). The advection of temperature is characterized by one striking minimum at 925 hPa and a smaller one at 775 hPa. At night and in the morning (Panel a and b) the cold advection is strongest (around $-0.03 \frac{\text{K}}{\text{h}}$) and decreases during the day. The global climate models show stronger daily variations. In some models (NAVGEM01, CNRM AM, FGOALSs) the minimum is analyzed below 950 hPa, GISS ModelE and GEOS5 show the minimum of the advection of temperature higher than ERA-Interim. The diurnal cycle of the global climate models show an other development than ERA-Interim where the minimum is strongest at night/early morning (Panel a and b). The largest negative values in the models are observable in the afternoon (Panel d), then decrease during the night and show the weakest minimum of the day during the early morning. During most of the day the global climate models overestimate the cold advection with values up to $-0.14 \frac{\text{K}}{\text{h}}$ in the models GEOS5, NAVGEM01, CAM5ZMMicroCAPT, and MRI AGCM. GISS ModelE simulates the weakest minimum and the weakest daily variations of all models. The monthly variations are negligible in the models (not shown).

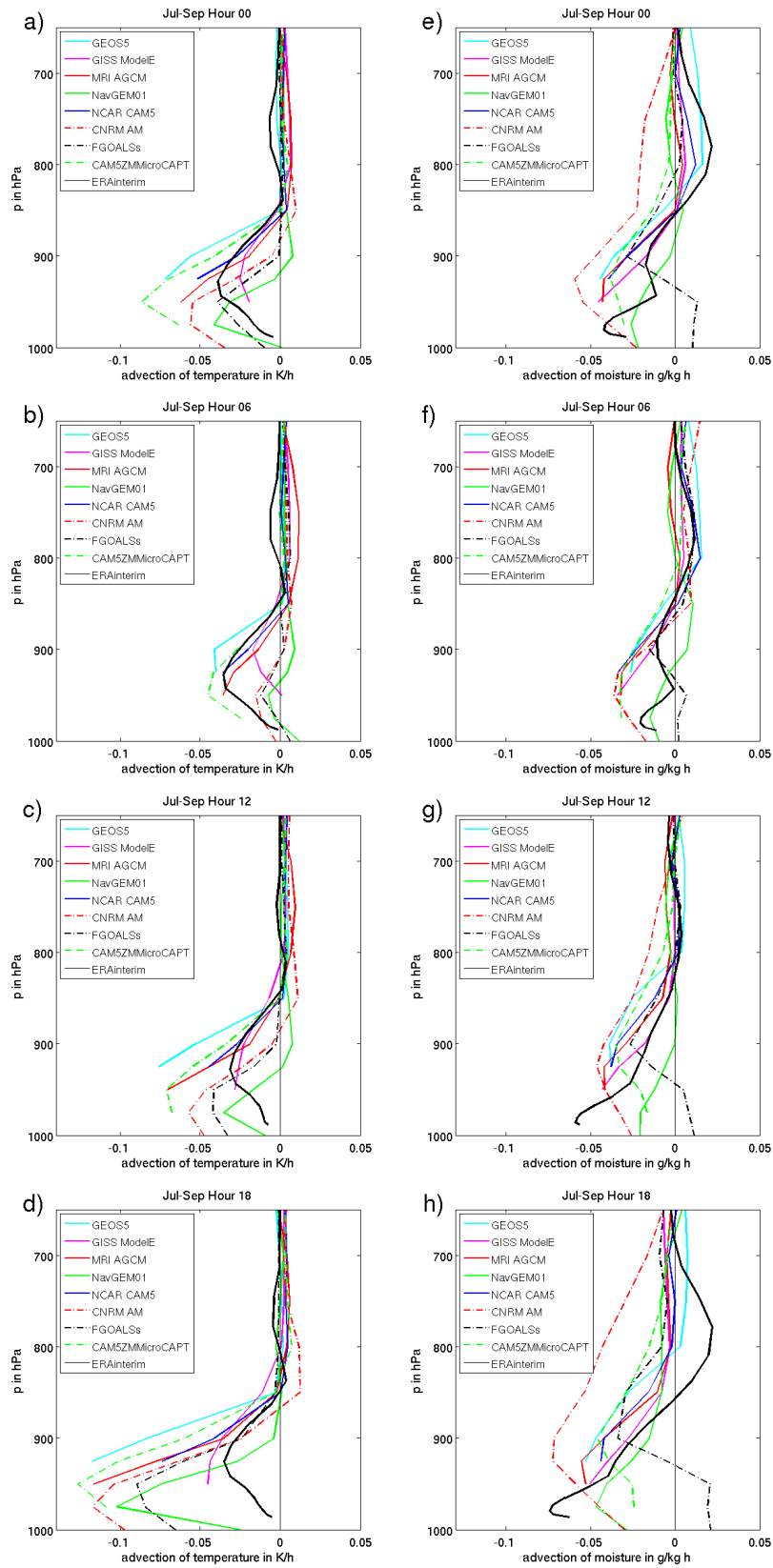


Figure 5.4: Mean vertical profiles in southern West Africa of temperature advection (first column) in $\frac{K}{h}$ and advection of moisture in $\frac{g}{kg h}$ averaged from 1991-2010 below 650 hPa at midnight (top column), at 06 UTC (second row), at midday (third row), and 18 UTC (bottom row) in the months July to September. The thick black line represents the results of ERA-Interim.

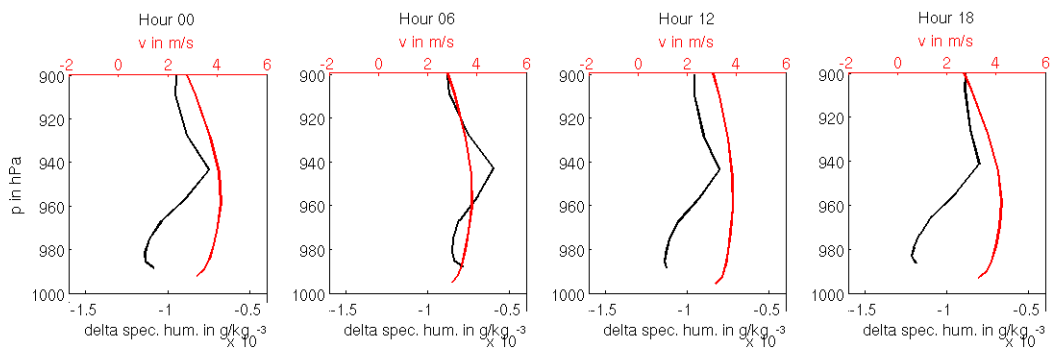


Figure 5.5: Mean vertical profiles of delta specific humidity in $\frac{\text{g}}{\text{kg}}$. The specific humidity at position 1 is subtracted from the values at position 3. The meridional wind component is used from position 2 in $\frac{\text{m}}{\text{s}}$ of ERA-Interim (positions are described in section 3.7).

The advection of moisture in ERA-Interim (Figure 5.4, right) shows negative values below 850 hPa and positive above. Local minima are simulated at 980 hPa and 900 hPa, one maximum with positive values at 800 hPa. In remembrance of the results in the CMIP5 data set (section 4.2), the dry advection from the Atlantic in the lower levels can be explained by the monsoonal SMC. The shallow return flow of this circulation is found at 800 hPa, where the maximum is visible. It is characterized by moist advection because of the shallow return flow of the monsoonal SMC. The maximum in ERA-Interim at 800 hPa is highest in the afternoon and night (Panel h and e) and decreases during the day. The dry advection near the ground is separated into two local minima. At midnight (Panel e), the lowest minimum with less than $-0.05 \frac{\text{g}}{\text{kg h}}$ is more pronounced than the second minimum above. In the morning (Panel f), the dry advection weakens. During the day until afternoon (Panel g and h), the dry advection strengthens and reaches its maximum in the afternoon with up to $-0.07 \frac{\text{g}}{\text{kg h}}$. During the day, the second minimum vanishes. These two minima in the lower parts appear because of weaker differences in the specific humidity at 950 hPa (Figure 5.5). The delta of specific humidity was calculated out of the values at position 1 subtracted from the values at position 3 (positions are described in section 3.7). The notch in the delta of specific humidity is heaviest at 06 UTC, when the two minima in the advection of moisture are best observable. During the day, the notch at 950 hPa is weaker, which means that the differences in the vertical structure of the delta of specific humidity are weaker. Due to this reason the minima in the advection of moisture are less pronounced during the day.

The global climate models show large differences to ERA-Interim. None of the models shows the split of the minimum below 900 hPa as it is produced in ERA-Interim. The minimum in the lower part is simulated in most of the models at around 950 hPa where ERA-Interim shows a notch in the vertical profile. The development of the dry advection in the models starts during the day and reaches its full extent in the afternoon (Panel h). In the early morning (Panel f), the dry advection near the ground is smallest. Except for the model NAVGEM01, all global climate models overestimate the dry advection compared to ERA-Interim. FGOALSs is too moist from

the ground up to 950 hPa where the values in the advection of moisture are positive. The maximum at 800 hPa with positive values in ERA-Interim is simulated well by GEOS5 AGCM during night to midday but the model shows differences in the afternoon. NAVGEM01 produces the maximum too low at 850 hPa in the night to early morning and simulates no maximum during the day and afternoon. So like before in the other variables, the models show problems in simulating the advection correctly compared to ERA-Interim.

5.5 Representation of Surface Solar Radiation

Clouds have an immense effect on the surface solar radiation, so when there are differences in the simulation of clouds, there must be differences in the surface solar radiation as well. As before, the models are compared to ERA-Interim but this time with the forecast of ECMWF because the variable surface solar radiation is only analyzed in the forecast. The medium-range

Table 5.1: Forecast of surface solar radiation (SSR) in ERA-Interim.

ECMWF forecasts	00 UTC	06 UTC	12 UTC	18 UTC
forecast initialized at	12 UTC	00 UTC	00 UTC	12 UTC
method to get six-hour resolution	$SSR_{18} - SSR_{00}$	SSR_{06}	$SSR_{12} - SSR_{06}$	SSR_{18}

forecasts of the ECMWF were made with 52 ensemble members which were initialized every day at zero and 12 UTC. The values in the variable surface solar radiation are accumulated from model initialization up to the chosen time-step. For example at 06 UTC, the values are accumulated from zero to 06 UTC. The time for the initialization is documented in Table 5.1. Since there are twelve-hourly and six-hourly forecasts, the latter has to be subtracted from the first to get a temporal resolution of six hours. For a better understanding, the method is shown in Table 5.1 in the bottom line. The index represents the time for which the forecast is made. Another problem is that the time description in the models differs from each other. So to find out which date described in the models belongs to 00, 06, 12, and 18 UTC, the diurnal cycle in the surface solar radiation can be used. At night the values of the surface solar radiation are small because the sun light is missing, while during the day the values increase. The results of these assignments are written down in Table 5.2 where the indexes represent the time description in the models.

Table 5.2: Time description in SSR.

Model	Hour 00	Hour 06	Hour 12	Hour 18
MRI AGCM	SSR_{18}	SSR_{00}	SSR_{06}	SSR_{12}
CAM5ZMMicroCAPT	SSR_{03}	SSR_{09}	SSR_{15}	SSR_{21}
GEOS5 AGCM	SSR_{21}	SSR_{03}	SSR_{09}	SSR_{15}
GISS ModelE	SSR_{21}	SSR_{03}	SSR_{09}	SSR_{15}

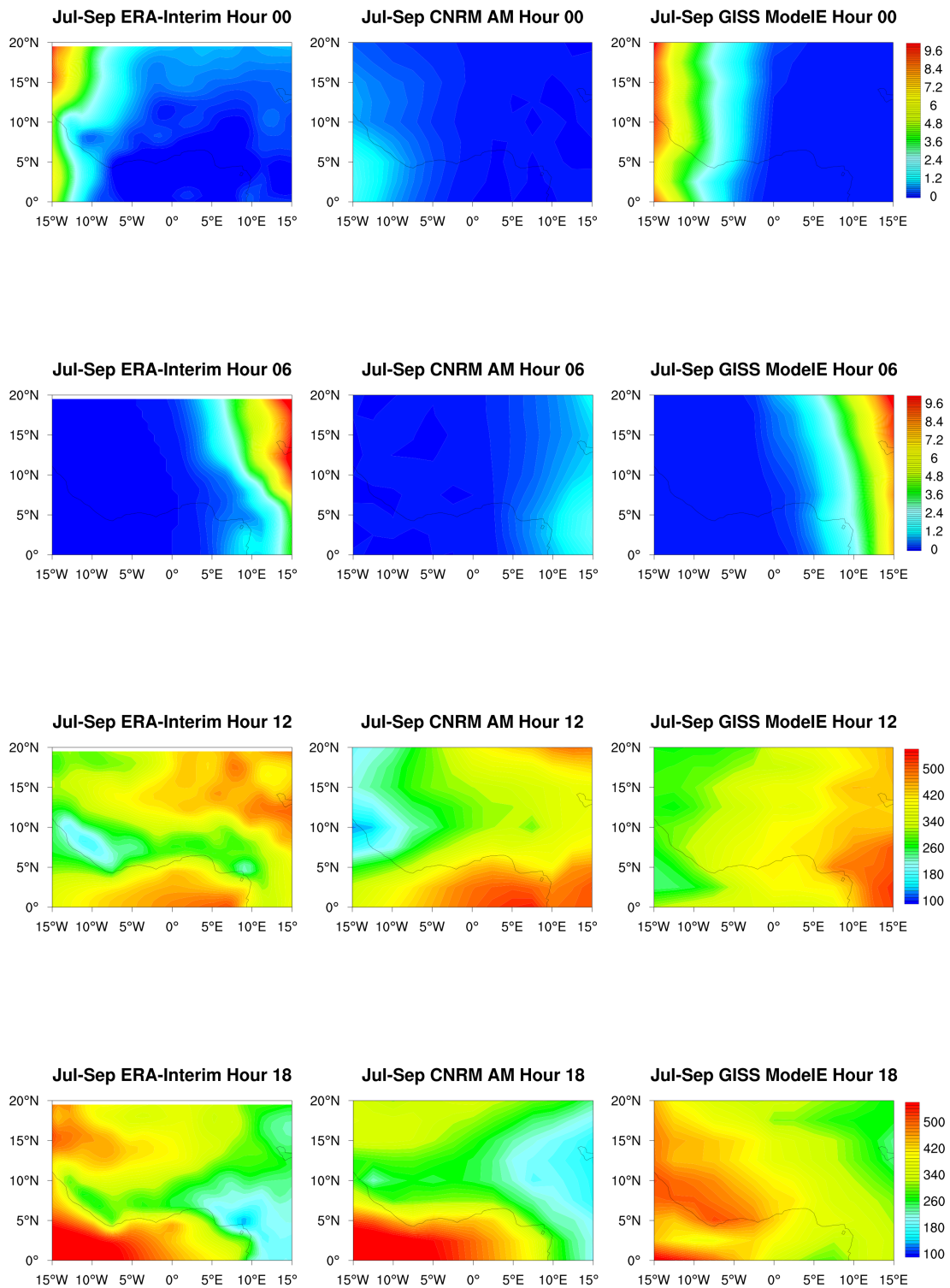


Figure 5.6: Diurnal cycle of surface net shortwave radiation in $\frac{W}{m^2}$ of ERA-Interim (first column), CNRM AM (second column), and GISS ModelE (third column) from 1991-2010; Note the different scales in the night/morning and the day/afternoon plots.

A horizontal view over the surface net shortwave radiation is represented in Figure 5.6. During the night and the early morning the values are around zero. At 00 UTC there are small values in the west because the values at 00 UTC are accumulated from 18 to 24 UTC, so this small values are the effect from the sunset in the evening. The same effect is visible during sunrise. During the day, the incoming solar radiation is high, only reduced by small albedo and clouds. For example in ERA-Interim the values are between $350\text{-}500 \frac{\text{W}}{\text{m}^2}$ along 15°N and around $250 \frac{\text{W}}{\text{m}^2}$ along the Guinea Coast in southern West Africa, so there must be clouds in this region. In the afternoon, the values over the Atlantic in the south are very high (more than $500 \frac{\text{W}}{\text{m}^2}$). Over land, especially in the north-east of Figure 5.6, the values are much smaller (around $150 \frac{\text{W}}{\text{m}^2}$), which can be explained by clouds in this region. During night and early morning, the effects of sunrise/sunset are smaller in CNRM AM compared to ERA-Interim. The surface solar radiation along the Guinea Coast is higher than in ERA-Interim with values up to $350 \frac{\text{W}}{\text{m}^2}$ and smaller in the western part of the Figure. In the vertical profile of the stratiform cloudiness in the southern part of West Africa, the model CNRM AM showed too few clouds (Figure 5.1). This can be the reason why the values in the surface solar radiation are higher in this region compared to ERA-Interim. Larger differences are observable between ERA-Interim and GISS ModelE. In ERA-Interim the values along the coast in southern West Africa are smaller than in the neighboring regions which is the effect of cloudiness in this part. In GISS ModelE the values are much higher along the Guinea Coast (around $350 \frac{\text{W}}{\text{m}^2}$), so there are missing clouds in this region which reduce the radiation. In the afternoon, the values over the Atlantic in the north-western part of the Figure are smaller than in ERA-Interim. So perhaps GISS ModelE simulates too many clouds in this region which are not found in ERA-Interim. The differences between the models and ERA-Interim are substantial (partly more than $100 \frac{\text{W}}{\text{m}^2}$). This effect of clouds illustrates how important a realistic representation of cloudiness is. The results of the surface solar radiation in the other models can be found in the appendix (Figure A.7 and A.8). The differences are large between the models. The model NAVGEM01 overestimates the surface solar radiation in the north compared to ERA-Interim and the model GEOS5 AGCM shows similar results as GISS ModelE.

The net surface solar radiation is influenced by all type of clouds, not only the low-level clouds. Hence the rank correlation between the surface solar radiation and the low-level cloudiness were calculated. For the calculation, the mean value of the surface solar radiation averaged over the horizontal box over southern West Africa (Figure 3.3) of each model at 12 UTC were used. The values were averaged over twenty years (1991-2010) in the months July to September. Then the rank numbers were correlated with the rank numbers of the maximal low-level cloudiness below 900 hPa. The low-level cloudiness were averaged over the same horizontal box in southern West Africa from 1991-2010. The result was $r = -0.38$, that means less low-level clouds are associated with higher surface solar radiation. But it is to note, that the value is insignificant to the level 0.9 (tested with the t-test, described in section 3.5).

In Knippertz et al. (2011), data from four ground stations were used from July-September in the years 1983-2007. Kumasi was one of the used ground station in this study and the mean value

was $147 \frac{\text{W}}{\text{m}^2}$. ERA-Interim analyzed from July-September in the years 1991-2010 values around $150 \frac{\text{W}}{\text{m}^2}$ (not shown), which is in the same range. The model CNRM AM simulates values around $180 \frac{\text{W}}{\text{m}^2}$ and the model GISS ModelE values around $200 \frac{\text{W}}{\text{m}^2}$ (not shown). The values of the models are larger than in the observations from the ground station in Kumasi, which can be explained by less cloudiness in the models compared to the observations.

The results of the other models can be found in the appendix (Figure A.7 and A.8). The model NAVGEM01 shows stronger net solar radiation along the Guinea Coast in southern West Africa compared to ERA-Interim. In contrast to this model, NCAR CAM5 has weaker net solar radiation than ERA-Interim, especially in the western part of the Figure. So probably NCAR CAM5 simulates more clouds than ERA-Interim.

5.6 Representation of the Tendency of Specific Humidity

An advantage over CMIP5 are the tendencies of moisture in GASS YoTC. In this section, case examples of models are chosen to take a closer look at the vertical profiles. These vertical profiles were averaged over the defined red box in southern West Africa (Figure 3.3) from 1991-2010.

For ERA-Interim only data from 2008 to 2009 are available, such that the results of ERA-Interim can not be compared to the different global climate models. During the night, there is a weak moistening near the ground due to turbulent diffusion in ERA-Interim (Figure A.9). Turbulent mixture is associated with moistening. The tendencies due to convection show a drying near the ground during the night, which intensify during the day. The ascending air caused by convection transports moisture from the ground to higher levels, such that the air near the ground gets drier.

In Figure 5.7, the diurnal cycles of CAM5ZMMicroCAPT, NAVGEM01, and GISS ModelE from July to September are represented. During the night in the model CAM5ZMMicroCAPT, the tendencies of moisture are weak. The tendency due to advection has a drying-out effect below 800 hPa and a moistening effect aloft, which is similar to the structure of the advection of moisture in section 5.4. This structure can be explained by the SMC. In 850 hPa there is a weak moistening due to boundary layer processes. This effect could be caused by mixing underneath the NLLJ. In the early morning, the tendency due to boundary layer processes is weaker, so there is less mixing caused by the NLLJ at this time. At 12 UTC the tendencies develop, especially the tendency of moisture due to boundary layer processes and the tendency due to convection. During the day, the turbulent boundary layer develops and leads to more turbulent mixing. This turbulent mixing causes a moistening, which is observable with a maximum at 900 hPa. At the same height, the tendency due to convection shows a minimum. Convection results in convergence at the ground and ascending above. This ascending air masses carry moisture away into higher levels, that is the reason why the tendency is negative below. There is also a moistening effect caused by evap-

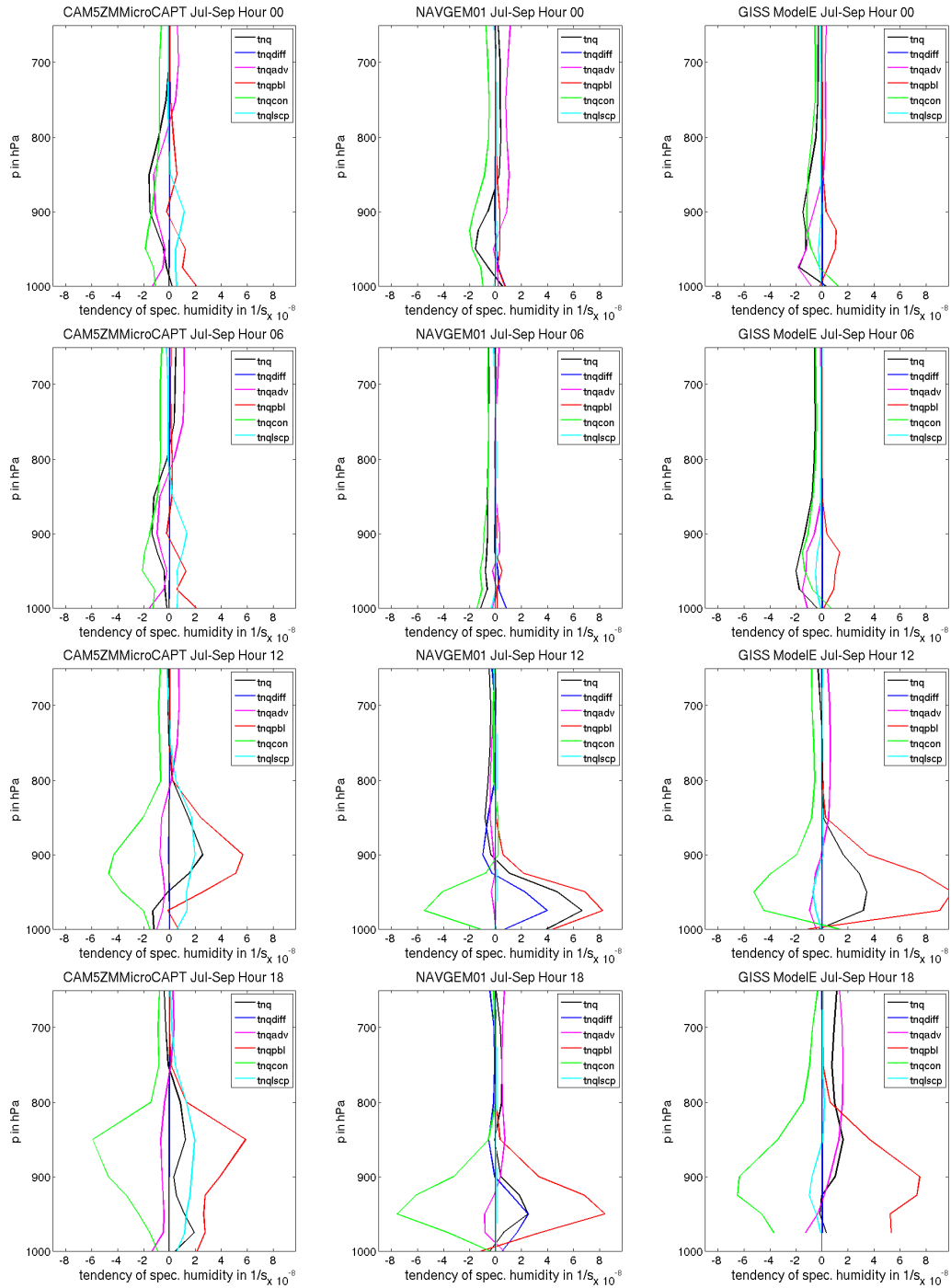


Figure 5.7: Diurnal cycle of tendencies of moisture averaged over defined red box at the Guinea Coast in southern West Africa (Figure 3.3) from 1991-2010 of the models CAM5ZMMicroCAPT (first column), NAVGEM01 (second column), and GISS ModelE (third column); black line: sum of all tendencies, blue line: tendency due to diffusion, pink line: tendency due to advection, red line: tendency due to boundary layer, green line: tendency due to convection and cyan line: tendency due to large scale cloud + precipitation.

oration of precipitation out of grid scale clouds. At 18 UTC, the position of the maximum in the tendency due to boundary layer processes and the minimum in the tendency due to convection raise to 850 – 900 hPa and intensify.

In the profiles of the model NAVGEM01, the diurnal cycle shows a clear development with weak tendencies at night and morning and larger tendencies from 12 UTC till the afternoon. At midday, the model simulates a great maximum in the tendency due to boundary layer processes at 975 hPa and a moistening in the same height in the tendency due to diffusion. The effect of diffusion is much greater than in the other models, so probably the definition of diffusion is different between the models. On the other hand, a drying effect is observable in the tendency due to convection. Compared to the model CAM5ZMMicroCAPT, the positions of the maxima and minima in the tendencies are at a lower height. The model NAVGEM01 simulates the low-level cloudiness at a comparable height as the cloudiness in ERA-Interim. CAM5ZMMicroCAPT simulates the low-level cloudiness too high. In the afternoon, the moistening due to turbulent mixing in the boundary layer and the drying-out due to convection intensify. The tendency due to advection shows a minimum below 900 hPa and a maximum aloft. The change of sign in the tendency due to advection is in a lower height than in the model CAM5ZMMicroCAPT (about 100 hPa lower).

As in the models described before, the model GISS ModelE shows weak tendencies during the night and early morning. The tendency due to boundary layer processes in the early morning shows a moistening at 950 hPa. This moistening could be caused by the mixing below the NLLJ. This moistening effect is larger than in the other models, so probably this model can simulate the NLLJ and the mixing of moisture better than the other models. At 12 UTC, the tendency due to processes in the boundary layer intensifies and the tendency due to convection shows a minimum at 950 hPa. The tendency due to grid scale clouds and precipitation shows a weak drying-out at 950 hPa, which is strange because it would be expected that there is a moistening due to evaporation of precipitation.

The results of the other global climate models can be found in the appendix (Figure A.10 and A.11). During the night, the tendencies are weak and intensify during the day. GEOS5 AGCM simulates the maximal tendencies during the day above 900 hPa. The model MRI AGCM shows a strange structure in the vertical profile of the tendency due to advection and due to boundary layer processes in the early morning and at midday. In the afternoon, the absolute values of the tendencies are much weaker than in the other models. Probably there is a six-hour shift in the data of MRI AGCM.

5.7 Representation of the Tendency of Temperature

The vertical profiles of the tendencies of temperature in the global climate models were averaged over the defined box in southern West Africa (Figure 3.3) from 1991-2010. As before in the tendencies of moisture, ERA-Interim has only data for 2008 and 2009. This is not enough for a

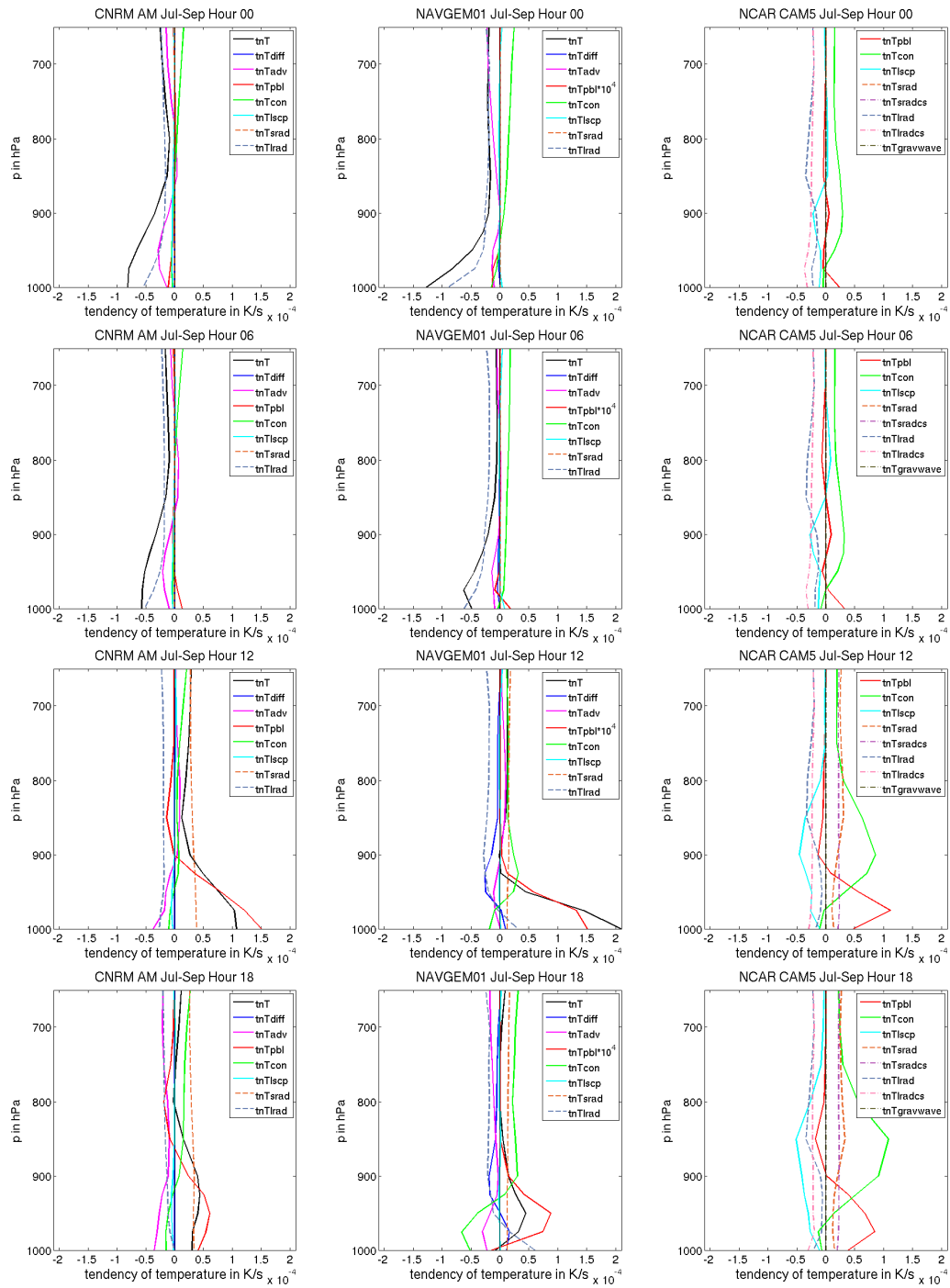


Figure 5.8: Diurnal cycle of tendencies of temperature averaged over defined red box at the Guinea Coast from 1991-2010 of the models CNRM AM (first column), NAVGEM01 (second column), and NCAR CAM5 (third column); black line: sum of all tendencies, blue line: due to diffusion, pink line: due to advection, red line: due to boundary layer processes, green line: due to convection, cyan line: due to large scale cloud + precipitation, green broken line: due to shortwave radiative heating, purple broken line: due to shortwave radiative heating clear sky, gray broken line: due to longwave radiative heating, rose broken line: due to shortwave radiative heating clear sky, khaki broken line: due to orog. gravity wave drag.

comparison with the different global climate models, which cover twenty years. The tendencies of temperature in ERA-Interim are weak during the night (Figure A.9, in the appendix). During the day, the convection is associated with heating at 900 hPa. At the same height there is a cooling from the cloud scheme of ERA-Interim. The energy for evaporation of precipitation out of the clouds is taken from the environment, such that the air cools down.

The vertical profiles of CNRM AM, NAVGEM01, and NCAR CAM5 are analyzed in Figure 5.8. During the night, the tendencies of temperature in the model CNRM AM are negative near the ground and around zero above. The absolute value of the tendency due to longwave radiative heating is greatest near the ground because of radiative cooling during night. This longwave cooling depends on clouds, so in case there are more clouds, the cooling effect would be weaker. The tendency due to advection shows a cooling at 950 hPa. Cold air advection at this height is represented in the results of section 5.4 as well. Cold air advection changes the stability in the low-levels and favors the development of turbulent eddies below the NLLJ. These turbulent eddies mix moisture from the ground to higher levels, which favors low-level cloud formation during the night. At 12 UTC, the sum of all tendencies is positive, mostly because of the tendency due to boundary layer processes. Turbulent mixing leads to heating. There is also a heating because of shortwave radiation and a slight cooling due to longwave radiation. Solar radiation heats up the ground, such that the tendency due to shortwave radiation shows the maximum at the ground. In the afternoon, the tendency due to boundary layer processes gets smaller but the values are still positive. The advection causes a cooling effect, as before at 12 UTC.

The model NAVGEM01 shows a similar behavior with negative values during the night and mostly positive values during the day. The tendency due to boundary layer processes is a factor of 10^4 too high compared to the other terms. Perhaps there is a wrong unit description because the sum of all tendencies (tnT) is not that high. The cooling effect due to longwave radiation during the night is greater than in CAM5ZMMicroCAPT. Perhaps the model NAVGEM01 simulates less clouds during the night than the model CAM5ZMMicroCAPT. During the day, there is a heating because of turbulent mixing in the boundary layer. Like before in the tendencies of moisture, the model NAVGEM01 shows greater values in the tendency due to diffusion compared to the other models, which can be explained by different definitions for this variable used in the models. At 18 UTC, the tendency due to boundary layer processes gets weaker and the effect of convection intensifies. Below 925 hPa the convection leads to cooling, aloft the convection is associated with heating. The convergence at the ground and the ascending above caused by convection transports warm air from the ground to higher levels. That is the reason for cooling near the ground and heating aloft.

During the night and early morning, the values of the tendencies are small in the model NCAR CAM5. The cooling of longwave radiation is weaker than in both models described before. Hence this model simulates more clouds than the others. During the day, the tendency due to convection shows a cooling effect near the ground and a heating effect at 900 hPa. In the same height (900 hPa), the tendency due to grid scale clouds and precipitation shows a slight cooling. Evap-

oration gets its energy from the environment, that is the reason why there is a cooling due to that process. The turbulent mixing in the boundary layer during the day leads to heating near the ground and to cooling at 900 hPa with slight negative values. In this model, the tendency due to convection is greater than in the models described before. Also the height of the maximal values in the different tendencies are higher than for example in the model NAVGEM01. So the height of the maximal values in the tendencies differs between the models and that fact can be important for the analysis of low-level cloud formation.

The results of the other global climate models can be found in the appendix (Figure A.12 and A.13). During the night, the absolute values of the tendencies are small but grow during the day. CAM5ZMMicroCAPT shows a cooling near the ground and a heating at 900 hPa during the day caused by convection. The effect of convection is greater in this model than in the other global climate models. At midday, the heating due to turbulent mixing in GEOS5 AGCM is stronger compared to the other models. GISS ModelE shows less variations during the day and the absolute values of the tendencies are weaker than in the other models.

5.8 Rank Correlation

Table 5.3: Rank correlation in July (top), August (second part) and September (bottom) of stratiform cloudiness (cls) with wind speed, advection of temperature (advT), and advection of moisture (advq); italics and bold value: value is significant to the level 0.95.

July Hour	cls/wind speed	cls/advT	cls/advq
00	<i>-0.62</i>	-0.36	-0.33
06	<i>-0.74</i>	-0.43	-0.45
12	-0.29	0.02	-0.14
18	-0.29	-0.07	-0.12
total	-0.48	-0.05	-0.29
August Hour	cls/wind speed	cls/advT	cls/advq
00	<i>-0.57</i>	0	-0.31
06	<i>-0.88</i>	-0.21	-0.43
12	-0.43	-0.05	-0.14
18	-0.33	0.12	-0.02
total	<i>-0.62</i>	0.24	-0.29
September Hour	cls/wind speed	cls/advT	cls/advq
00	-0.29	-0.07	-0.02
06	-0.45	0.12	0.07
12	-0.12	0.05	0.12
18	-0.21	-0.12	-0.12
total	-0.29	0	-0.02

With regard to statistical analysis, calculating rank correlations can be advantageous to find con-

nections between several variables. The approach for the calculation is similar to the one in section 4.3. The variables were formed in two vectors in which each value represents one model. The values were built out of the mean vertical profiles of each model which were averaged over 1991-2010 in the defined horizontal box near the Atlantic coast (Figure 3.3). The value of each model consists out of the maximal value below 900 hPa and each result was ordered in the vector with its rank position number. In this analysis eight models were used.

The diurnal cycles of the rank correlation between the stratiform cloudiness and the wind speed, the advection of temperature and moisture are represented in Table 5.3. Significant values to the level 0.9 are marked as italics and bold. The statistical significance is tested with the t-test. First the results of the rank correlation between the stratiform low-level cloudiness and the maximal wind speed below 900 hPa are described. The values are negative during the whole day. It can be assumed that a strong NLLJ drives turbulence which leads to mixing of moisture in higher levels where cloudiness develops. The turbulent eddies also mix down momentum from the jet to the ground which could cause the jet to slow down. So the more mixing, the more cloudiness can develop, but the jet weakens as well. So the rank correlation gets negative. The absolute values in July increase from the night to the morning when the coefficient is largest (-0.74) and decrease during the day (-0.29). In July and August the rank correlation is significant at night and in the morning. In August the rank correlation of all time-steps is significant as well (-0.62). In September the values are much smaller, so the statistical connection between these two variables is weaker. The rank correlation between the wind speed and the low-level cloudiness between the CMIP5 models shows positive values (section 4.3). These different results can be caused by the choice of different models which were used for the calculation. Looking at the rank correlation between the low-level stratiform cloudiness and the advection of temperature, it attracts attention that all values are insignificant. In July the values are negative at night and morning with values up to -0.43 and around zero during the day. From July to September the rank correlation coefficient gets smaller with values around zero. A negative correlation at night and morning in July means that cold advection is connected with more cloudiness, which is consistent with Schuster et al. (2013). Cold air advection connected with wind shear below the NLLJ leads to turbulent mixing of moisture. The cold air advection destabilizes the low-levels and turbulent eddies can develop. These turbulent eddies mix moisture to higher levels where clouds can form. So cold advection and the NLLJ are connected in the process of low-level cloud formation. Insignificant values are calculated for the rank correlation between the low-level stratiform cloudiness and the advection of moisture. The values are mostly negative or around zero. In July and August the rank correlation coefficients vary between negative values at night and morning and values near zero during the day. In September the rank correlation is small in all time-steps. Negative correlation means that dry advection is associated with more low-level cloudiness, which is surprisingly because it would be expected that dry air has a negative effect for cloud formation. The rank correlation was made with only eight models, so the found results in this table are hardly useful.

So far, the rank correlation was made out of the differences between the models. Figure 5.9

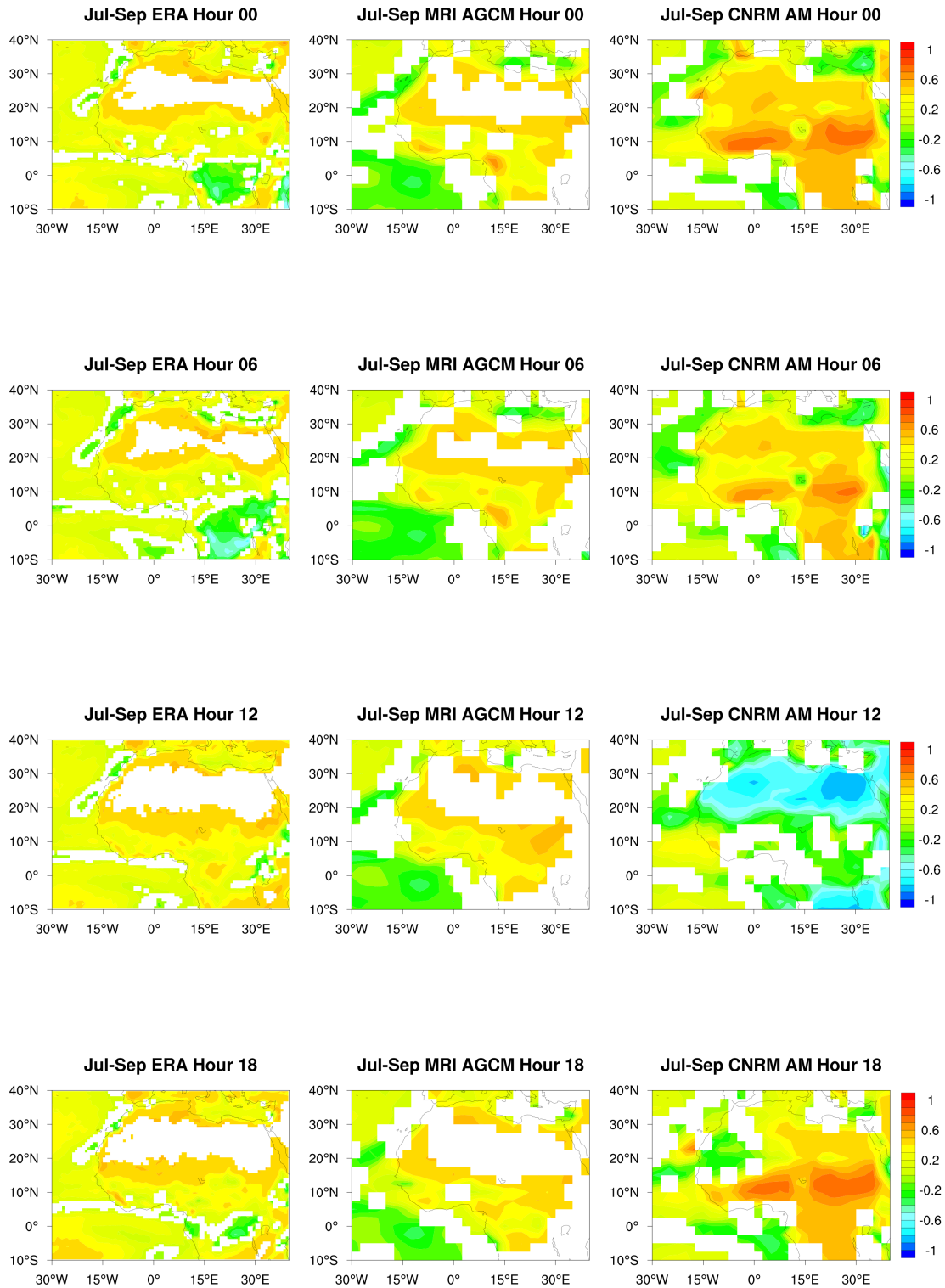


Figure 5.9: Rank correlation between the maximal value of stratiform cloud fraction and wind speed below 900 hPa at midnight (top row), at 06 UTC (second row), at midday (third row) and 18 UTC (bottom row) in the months July to September of ERA-Interim (first column), MRI AGCM (second column), and CNRM AM (third column); Significant values to the level 0.9 in contours.

shows the rank correlation between the low-level stratiform cloudiness and the maximal wind speed below 900 hPa for each model. The two vectors, which are important for the calculation, were formed out of the maximal values below 900 hPa at each lon x lat grid-point. These two vectors vary over twenty years with a temporal resolution of six hours, so the size is much greater than in the calculation used in the table before. To analyze the diurnal cycle in July to September, only data in the particular time was chosen. Now it is possible to see the rank correlations over whole West Africa for each model separately. The models MRI AGCM and CNRM AM are compared to ERA-Interim. White areas in the Figures represent insignificant values to the level 0.9.

First the results of ERA-Interim are discussed. Over most of the domain the correlation is positive, except of the coast in the north-west and in the region of Congo and Angola. At night and in the morning the negative correlation in Congo and Angola becomes more intensive and turns into a positive correlation during the day. Over the Sahara, the values are insignificant. The area in the southern part of West Africa is positive, but the variations during the day are weak. In the model MRI AGCM the domain over the Sahara is insignificant as well. It attracts attention that more areas show insignificant values than in ERA-Interim. Over land the correlation is positive, over the Atlantic the values are negative, except the region in the north-west. At night and in the morning, the rank correlation at the Guinea Coast in southern West Africa shows areas with higher values (Ivory Coast and Cameroon). During the day the correlation gets weaker. The model CNRM AM shows great differences to ERA-Interim. At night, a band of very high rank correlation coefficients at 10° N is observable which includes the area of the Guinea Coast in southern West Africa. Over the Sahara the values are positive and significant. In the early morning the values get a bit weaker, nevertheless the values are still highly positive at the band at 10° N. At midday, the rank correlation changes. Now the values are highly negative over the Sahara and slightly negative over the whole land masses. In the region at the coast in southern West Africa the values are insignificant. In the afternoon, the band with positive values at 10° N revives and the values over the land masses of West Africa are positive like before. In Table 5.3 the rank correlation between the stratiform low-level cloudiness and the maximal wind speed below 900 hPa is negative. In contrast to this result, the rank correlation is positive in the same area at the Guinea Coast in southern West Africa in the horizontal view for each model (Figure 5.9). So looking at each model separately the connection between cloudiness and wind speed changes. A stronger wind is associated with more cloudiness. This result is similar to the results of the models in the CMIP5 data set (section 4.3). The higher wind speed in the NLLJ produces more turbulent eddies which mix up moisture in higher levels where clouds can form. So the mixing down of momentum from the jet to the ground is not that strong. This result can be found in the other global climate models as well (Figure A.14 to A.15).

More calculated rank correlations were made for the low-level stratiform cloudiness and the tendencies of moisture (Table 5.4). The approach to calculate these rank correlations is consistent with the one for Table 5.3. Here the focus is on the differences between the models, so

Table 5.4: Rank correlation in July (top), August (second part) and September (bottom) of stratiform cloudiness (cls) with tendency of specific humidity total (tnq), due to advection (tnqadv), due to convection (tnqcon), due to boundary layer processes (tnqpbl) due to large scale clouds and precipitation (tnqlscp), and due to diffusion (tnqdiff); italics and bold value: value is significant to the level 0.9.

Jul Hour	cls/tnq	cls/tnqadv	cls/tnqcon	cls/tnqpbl	cls/tnqlscp	cls/tnqdiff
00	-0.39	-0.26	0.1	-0.12	0.45	0.52
06	0.04	0.26	0.1	0.33	0.4	0.52
12	<i>-0.61</i>	-0.03	-0.26	-0.33	<i>0.71</i>	0.31
18	0.21	-0.49	0.05	-0.29	<i>0.62</i>	-0.29
Aug Hour	cls/tnq	cls/tnqadv	cls/tnqcon	cls/tnqpbl	cls/tnqlscp	cls/tnqdiff
00	-0.32	-0.43	0.1	-0.45	0.4	0.52
06	0.21	0	0.31	0.24	0.43	<i>0.62</i>
12	-0.43	-0.07	-0.24	-0.48	<i>0.64</i>	<i>0.62</i>
18	<i>0.54</i>	-0.43	0.12	-0.24	0.48	-0.29
Sep Hour	cls/tnq	cls/tnqadv	cls/tnqcon	cls/tnqpbl	cls/tnqlscp	cls/tnqdiff
00	-0.43	-0.03	0.1	-0.12	<i>0.53</i>	0.52
06	-0.11	-0.21	-0.1	0.4	0.07	<i>0.62</i>
12	-0.07	-0.07	-0.29	-0.24	<i>0.62</i>	0.31
18	0.43	<i>-0.54</i>	0.1	-0.26	<i>0.69</i>	-0.29

whether a model with more low-level cloudiness has automatically higher values in the variable tendency of moisture compared to the other models. The time description in the models CAM5ZMMicroCAPT, GEOS5 AGCM, and GISS ModelE are different to the other models. So like in the variable surface solar radiation, the described time in the models were rearranged as documented in Table 5.2. The model GEOS5 AGCM has no data for the years 1995 and 1996, so these years are missing in the results of the tendencies in this model.

At night in July (Table 5.4) the value of the total tendency of moisture is negative, just as the tendency of moisture due to advection. Positive values show the correlations between the stratiform cloudiness and the tendency of moisture due to large scale clouds and precipitation with 0.45 and the correlation with the tendency due to diffusion (0.52). In the early morning, the correlation coefficients stay small which changes at midday. At 12 UTC, the correlation with the tendency due to large scale clouds and precipitation is positive (0.71) but the correlation with the total tendency of moisture shows a minimal value (-0.61), like the tendency due to convection and due to boundary layer processes. So during the day, convection starts by less stable conditions in the boundary layer and transports moisture from the ground to higher levels where clouds can form. A source of moisture is evaporation of precipitation that is the reason why the correlation with the tendency due to large scale clouds and precipitation is highly positive at midday. In the afternoon, this correlation stays positive but the tendencies due to advection, boundary layer processes, and diffusion show negative values at this time. The advection transports moisture away, so that the

Table 5.5: Rank correlation in July (top), August (second part) and September (bottom) of stratiform cloudiness (cls) with tendency of temperature total (tnT), due to advection (tnTadv), due to convection (tnTcon), due to boundary layer processes (tnTpbl) due to large scale clouds and precipitation (tnTlscp), and due to diffusion (tnTdiff); italics and bold value: value is significant to the level 0.9.

Jul Hour	cls/tnT	cls/tnTadv	cls/tnTcon	cls/tnTpbl	cls/tnTlscp	cls/tnTdiff
00	0.43	0.14	0.71	0.62	-0.12	0.43
06	0.29	-0.21	0.69	0.79	-0.45	0.21
12	-0.36	-0.71	0.48	0.19	-0.57	0.68
18	-0.79	-0.46	0.57	0.19	-0.62	0.39
Aug Hour	cls/tnT	cls/tnTadv	cls/tnTcon	cls/tnTpbl	cls/tnTlscp	cls/tnTdiff
00	0.29	-0.18	0.52	0.76	0.1	0.32
06	0.21	-0.46	0.55	0.79	-0.26	0.43
12	-0.39	-0.57	0.62	0.19	-0.55	0.61
18	-0.75	-0.43	0.48	0.45	-0.36	0.43
Sep Hour	cls/tnT	cls/tnTadv	cls/tnTcon	cls/tnTpbl	cls/tnTlscp	cls/tnTdiff
00	0.64	-0.32	0.62	0.6	-0.1	0.39
06	0.57	-0.46	0.64	0.62	-0.24	0.61
12	0.11	-0.25	0.5	0.24	-0.45	0.79
18	-0.75	-0.46	0.57	0.33	-0.69	0.54

specific humidity decreases and this moisture is missing for the formation of clouds. The behavior of the diurnal cycles of the rank correlation coefficients in August and September are mostly the same as in July. There are little changes in the magnitude but the development stays similar.

The diurnal cycle of the tendencies of temperature are documented in the Tables 5.5 and 5.6. In the data of the model FGOALSs, the year 1991 is missing in the variable tnTpbl, like in the variable tnTlrad the year 2001 and there is no data for the variable tnTsradi in 1999. Like in the data of tendencies of moisture, the years 1995 and 1996 are missing in the model GEOS5 AGCM and the time descriptions in the models CAM5ZMMicroCAPT, GEOS5 AGCM, and GISS ModelE are rearranged as described before. In July the correlation between the maximal stratiform cloudiness below 900 hPa and the tendency of temperature (total) is positive at night (Table 5.5). Higher values are calculated for the correlations with the tendency due to convection (0.71) and due to boundary layer processes (0.62). At 06 UTC, the correlation with the total tendency of temperature is still positive but weaker. The correlation with the tendency due to advection is negative, so the low-level cloudiness increases with cold advection. Also the correlation with the tendency due to large scale clouds and precipitation is negative. Contrary to these results, the correlations with the tendency due to convection and due to processes in the boundary layer are highly positive as before at night (up to 0.79). So these tendencies can play an important role for the low-level cloud formation during the night. At 12 UTC, the correlation with the total tendency of temperature turns to a negative value, like the tendencies due to advection with -0.71 and due

Table 5.6: Rank correlation in July (top), August (second part) and September (bottom) of stratiform cloudiness (cls) with tendency of temperature due to shortwave radiative heating (tnTsrاد) and due to advection (tnTadv), due to shortwave radiative heating (tnTlrاد); italics and bold value: value is significant to the level 0.9.

Jul Hour	cls/tnTlrاد	cls/tnTsrاد
00	<i>0.6</i>	
06	<i>0.74</i>	
12	<i>0.52</i>	-0.07
18	-0.26	-0.33
Aug Hour	cls/tnTlrاد	cls/tnTsrاد
00	<i>0.74</i>	
06	<i>0.79</i>	
12	<i>0.55</i>	-0.19
18	0.14	-0.33
Sep Hour	cls/tnTlrاد	cls/tnTsrاد
00	<i>0.81</i>	
06	<i>0.64</i>	
12	<i>0.55</i>	-0.1
18	0	-0.24

to large scale clouds and precipitation with -0.57 . Evaporation of rain leads to cooling because the energy for this process is taken from the environment. At the afternoon these correlations are still negative. Like in the tendencies of moisture, the behavior of the diurnal cycles in the rank correlation coefficients in August and September are similar to the one in July.

The correlations with the tendencies of temperature due to radiative heating are documented in Table 5.6. The correlation with the tendency due to longwave radiation are highly positive from midnight to 12 UTC and the values are small in the afternoon. A contrary behavior shows the correlation with the tendency due to shortwave radiative heating. Here the values are weakly negative during the day. During the night, there is no solar radiation. That is the reason why the correlation with this values during the night are missing in this table. So longwave heating at night leads to more low-level clouds.

5.9 Summary of the Processes in the Models

The simulation of cloud formation is a complicated procedure and little biases show large effects (Schuster et al., 2013). In Figures 5.10 to 5.12 the different variables are summarized for each model. Each vertical line represents the p-coordinate at midnight (first vertical line), 06 UTC (second vertical line), midday (third vertical line), and 18 UTC (fourth vertical line). The numerals underneath the time descriptions are the differences compared to ERA-Interim of the maximal values of cloudiness below 800 hPa (blue) and the differences to the maximal wind speed below

800 hPa (purple). The circles show the position and magnitude of the maximal cloud fraction in the model and the triangles the maximal wind speed. The tendencies of moisture and temperature are represented as arrows, the length shows the magnitude and the position at the vertical line the height of the maximal values. The maximal tendencies of temperature due to longwave and shortwave radiation are below the abscissa. The numbers are given in $\frac{\text{K}}{\text{day}}$. In the models MRI AGCM and NAVGEM01 the variable tendency of temperature due to processes in the boundary layer is a factor of 10^4 too high compared to the other terms. For a better representation, this variable is divided by this factor.

In the vertical profiles of the variable stratiform cloud fraction in the area at the Guinea Coast in southern West Africa (Figure 5.1), the models CAM5ZMMicroCAPT, NCAR CAM5, and CNRM AM show no or weak variations during the day. These models are summarized in Figure 5.10. The jet (maximal wind speed represented as triangles) is located below the maximal cloud fraction in all of these models. So the jet can influence the cloud formation only weakly. Also remarkable is that the jet is simulated too strong in CAM5ZMMicroCAPT and CNRM AM compared to ERA-Interim. The most important tendencies of moisture and temperature are the tendencies due to convection and due to boundary layer processes. At night and early morning, the absolute values of the tendencies are small in CAM5ZMMicroCAPT. Near the ground, the boundary layer processes are associated with weak heating and moistening. At the jet level there is a cooling due to advection. Cold advection destabilizes the low-levels, so that turbulent eddies below the jet level can develop easier. During the day, the tendencies intensify and raise to higher levels whereas the maximal cloud fraction gets smaller and the jet level sinks. The drying-out and heating effect due to convection is maximal during the day between 925 and 850 hPa. Convection is associated with ascending, which carries warm air from the ground to higher levels, such that the ground gets cooler and the levels aloft warmer. In CAM5ZMMicroCAPT the heating effect due to convection is stronger at higher levels than the cooling effect near the ground. The heating due to boundary layer processes is maximal at midday near the ground at 950 hPa. Turbulent mixing in the boundary layer during the day leads to heating. In NCAR CAM5, the tendencies are weak at night and morning at lower levels and grow during the day at higher levels. The maximal heating due to turbulent mixing in the boundary layer is during the day at 950 hPa. At 850 hPa, there is a heating due to convection, where the maximal cloud fraction can be found. So the heating in higher levels is stronger than the cooling in low-levels caused by convection. The model CNRM AM simulates too few clouds compared to ERA-Interim and too high. During the night, the tendencies are weak but intensify during the day. At midday, the heating due to turbulent mixing in the boundary layer is maximal near the ground at 975 hPa. The turbulent mixing in the boundary layer during the day is also associated with moistening, which is maximal between 925 and 850 hPa. The effect of convection is weaker than in the described models before, in which the heating is maximal during the day at around 850 hPa.

The models MRI AGCM, NAVGEM01, and GISS ModelE are summarized in Figure 5.11. These models have shown a similar behavior in the vertical structure of the stratiform cloud fraction as

ERA-Interim, but the values are too small (NAVGEM01 and GISS ModelE) or the height of the maximal cloud fraction is too high (MRI AGCM). All three models underestimate the magnitude of the jet and the size of the low-level cloudiness compared to ERA-Interim. MRI AGCM simulates the jet underneath the maximal cloudiness, like the three models presented before and the magnitude of the jet is too weak compared to ERA-Interim (up to $-2 \frac{m}{s}$). The location of the jet level (1000 hPa) seems to be an error with the inter- and extrapolation of model layers to pressure levels. Normally the wind speed lessens with lower height. At 06 UTC, the tendency of moisture due to advection is weakly positive underneath the maximal cloudiness and there is a weak drying due to convection at the height of the maximal cloudiness. The convection has not jet developed, such that the negative tendency of moisture due to convection is small in the morning. At midday, the absolute values in the tendencies of moisture due to advection and convection increase, the cloudiness raises to 850 hPa where moistening due to boundary layer processes and heating due to convection are simulated. During the day, the convection develops in a less stable boundary layer, which leads to heating and moistening. At night and in the afternoon, the tendencies get weaker than during the day. This behavior is different from the three models described before. Probably there is a six-hour shift in the data of the different tendencies in MRI AGCM. The tendency of moisture due to boundary layer processes is weaker than in the other described models but the advection plays a more important role. In the models MRI AGCM and NAVGEM01 the tendency of temperature due to boundary layer processes is much greater than the other tendencies. This can be a unit problem. At night and the early morning, the jet level is in the same height as the maximal cloud fraction in the model NAVGEM01, but the magnitude is weaker compared to ERA-Interim. As described in Schuster et al. (2013), the jet influences the low-level cloud formation. The wind shear underneath the NLLJ produces turbulent eddies which mix moisture from the ground to higher levels. For the formation of these turbulent eddies, the nocturnal boundary layer has to be less stable, that is the reason why cold air advection has a positive effect for the formation of turbulence during the night. With the mixing of moisture, low-level clouds can form during the night. The tendencies are small during night and increase during the day but stay in lower levels. In the other models described before, the maximal values in the different tendencies are at a higher level (up to 800 hPa). This phenomenon is also observable in the model GISS ModelE. Here the maximal values in the different tendencies are below 900 hPa. This model simulates two local maxima in the cloudiness below 800 hPa at night. The lower maximum is located in nearly the same height as the jet at 975 hPa. In the morning, the cloudiness increases and the level of maximal cloud fraction raises to 950 hPa where the maximal tendencies of moisture are located. So the jet seems to have a positive effect for clouds in the low-levels (below 900 hPa). At 12 UTC, the tendencies are greatest and the cloudiness raises to 800 hPa with smaller values. The turbulent mixing in the boundary layer is associated with heating and moistening. In NAVGEM01 and GISS ModelE, the cooling effect of convection near the ground is greater than the heating aloft during the day. That fact is different to the models in Figure 5.10, which show a stronger heating in higher levels caused by convection. In the afternoon, the tendencies in GISS ModelE decrease a bit and get weakest at night.

The last two models summarized in Figure 5.12 can not be related to the two groups. GEOS5 AGCM shows a different diurnal cycle than ERA-Interim. At night, there are too few clouds and they are located too high at 850 hPa. The strength of the jet is simulated well at a height of 950 hPa. In the morning, the cloudiness drops to 925 hPa but stays small, whereas the jet strengthens. During the day, the jet slows and the cloudiness raises and increases. So the behavior of the jet development is simulated well but the model shows problems with the simulation of low-level clouds. At night, the tendency of moisture due to boundary layer processes is located near the ground but raises during the course of the day with maximal values at 12 UTC in 850 hPa. The tendency of moisture due to convection shows negative values above 850 hPa during the whole day. The model FGOALSs simulates no stratiform cloudiness below 700 hPa, so in this model the formation of low-level clouds cannot be analyzed.

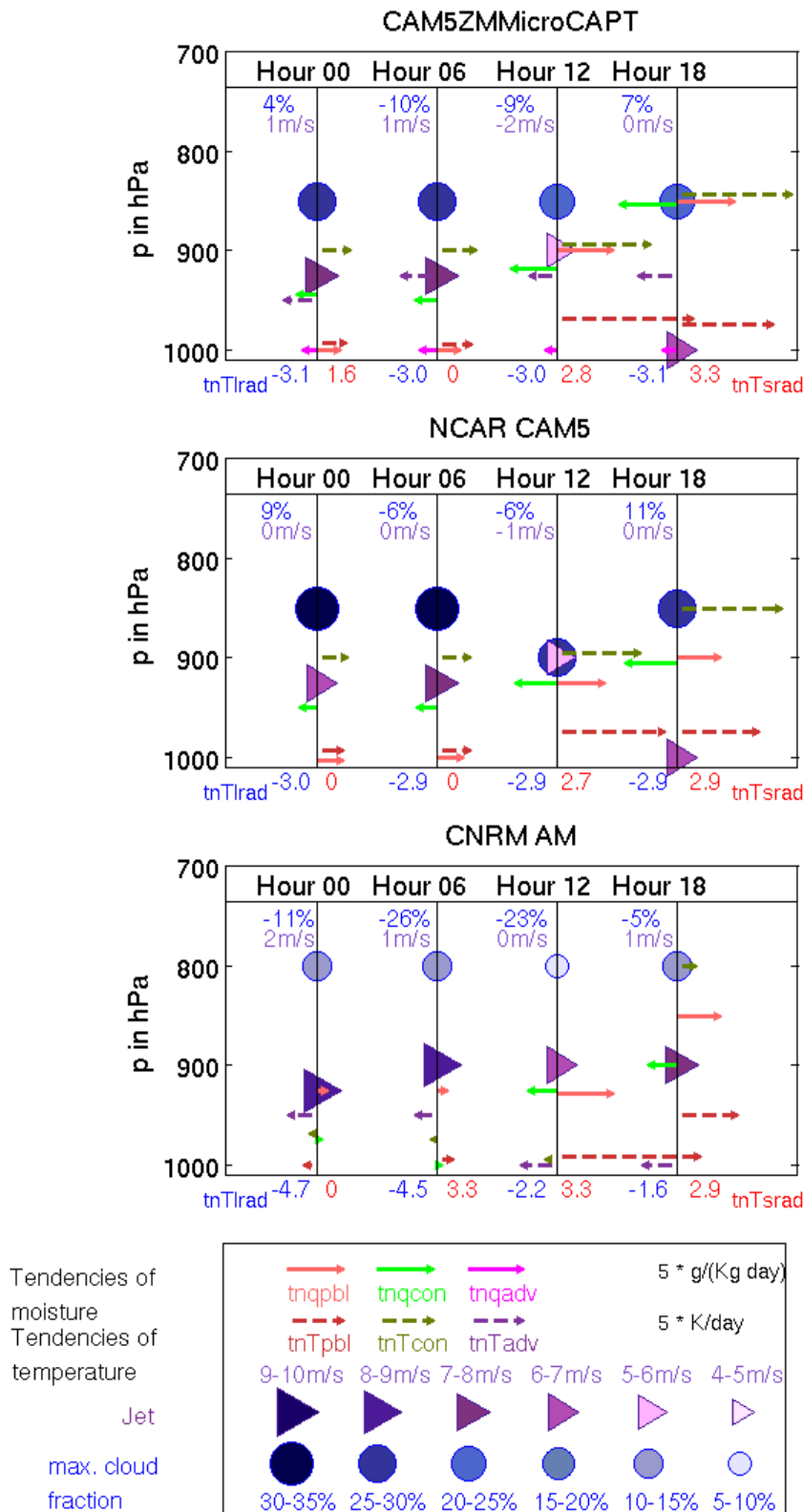


Figure 5.10: Summary of the diurnal cycle of the variables max. low-level cloudiness (blue circle) and NLLJ (purple triangle) in symbols and the max. tendencies marked with arrows; differences to low-level maximal cloudiness of ERA-Interim is shown in blue numerals below time description in % and differences to maximal wind speed below 900 hPa of ERA-Interim is shown in purple underneath; max. tendency due to longwave radiation is shown in blue numerals below the abscissa, aside the max. tendency due to shortwave radiation in red numerals.

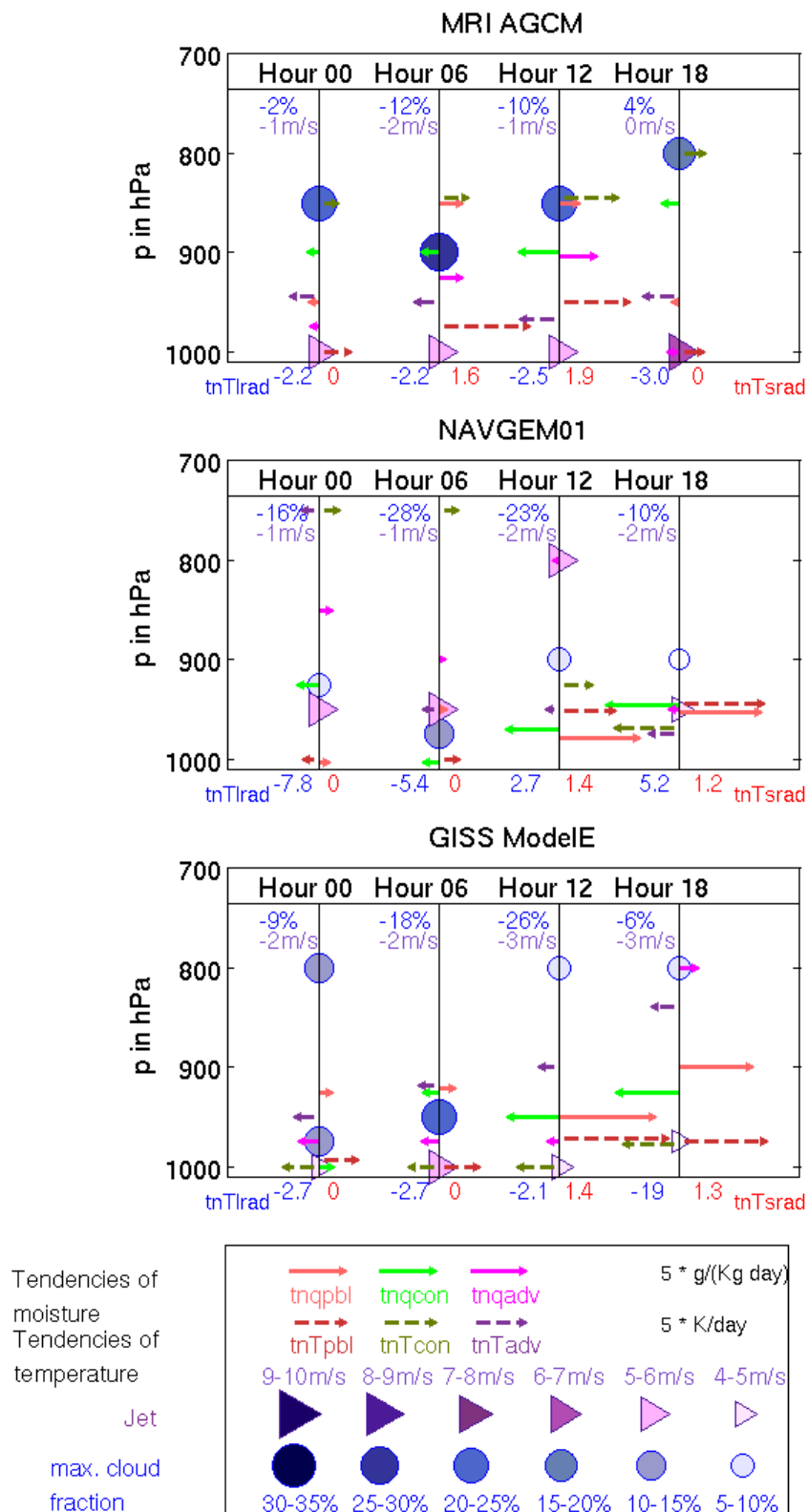


Figure 5.11: Summary of the diurnal cycle of the variables max. low-level cloudiness (blue circle) and NLLJ (purple triangle) in symbols and the max. tendencies marked with arrows; differences to low-level maximal cloudiness of ERA-Interim is shown in blue numerals below time description in % and differences to maximal wind speed below 900 hPa of ERA-Interim is shown in purple underneath; max. tendency due to longwave radiation is shown in blue numerals below the abscissa, aside the max. tendency due to shortwave radiation in red numerals.

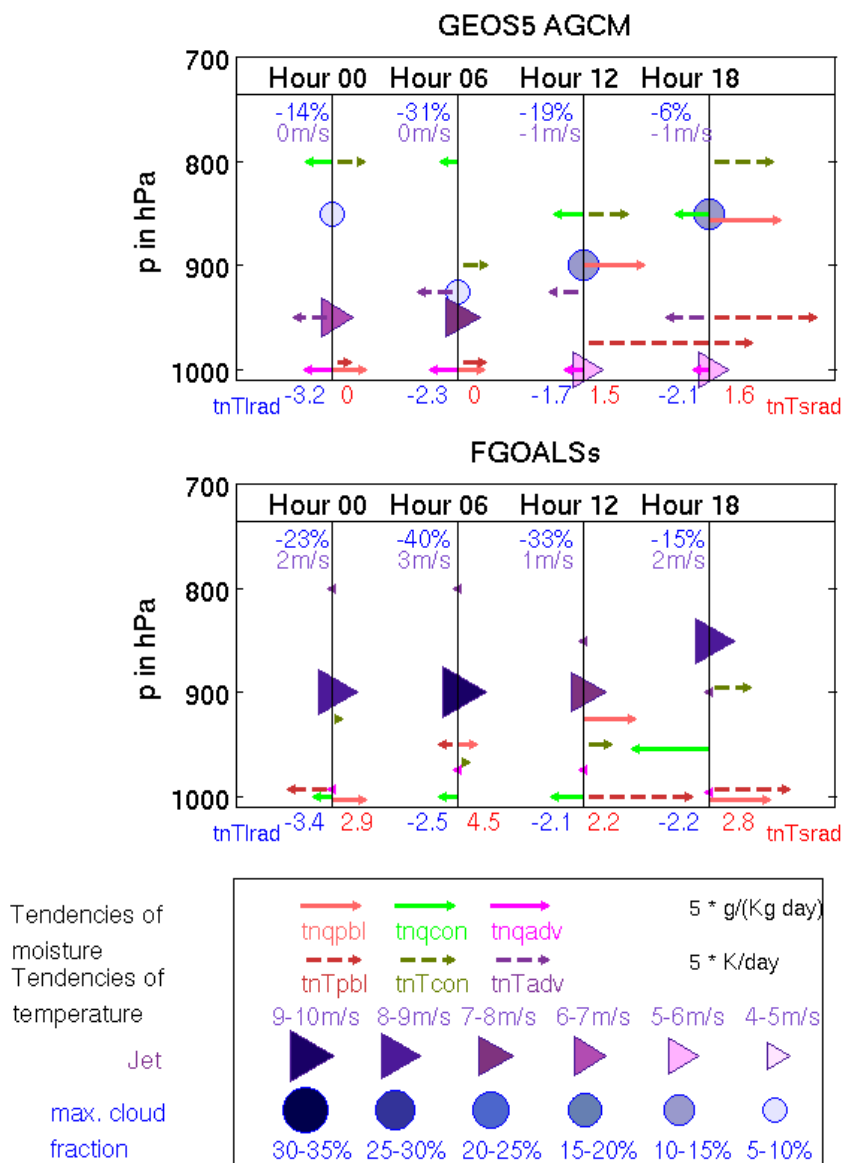


Figure 5.12: Summary of the diurnal cycle of the variables max. low-level cloudiness (blue circle) and NLLJ (purple triangle) in symbols and the max. tendencies marked with arrows; differences to low-level maximal cloudiness of ERA-Interim is shown in blue numerals below time description in % and differences to maximal wind speed below 900 hPa of ERA-Interim is shown in purple underneath; max. tendency due to longwave radiation is shown in blue numerals below the abscissa, aside the max. tendency due to shortwave radiation in red numerals.

6. Discussion, Summary and Outlook

The overarching aim of this work is to improve global climate models and the weather forecast over West Africa with regard to the representation of low-level cloud formation. At the Guinea Coast during the summer monsoon, low-level cloudiness is observable at night and early morning and vanishes during the day. This behavior is explained in the studies of Schuster et al. (2013) and Gounou et al. (2012). During the night, a NLLJ forms because of a large surface pressure gradient from the heat-low over the Sahara to the Atlantic. The wind shear underneath the jet induces turbulent eddies which mix up moisture from the ground to higher levels and favor cloud formation. Connected with cold advection, which destabilizes the low-levels, turbulent eddies can develop easier. During the day, the NLLJ slows because of the turbulence, which grows during the day due to solar radiation. To answer the question, how climate global models represent this low-level cloudiness during the phase of the wet monsoon, two different data sets were used. At first the results of the different models of CMIP5, in which the variables were averaged over 1979-2008, are described:

- In ERA-Interim the cloudiness below 800 hPa is split in two maxima: at 850 hPa, the low-level clouds, and at 950 hPa, the ultra-low clouds. This structure is not simulated in most of the examined climate models.
- Further differences from ERA-Interim to the global climate models are the height and the extension of the clouds. Some models simulate the clouds too high, others overestimate the cloud cover or simulate no low-level clouds at all.
- Like in the variable cloudiness, there is a large spread between the models looking at the vertical structure of the wind speed. Most models overestimate the strength of the jet.
- The cold advection is also overestimated in the global climate models and the SMC is located on different levels compared to the results of ERA-Interim. The monsoonal SMC described by Zhang et al. (2008) is characterized by a low-level flow from the ocean toward the heat-low over the Sahara and a shallow return flow, which interfuses the heavy rainbands of the monsoon and leads to moist advection at this height. Over the ocean the air descend, meanwhile dryer air from above can mix into the descending air masses, which leads to dry advection near the ground. The global climate models simulate the height of the shallow return flow too high and the moist advection is too weak compared to ERA-Interim.

- The rank correlation between the maximal wind speed below 900 hPa and the low-level cloudiness shows a positive connection. That means that a strong jet induces wind shear and turbulent eddies which mix up moisture into higher levels and favor cloud formation.
- The rank correlation between the low-level cloudiness and the advection of temperature is small, so there is no significant statistical connection between these two variables. The same result is calculated for the rank correlation with the advection of moisture. The values are slightly negative but insignificant to the level 0.95.

What are the reasons for the differences in the formation of low-level clouds in the different models? All in all, the global climate models in CMIP5 show large differences in the simulation of low-level clouds compared to ERA-Interim which can be caused by a different simulated NLLJ or too strong cold advection. But the statistical connection between the low-level cloudiness and the advection is small, so perhaps the advection plays a smaller role in the formation of low-level clouds than described in Schuster et al. (2013) or the models are inconsistent. The rank correlation of one variable can not resolve whole processes, such that the advection can be important in collaboration with other variables even though the correlation is small. Problematic is the temporal resolution in the models of CMIP5 with mostly daily or even monthly mean data. This is not enough to analyze the diurnal cycle of the formation of low-level clouds at the Guinea Coast. An other disadvantage is that there are no diabatic terms in the data set of CMIP5.

The second data set of GASS YoTC has a temporal resolution of six hours, so here is the chance for an analysis of the diurnal variations. In the vertical structure of ERA-Interim the clouds develop during night and reach the maximum in the early morning at a height of 950 hPa. Afterward the clouds raise during the day and decrease in the afternoon. This is very typical for this region during the wet monsoon and described in Schuster et al. (2013) and Gounou et al. (2012). The global climate models differ from ERA-Interim in the following points:

- Some models show no or less diurnal variations in the cloudiness, others represent the diurnal cycle of the low-level clouds well but the values are too small. One model simulates the behavior of the diurnal variations well but the height of the clouds is too high.
- In the variable wind speed, most models overestimate the magnitude. In some models the jet level is too low, so that the jet is uncoupled from the cloud formation. Two models simulate the jet level above the low-level cloudiness during the night and early morning, which is consistent with the theory discussed in Schuster et al. (2013) and Gounou et al. (2012).
- Less diurnal variations are observed in the vertical structure of the cold advection in ERA-Interim. The different models show stronger variations during the day and mostly overestimate the cold advection.
- The vertical structure of the advection of moisture shows a drying underneath 850 hPa and a moistening above in the data of ERA-Interim. This vertical structure can be explained with

the monsoonal SMC. The global climate models have problems to simulate the shallow return flow, being too dry at this height. Also near the ground, the global climate models show mostly a drier advection compared to ERA-Interim.

- The calculated rank correlation between the low-level cloudiness and wind speed shows negative values by comparing the models to each other and positive values for the calculation which were made for each model separately. The wind shear underneath the jet produces turbulent eddies which mix moisture from the ground to higher levels. These turbulent eddies also mix down momentum from the jet to the ground which weakens the jet and the rank correlation becomes negative. So comparing the models to each other the process of mixing down of momentum dominates. Calculating the rank correlation for each model separately, the correlation gets positive, such that the mixing of moisture underneath the jet has a positive effect for low-level cloud formation.
- The rank correlation between the low-level cloudiness and the advection of temperature and moisture is small. This results is in common with the results calculated with the CMIP5 models.
- Models with a weak diurnal cycle in the cloudiness simulate the cloudiness too high. Models which underestimate the extension of the low-level clouds have a weaker jet than ERA-Interim.
- The two models with a well simulated diurnal cycle of cloudiness show strong tendencies due to boundary layer processes (positive values) and due to convection (negative values, but smaller than due to boundary layer processes) during midday and the afternoon below 900 hPa. Models which simulate the cloudiness too high simulate these two tendencies at higher levels (above 900 hPa).

The data set of GASS YoTC opens more options than the one of CMIP5. The temporal resolution and the tendencies of specific humidity and temperature give the chance to gain more insight into cloud formation in global climate models. The analyzed global climate models have problems to simulate the cold and dry advection, the strength and vertical position of the NLLJ and the extension and diurnal variations of the low-level stratiform cloudiness. So as described before, models which simulate the low-level cloudiness at the right height show the maximal values in the tendencies below 900 hPa, so perhaps the height of these maximal values in the tendencies is important for the simulation of the right height of cloudiness. Models which simulate too few low-level clouds show a weaker NLLJ than ERA-Interim, so the wind speed seems to be important as well. As in Schuster et al. (2013), the turbulence caused by the wind shear underneath the NLLJ is one main part of low-level cloud formation which is underlined by the results of this work.

Outlook

There are still open questions left. The problems in climate models by simulating the low-level cloud formation are not completely understood yet, but this study shows in which variables differences can be found between the models and which ones are connected to low-level clouds. Like in the study of Schuster et al. (2013), the NLLJ might play an important role, as the tendencies of temperature and moisture. For an even better understanding of the simulation of cloud formation in the different global climate models, more open questions have to be answered such as the analysis of the different parametrization which are used in the models or a detailed analysis of the stability. The available data of ERA-Interim for the tendencies of moisture and temperature (2008-2009) were not enough for a comparison with the different global climate models of YoTC, in which data from 1991-2010 were used. To compare the models to ERA-Interim, the models can be analyzed for the years 2008-2009. If the results of these two years are similar to the climatological result in the models, it can be assumed that the results of ERA-Interim in these two years are representative for 1991-2010 as well. Then the data of ERA-Interim for the tendencies of moisture and temperature can be compared to the results of the different models. Furthermore more models can be included to the analysis like coupled atmosphere-ocean models. As a future work, modeling with ICON (ICOsahedral Nonhydrostatic), the new climate model of the Deutscher Wetterdienst (DWD) and the Max Planck Institute, can be useful because this new climate model gives the chance to change the horizontal resolution over a special region for example West Africa, so that more processes can be directly simulated instead of parameterized. In the project DACCIWA, the understanding of low-level cloud formation and the physical processes behind it can be analyzed better with new measurements in the region of southern West Africa. Also more modeling with different climate models, which is also included in DACCIWA, is useful to find model errors and to improve the representation of low-level clouds in climate models.

A. Appendix

Rank Correlation CMIP5

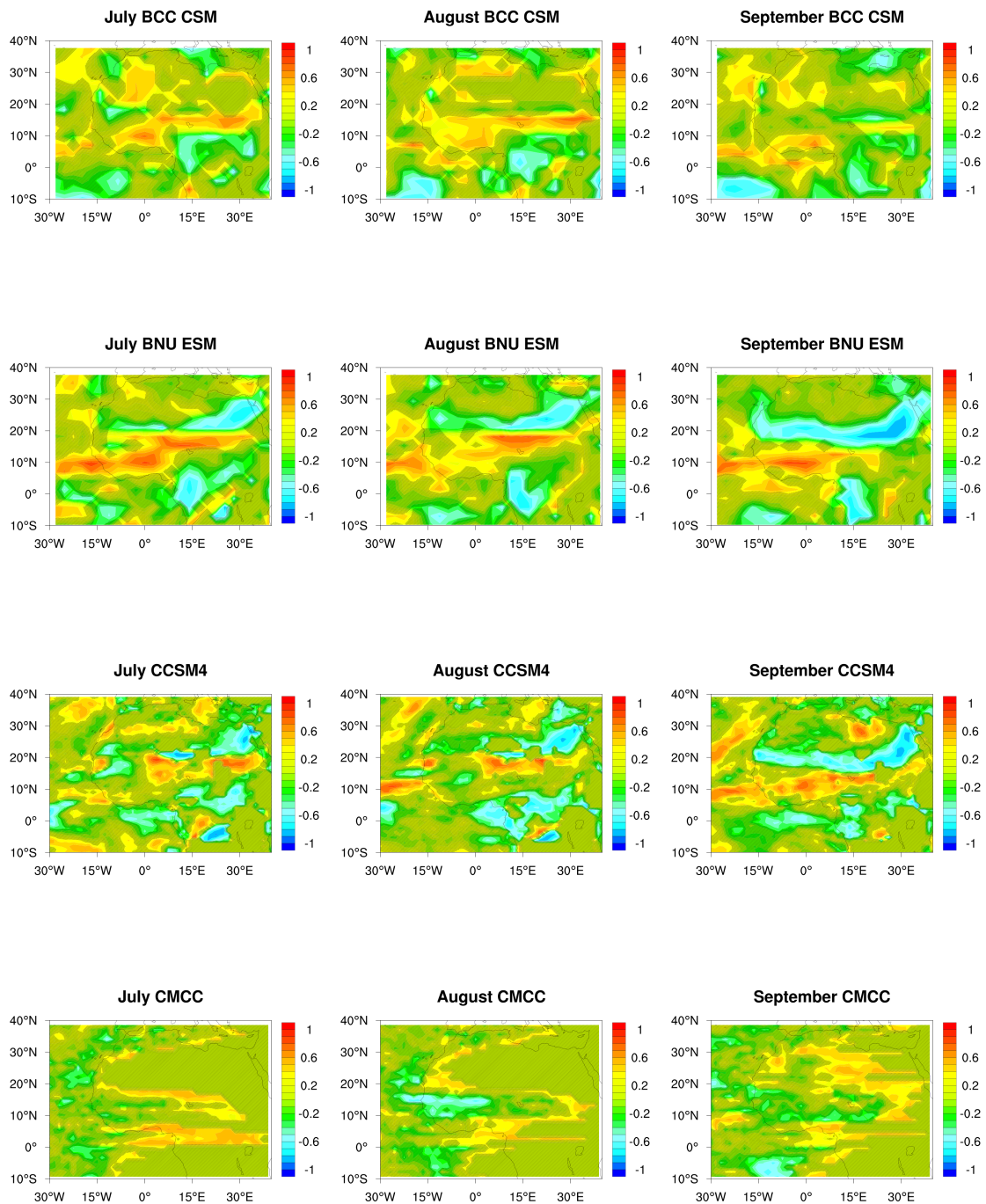


Figure A.1: Rank correlation between the maximal value of cloud fraction and wind speed below 900 hPa in the months July (first column), August (second column), and September (third column) of BCC CSM (top row), BNU ESM (second row), CCSM4 (third row), and CMCC (bottom row); Insignificant values to the level 0.9 are shaded.

Rank Correlation CMIP5

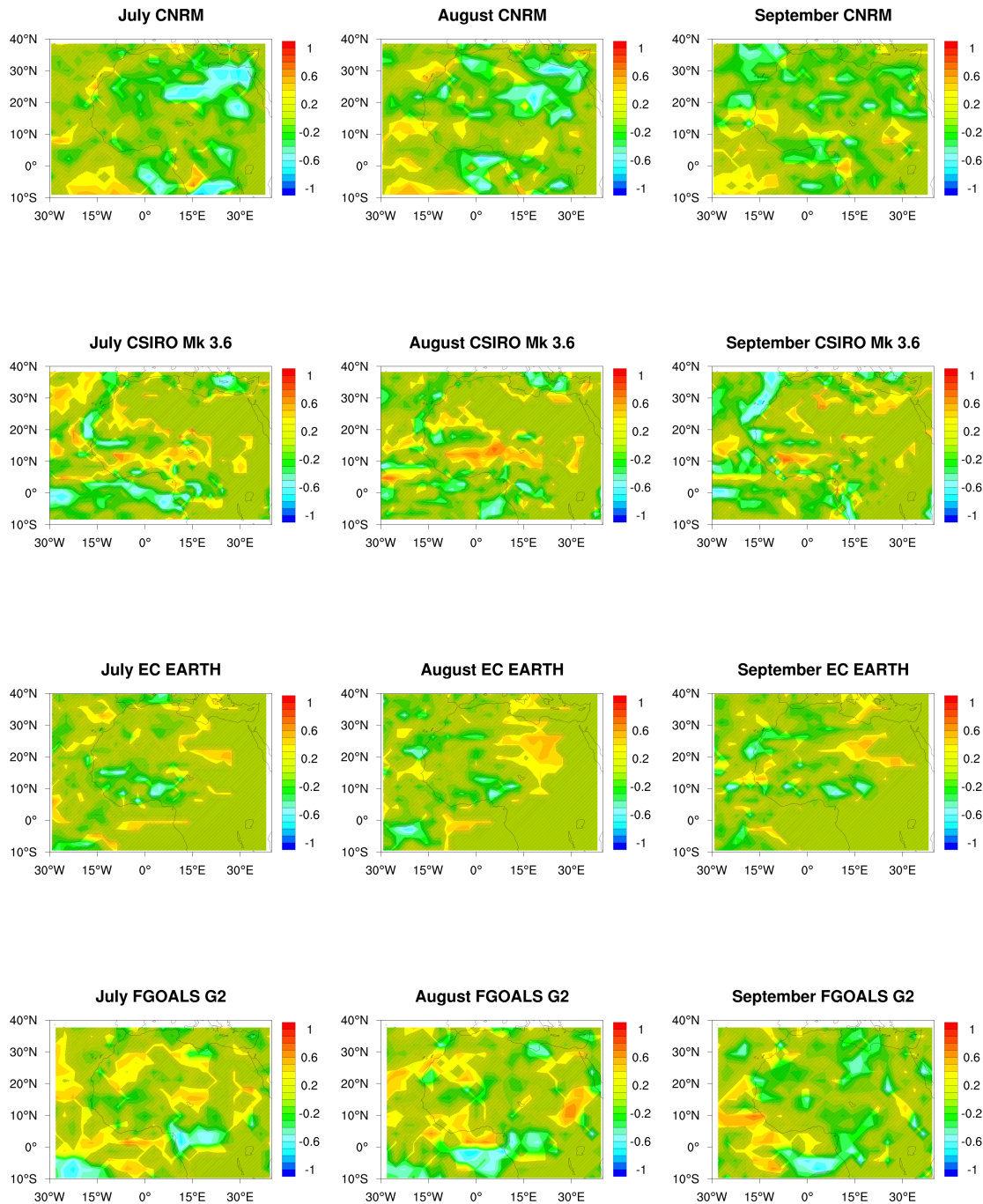


Figure A.2: Rank correlation between the maximal value of cloud fraction and wind speed below 900 hPa in the months July (first column), August (second column), and September (third column) of CNRM (top row), CSIRO Mk 3.6 (second row), EC EARTH (third row), and FGOALS G2 (bottom row); Insignificant values to the level 0.9 are shaded.

Rank Correlation CMIP5

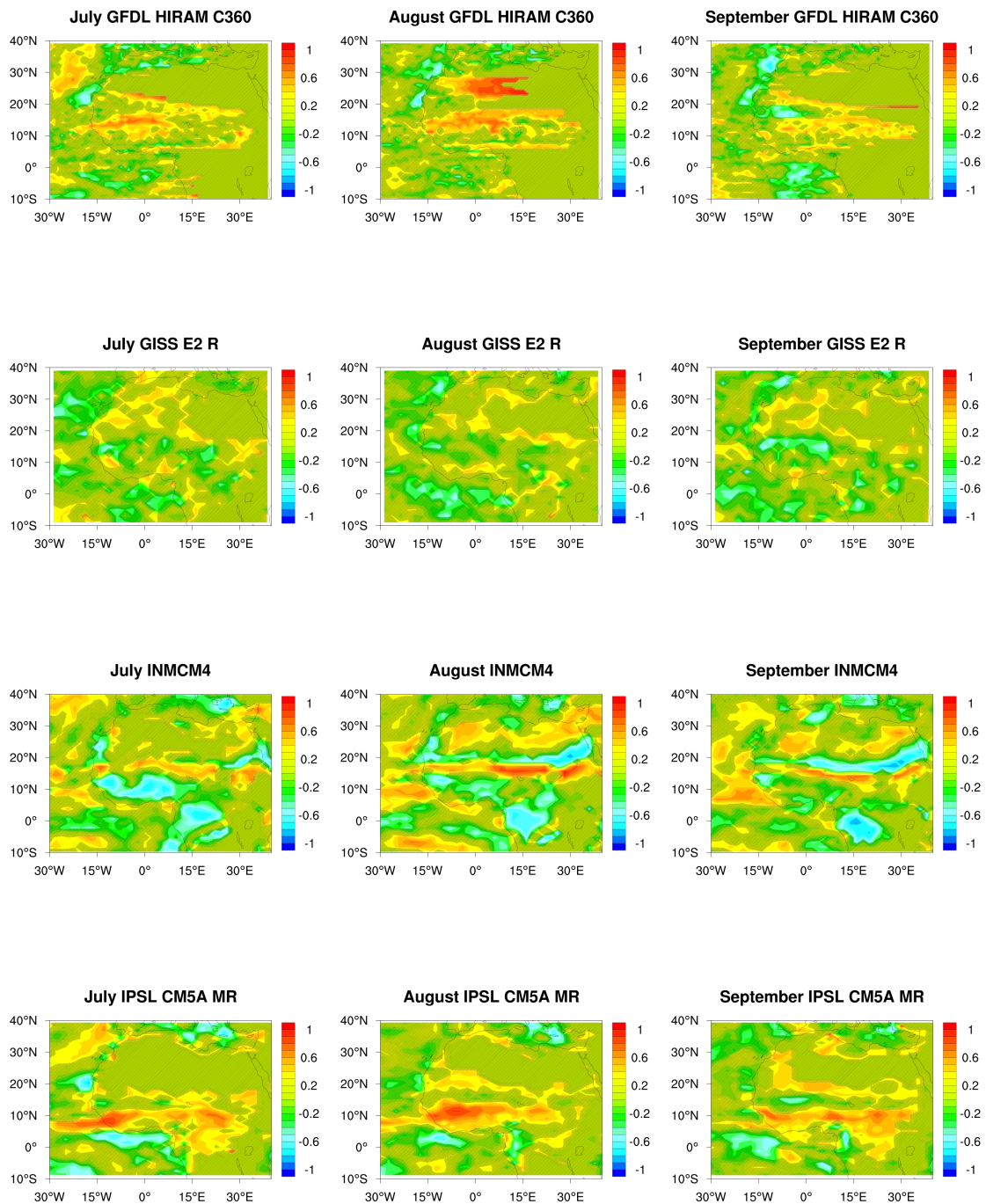


Figure A.3: Rank correlation between the maximal value of cloud fraction and wind speed below 900 hPa in the months July (first column), August (second column), and September (third column) of GFDL HIRAM C360 (top row), GISS E2 R (second row), INMCM4 (third row), and IPSL CM5A MR (bottom row); Insignificant values to the level 0.9 are shaded.

Rank Correlation CMIP5

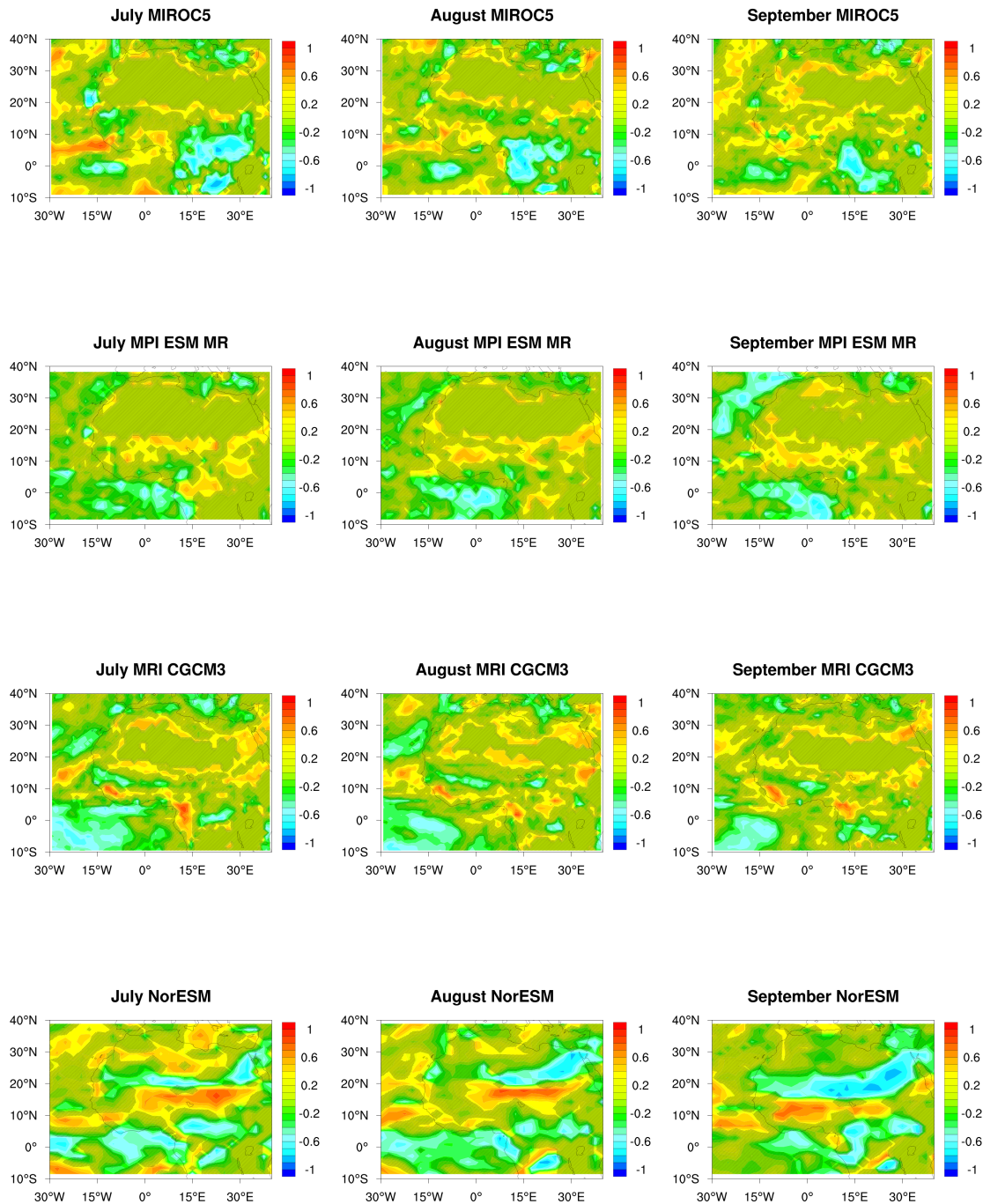


Figure A.4: Rank correlation between the maximal value of cloud fraction and wind speed below 900 hPa in the months July (first column), August (second column), and September (third column) of MIROC5 (top row), MPI ESM MR (second row), MRI CGCM3 (third row), and NorESM (bottom row); Insignificant values to the level 0.9 are shaded.

Total Low-Level Stratiform Cloudiness and Wind Speed YoTC

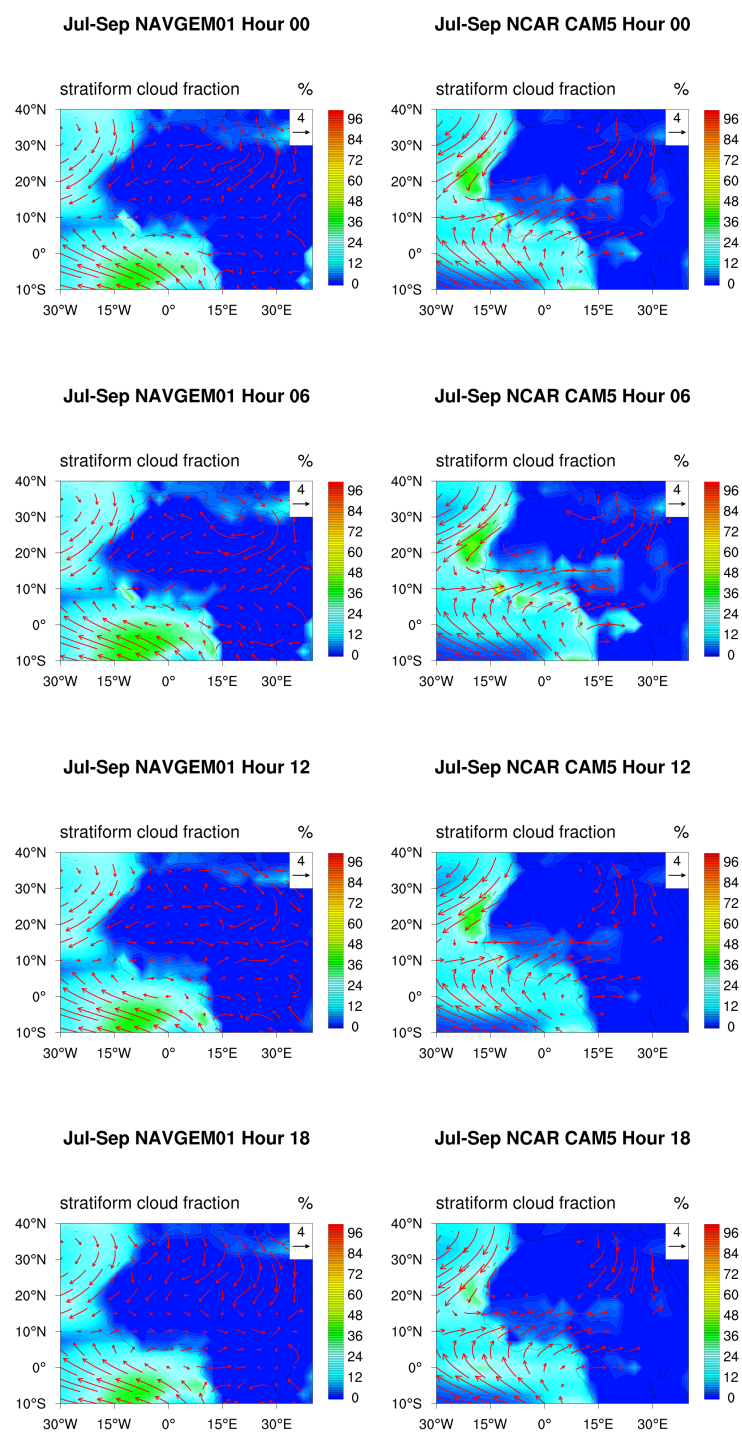


Figure A.5: Horizontal view of total stratiform cloudiness below 900 hPa (countours) and wind vectors (arrows) at 900 hPa of NAVGEM01 (first column) and NCAR CAM5 (second column) at midnight (top row), at 06 UTC (second row), at midday (third row) and 18 UTC (bottom row) in the months July to September.

Total Low-Level Stratiform Cloudiness and Wind Speed YoTC

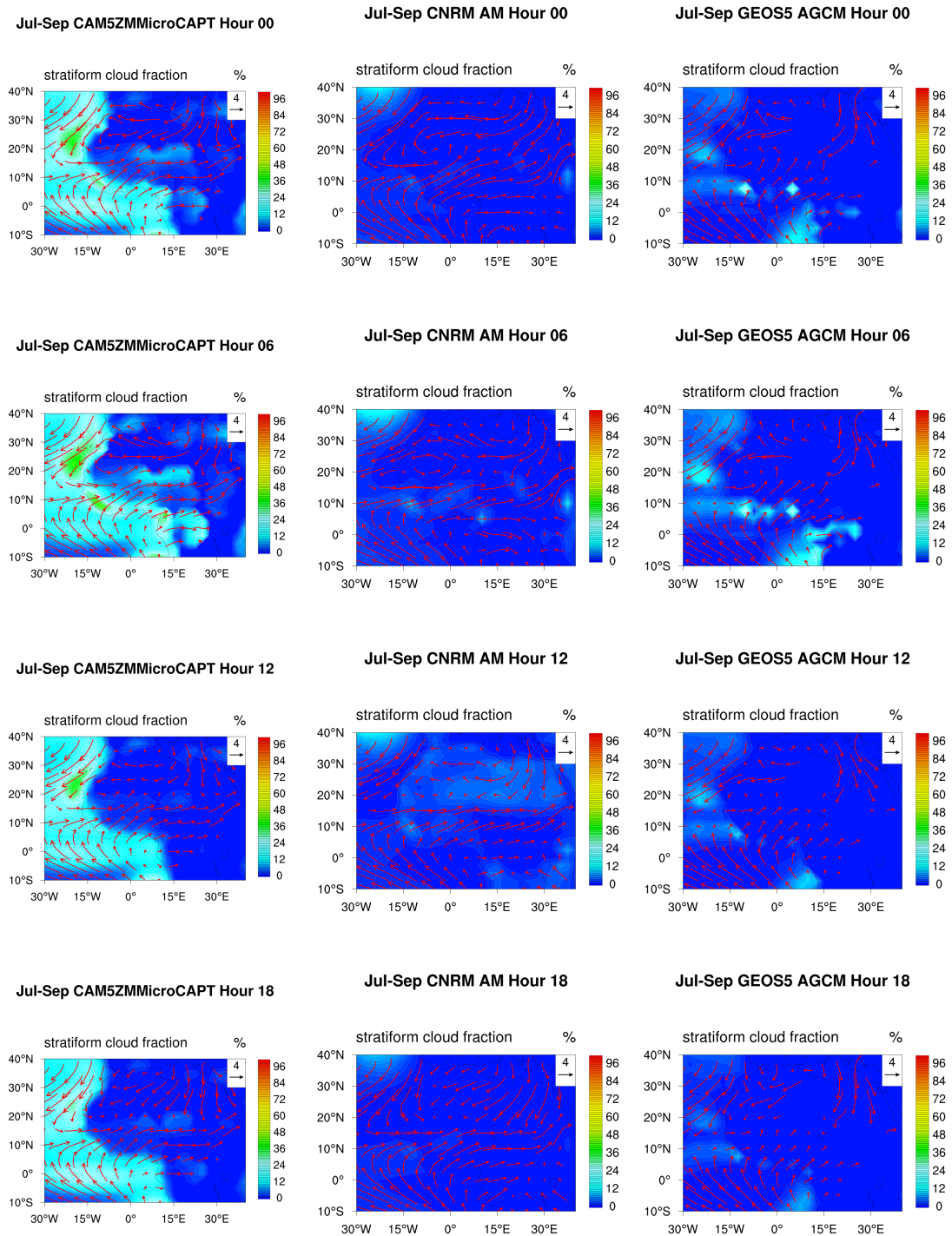


Figure A.6: Horizontal view of total stratiform cloudiness below 900 hPa (countours) and wind vectors (arrows) at 900 hPa of CAM5ZMMicroCAPT (first column), CNRM AM (second column), and GEOS5 AGCM (third column) at midnight (top row), at 06 UTC (second row), at midday (third row) and 18 UTC (bottom row) in the months July to September.

Surface Solar Radiation YoTC

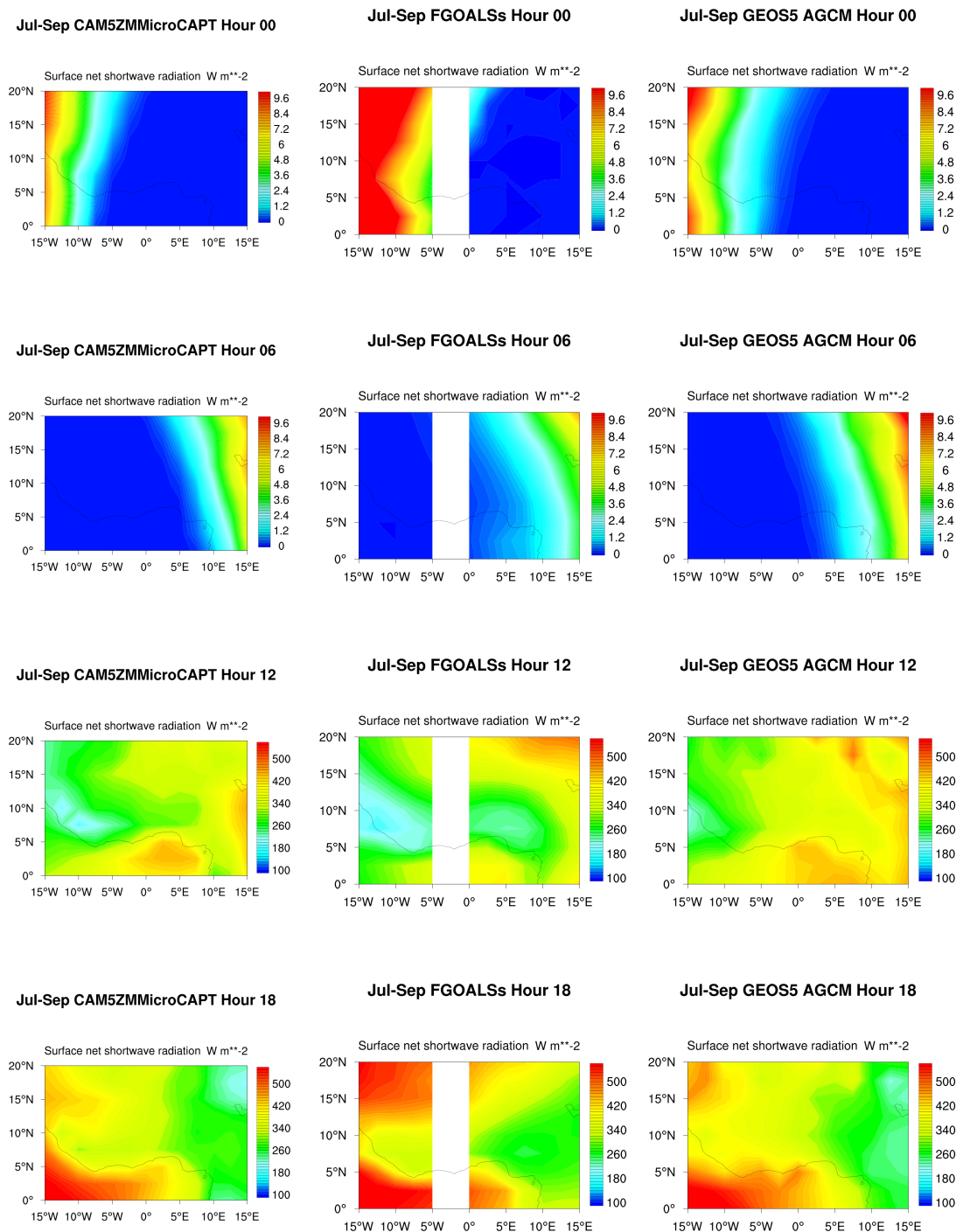


Figure A.7: Diurnal cycle of surface net shortwave radiation in CAM5ZMicroCAPT (first column), FGOALSs (second column), and GEOS5 AGCM (third column); Note the different scales in the night/morning and the day/afternoon plots.

Surface Solar Radiation YoTC

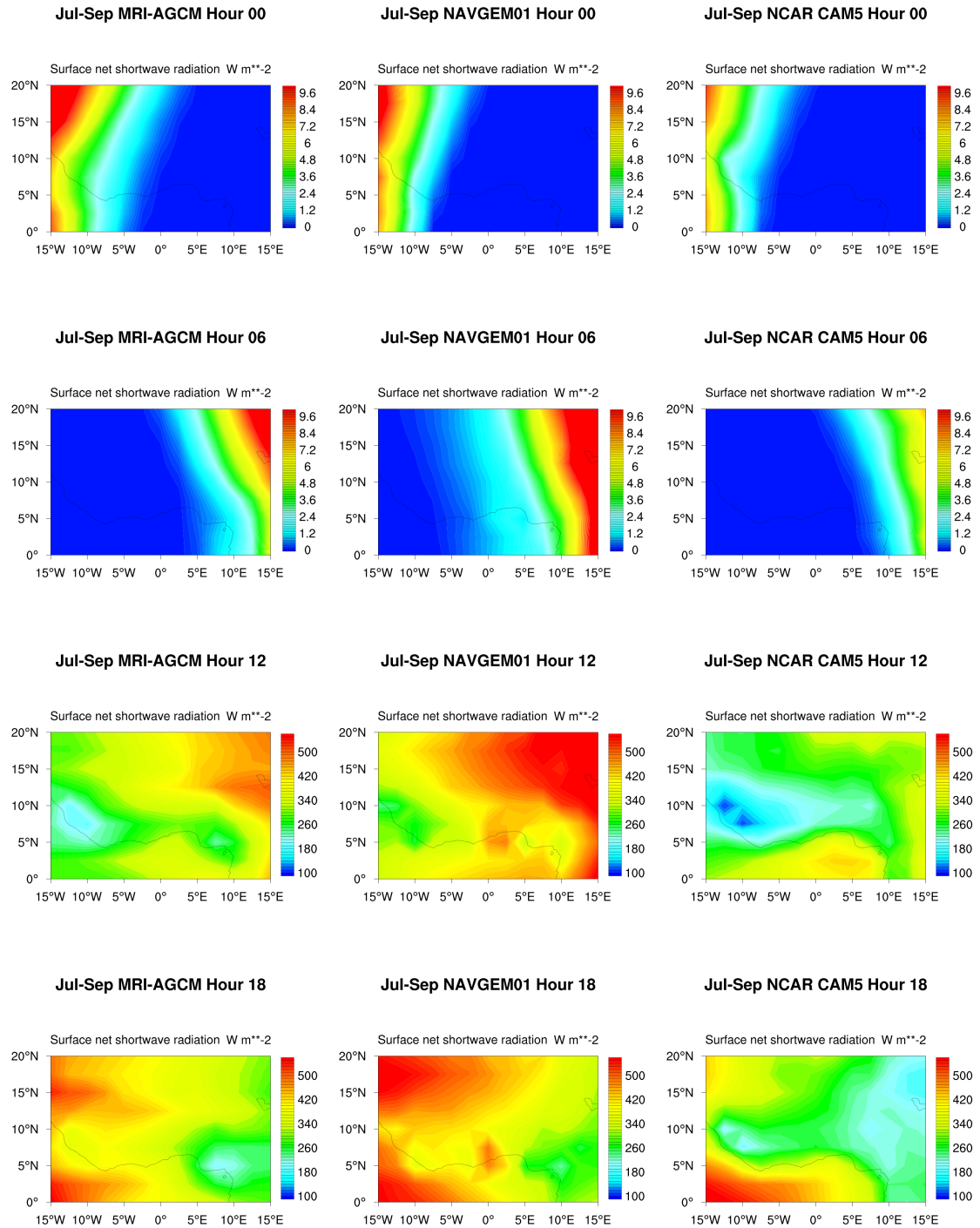


Figure A.8: Diurnal cycle of surface net shortwave radiation in MRI AGCM (first column), NAVGEM01 (second column), and NCAR CAM5 (third column); Note the different scales in the night/morning and the day/afternoon plots.

Tendencies of Moisture and Temperature ERA-Interim

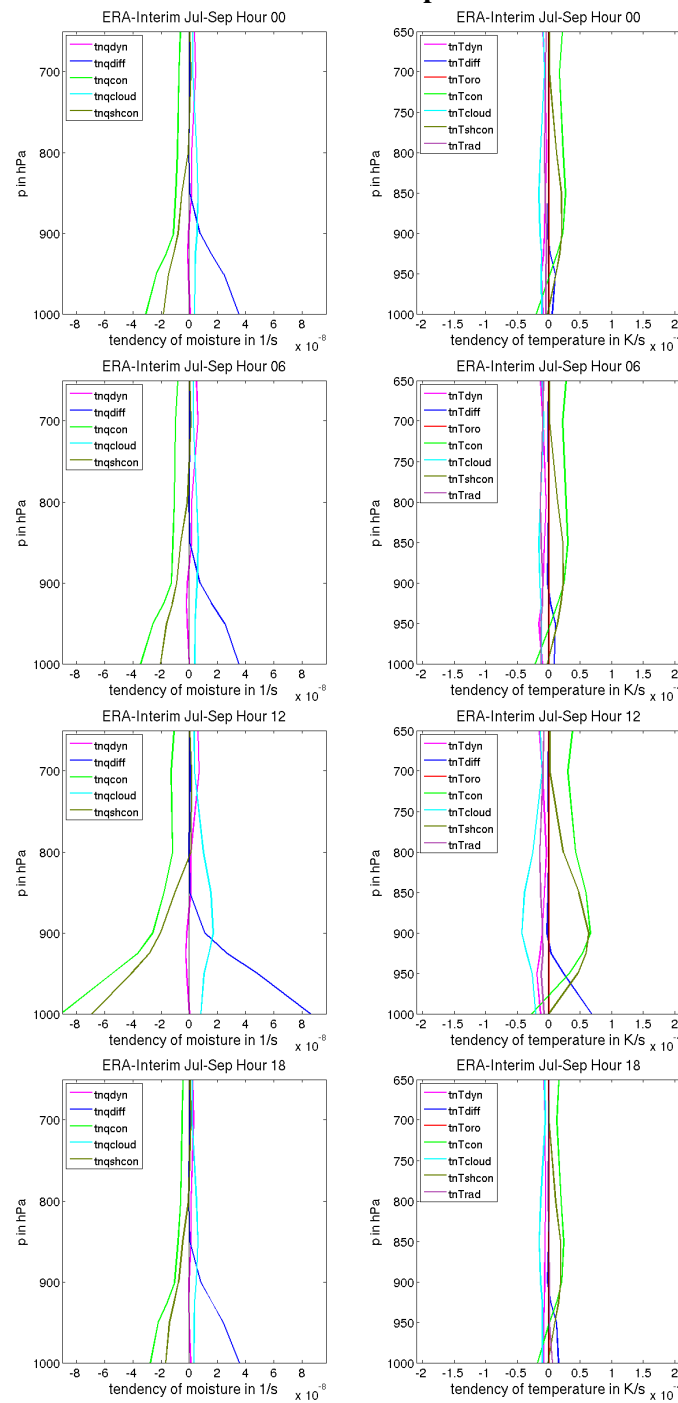
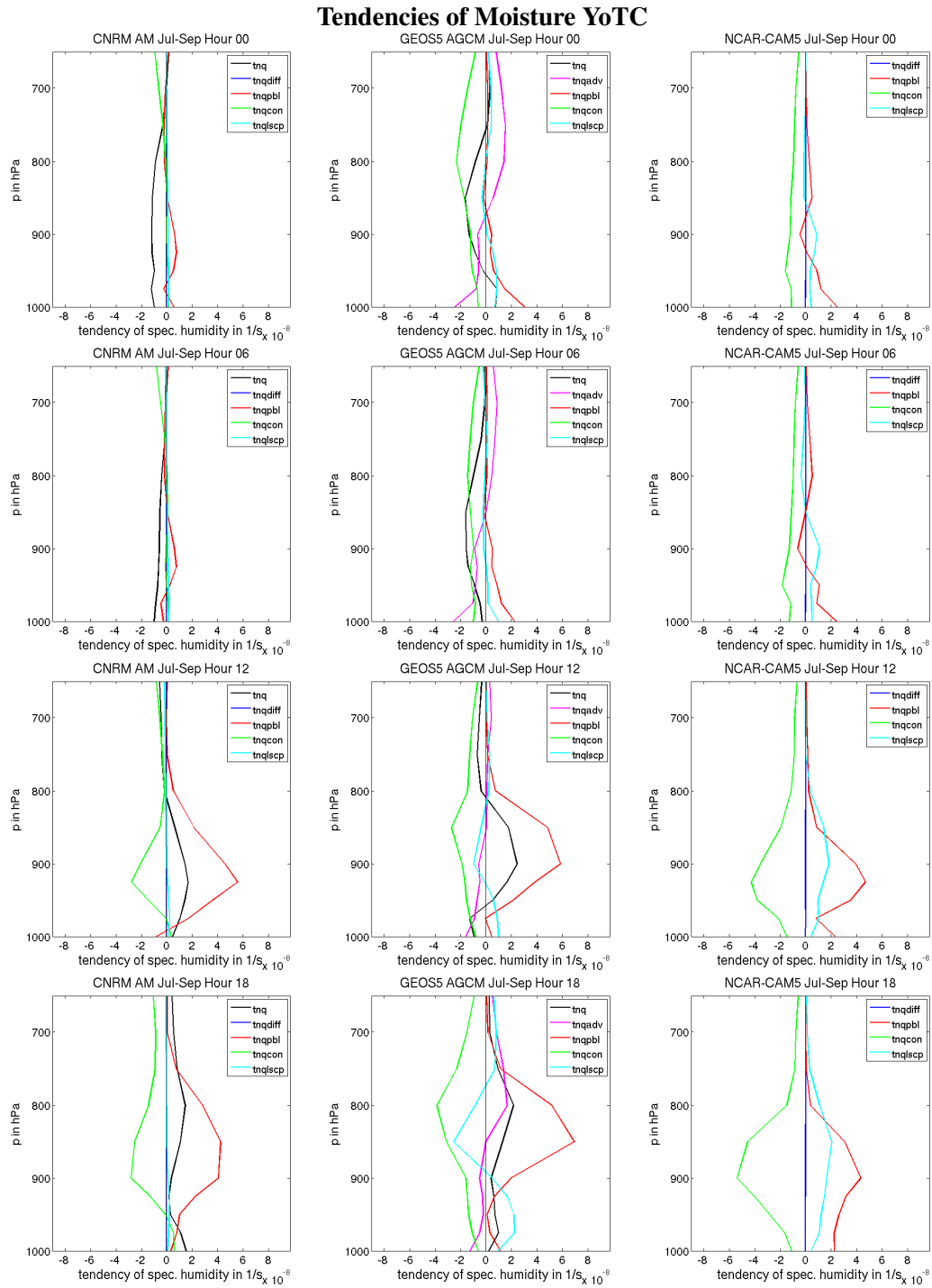


Figure A.9: Diurnal cycle of tendencies of moisture (left) and temperature (right) averaged over defined red box at the Guinea Coast in southern West Africa (Figure 3.3) from 2008-2009 of ERA-Interim; pink line: tendency due to dynamics, blue line: tendency due to turbulent diffusion + subgrid orography, red line: tendency due to subgrid orography, green line: tendency due to convection, cyan line: tendency due to clouds dark green line: tendency due to shallow convection, and purple line: tendency due to radiation.



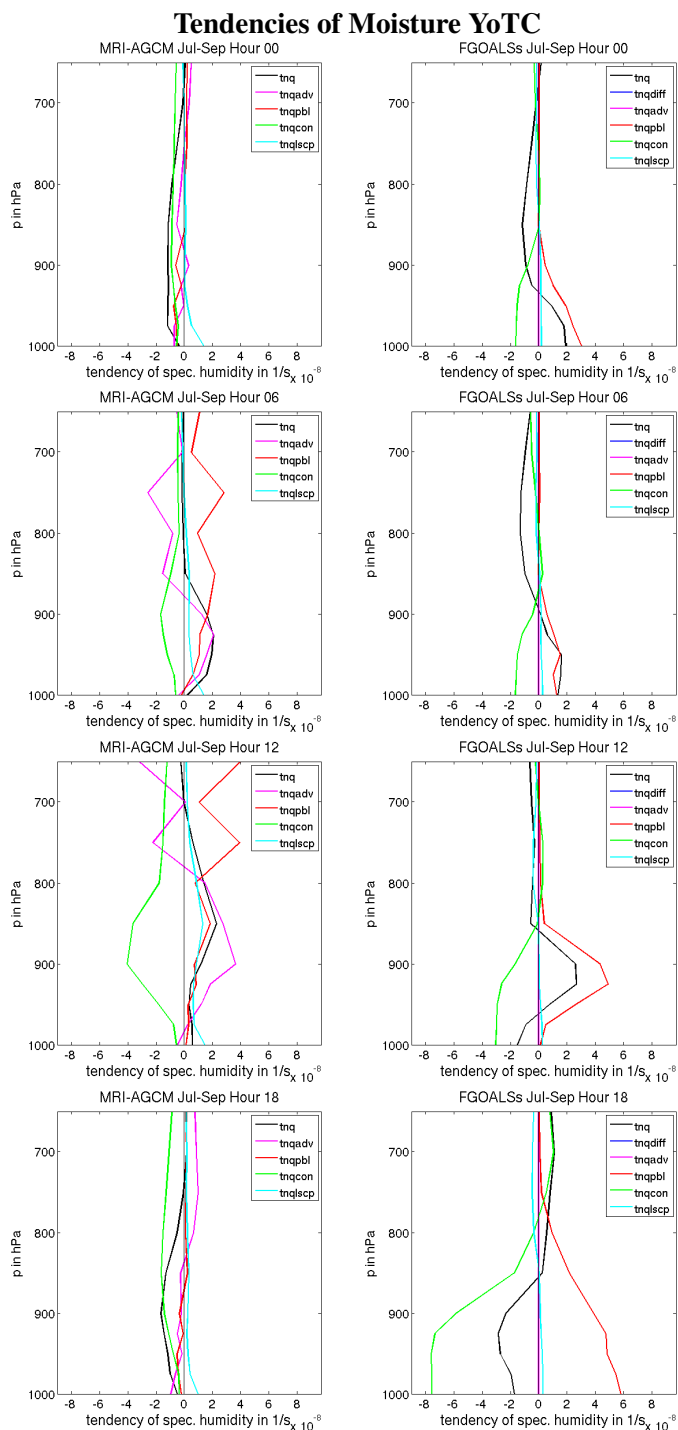


Figure A.11: Diurnal cycle of tendencies of moisture averaged over defined red box at the Guinea Coast in southern West Africa from 1991-2010 of the models MRI AGCM (first column) and FGOALSs (second column); black line: sum of all tendencies, blue line: tendency due to diffusion, pink line: tendency due to advection, red line: tendency due to boundary layer, green line: tendency due to convection and cyan line: tendency due to large scale cloud + precipitation.

Tendencies of Temperature YoTC

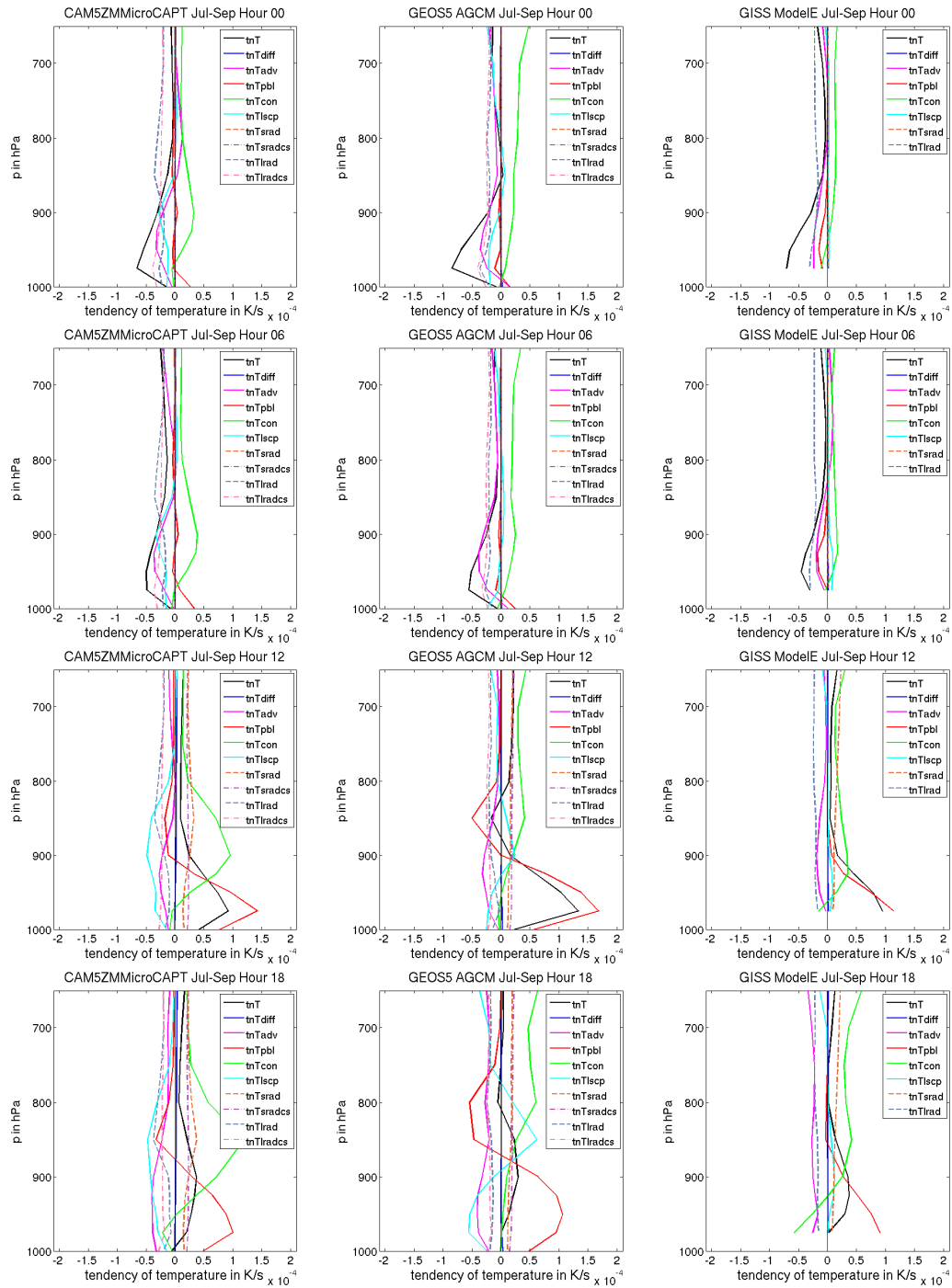


Figure A.12: Diurnal cycle of tendencies of temperature averaged over defined red box at the Guinea Coast from 1991-2010 of the models CAM5ZMicroCAPT (first column), GEOS5 AGCM (second column) and GISS ModelE (third column); black line: sum of all tendencies, blue line: due to diffusion, pink line: due to advection, red line: due to boundary layer, green line: due to convection, cyan line: due to large scale cloud + precipitation, green broken line: due to shortwave radiative heating, purple broken line: due to shortwave radiative heating clear sky, gray broken line: due to longwave radiative heating, rose broken line: due to shortwave radiative heating clear sky, khaki broken line: due to orog. gravity wave drag.

Tendencies of Temperature YoTC

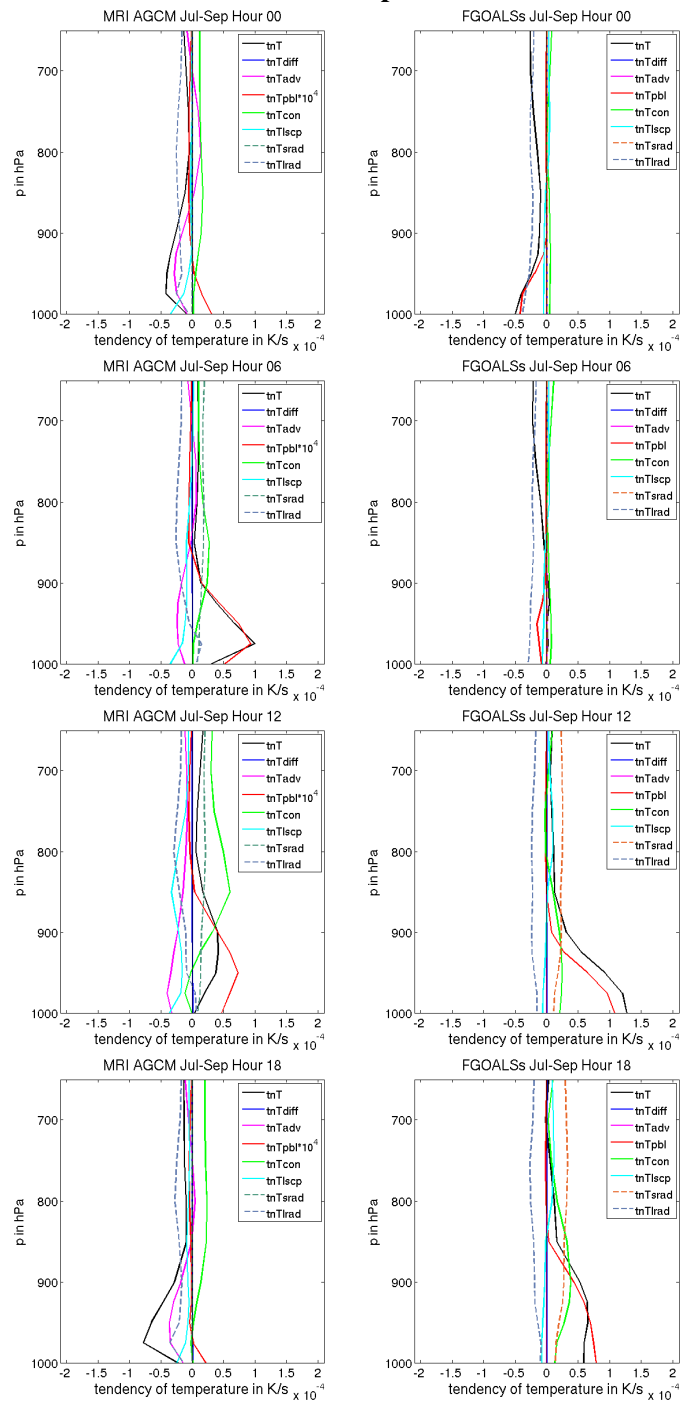


Figure A.13: Diurnal cycle of tendencies of temperature averaged over defined red box at the Guinea Coast from 1991-2010 of the models MRI AGCM (first column) and FGOALSs (second column); black line: sum of all tendencies, blue line: due to diffusion, pink line: due to advection, red line: due to boundary layer, green line: due to convection, cyan line: due to large scale cloud + precipitation, green broken line: due to shortwave radiative heating, purple broken line: due to shortwave radiative heating clear sky, gray broken line: due to longwave radiative heating, rose broken line: due to shortwave radiative heating clear sky, khaki broken line: due to orog. gravity wave drag.

Rank Correlation YoTC

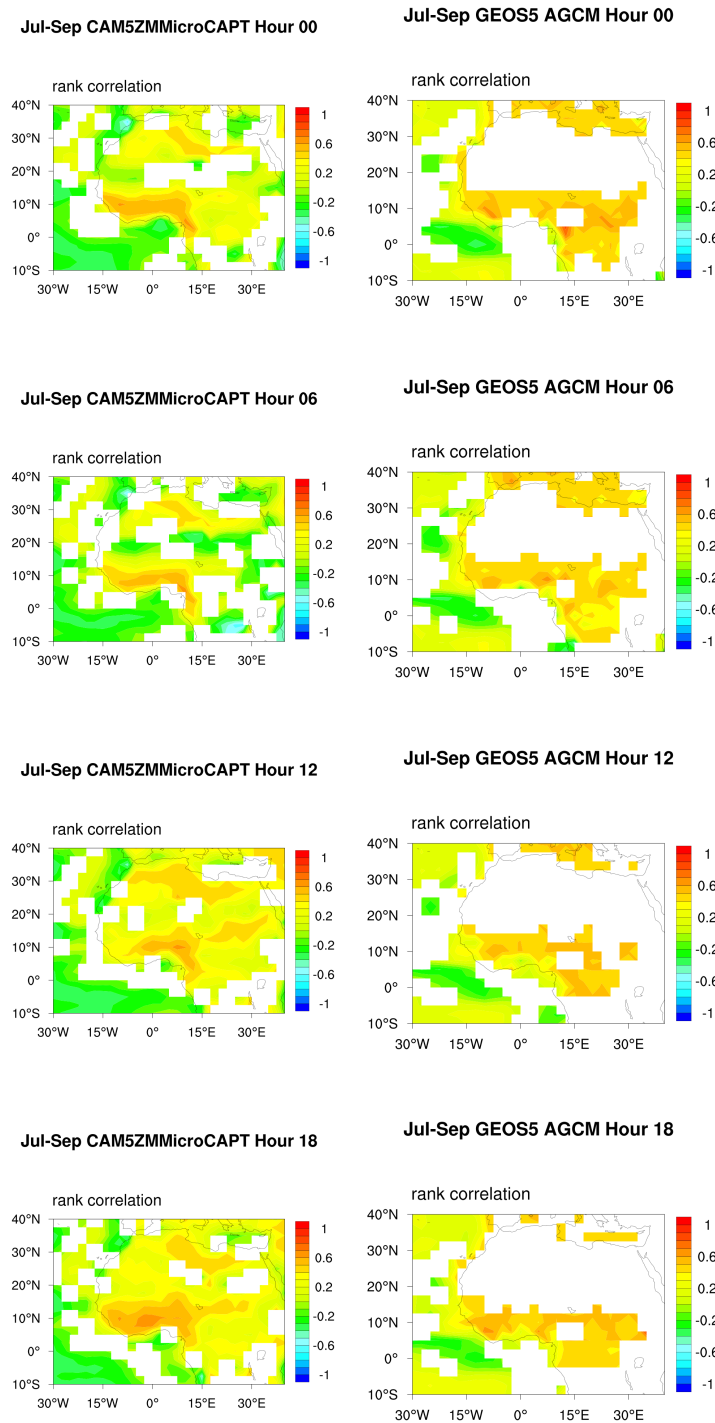


Figure A.14: Rank correlation between the maximal value of stratiform cloud fraction and wind speed below 900 hPa at midnight (top row), at 06 UTC (second row), at midday (third row) and 18 UTC (bottom row) in the months July to September of CAM5ZMMicroCAPT (first column), and GEOS5 AGCM (second column); Significant values to the level 0.9 in contours.

Rank Correlation YoTC

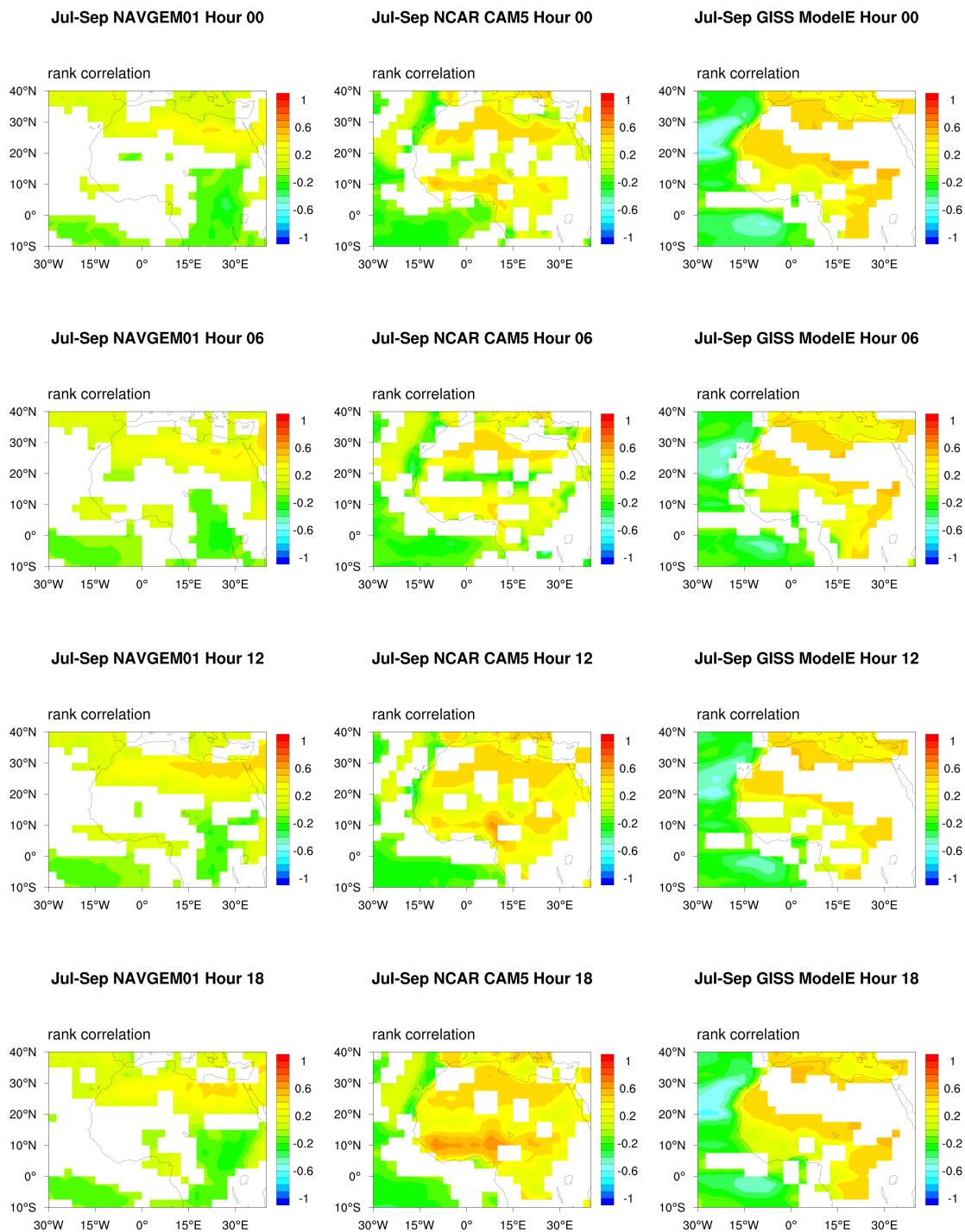


Figure A.15: Rank correlation between the maximal value of stratiform cloud fraction and wind speed below 900 hPa at midnight (top row), at 06 UTC (second row), at midday (third row) and 18 UTC (bottom row) in the months July to September of NAVGEM01 (first column), NCAR CAM5 (second column), and GISS ModelE (third column); Significant values to the level 0.9 in contours.

List of Acronyms

Coupled Model Intercomparison Project Phase 3	CMIP3
Coupled Model Intercomparison Project Phase 5	CMIP5
GEWEX Atmosphere System Study	GASS
Year of Tropical Convection	YoTC
ReAnalysis-Interim	ERA-Interim
European Centre for Medium-Range Weather Forecasts	ECMWF
Cloud Feedback Model Intercomparison Project	CFMIP
Cloud feedback model intercomparison project Observation Simulator Package	COSP
National Oceanic and Atmospheric Administration	NOAA
World Climate Research Program	WCRP
Observing System Research and Predictability Experiment	THORPEX
World Weather Research Program	WWRP
Tropical Rainfall Measuring Mission precipitation radar	TRMM
InterTropical ConvergenceZone	ITCZ
InterTropical Front	ITF
Nocturnal Low-Level Jet	NLLJ
Shallow Meridional Circulation	SMC
Sea Surface Temperature	SST
Surface Solar Radiation	SSR
Cloud fraction	cl
Cloud fraction stratiform	cls
Advection of moisture	advq
Advection of temperature	advT
Tendency of moisture (specific humidity)	tnq
Tendency of moisture due to advection	tnqadv
Tendency of moisture due to convection	tnqcon
Tendency of moisture due to boundary layer processes	tnqpbl
Tendency of moisture due to large scale clouds and precipitation	tnqlsep
Tendency of moisture due to diffusion	tnqdiff
Tendency of temperature	tnT
Tendency of temperature due to advection	tnTadv
Tendency of temperature due to convection	tnTcon
Tendency of temperature due to boundary layer processes	tnTpbl
Tendency of temperature due to large scale clouds and precipitation	tnTlsep
Tendency of temperature due to diffusion	tnTdiff
Tendency of temperature due to shortwave radiative heating	tnTsrاد
Tendency of temperature due to shortwave radiative heating clear sky	tnTsrادcs
Tendency of temperature due to longwave radiative heating	tnTlrad
Tendency of temperature due to longwave radiative heating clear sky	tnTlradcs
Tendency of temperature due to due to orographic gravity wave drag	tnTgravwave

Bibliography

- Abdou, K., Parker, D. J., Brooks, B., Kalthoff, N., and Lebel, T. (2010). The diurnal cycle of lower boundary-layer wind in the West African monsoon. *Quarterly Journal of the Royal Meteorological Society*, 136(S1):66–76.
- Couvreux, F., Guichard, F., Gounou, A., Bouniol, D., Peyrillé, P., and Köhler, M. (2014). Modelling of the Thermodynamical Diurnal Cycle in the Lower Atmosphere: A Joint Evaluation of Four Contrasted Regimes in the Tropics Over Land. *Boundary-Layer Meteorology*, 150(2):185–214.
- Dee, D., Uppala, S., Simmons, A., Berrisford, P., Poli, P., Kobayashi, S., Andrae, U., Balmaseda, M., Balsamo, G., Bauer, P., et al. (2011). The ERA-Interim reanalysis: Configuration and performance of the data assimilation system. *Quarterly Journal of the Royal Meteorological Society*, 137(656):553–597.
- Fink, A. (2006). Das Westafrikanische Monsunsystem. *Promet*, 32(3/4):114–122.
- Gounou, A., Guichard, F., and Couvreux, F. (2012). Observations of diurnal cycles over a West African meridional transect: Pre-monsoon and full-monsoon seasons. *Boundary-layer meteorology*, 144(3):329–357.
- Hall, N. M. and Peyrillé, P. (2006). Dynamics of the West African monsoon. In *Journal de Physique IV (Proceedings)*, volume 139, pages 81–99. EDP sciences.
- Hurrell, J. W., Hack, J. J., Shea, D., Caron, J. M., and Rosinski, J. (2008). A new sea surface temperature and sea ice boundary dataset for the Community Atmosphere Model. *Journal of Climate*, 21(19):5145–5153.
- Jiang, X. et al. (2014). Vertical Structure and Physical Processes of the Madden-Julian Oscillation: Exploring Key Model Physics in Climate Simulations. *Journal of Geophysical Research - Atmospheres*.
- Knippertz, P., Coe, H., Chiu, J. C., Evans, M. J., Fink, A. H., Kalthoff, N., Liousse, C., Mari, C., Allan, R. P., Brooks, B., et al. (2015). The DACCIWA project: Dynamics-aerosol-chemistry-cloud interactions in West Africa. *Bulletin of the American Meteorological Society*, (2015).

- Knippertz, P., Fink, A. H., Schuster, R., Trentmann, J., Schrage, J. M., and Yorke, C. (2011). Ultra-low clouds over the southern West African monsoon region. *Geophysical Research Letters*, 38(21).
- Lappen, C.-L. and Schumacher, C. (2012). Heating in the tropical atmosphere: what level of detail is critical for accurate MJO simulations in GCMs? *Climate dynamics*, 39(9-10):2547–2568.
- Linden, R., Fink, A. H., and Redl, R. (2015). Satellite-based climatology of low-level continental clouds in southern West Africa during the summer monsoon season. *Journal of Geophysical Research: Atmospheres*, 120(3):1186–1201.
- Mohr, K. I. and Thorncroft, C. D. (2006). Intense convective systems in West Africa and their relationship to the African easterly jet. *Quarterly Journal of the Royal Meteorological Society*, 132(614):163–176.
- Nam, C., Bony, S., Dufresne, J.-L., and Chepfer, H. (2012). The ‘too few, too bright’ tropical low-cloud problem in CMIP5 models. *Geophysical Research Letters*, 39(21).
- Parker, D., Burton, R., Diongue-Niang, A., Ellis, R., Felton, M., Taylor, C., Thorncroft, C., Bessemoulin, P., and Tompkins, A. (2005). The diurnal cycle of the West African monsoon circulation. *Quarterly Journal of the Royal Meteorological Society*, 131(611):2839–2860.
- Persson, A. and Grazzini, F. (2007). User Guide to ECMWF forecast products. *Meteorol. Bull.*, 3:153.
- Rácz, Z. and Smith, R. K. (1999). The dynamics of heat lows. *Quarterly Journal of the Royal Meteorological Society*, 125(553):225–252.
- Reynolds, R. W., Rayner, N. A., Smith, T. M., Stokes, D. C., and Wang, W. (2002). An improved in situ and satellite SST analysis for climate. *Journal of climate*, 15(13):1609–1625.
- Roehrig, R., Bouniol, D., Guichard, F., Hourdin, F., and Redelsperger, J.-L. (2013). The present and future of the West African monsoon: a process-oriented assessment of CMIP5 simulations along the AMMA transect. *Journal of Climate*, 26(17):6471–6505.
- Schrage, J. M. and Fink, A. H. (2012). Nocturnal continental low-level stratus over tropical West Africa: observations and possible mechanisms controlling its onset. *Monthly Weather Review*, 140(6):1794–1809.
- Schuster, R., Fink, A. H., and Knippertz, P. (2013). Formation and maintenance of nocturnal low-level stratus over the southern West African monsoon region during AMMA 2006. *Journal of the Atmospheric Sciences*, 70(8):2337–2355.
- Sultan, B. and Janicot, S. (2003). The West African monsoon dynamics. Part II: The “preonset” and “onset” of the summer monsoon. *Journal of climate*, 16(21):3407–3427.

- Waliser, D. E., Moncrieff, M. W., Burridge, D., Fink, A. H., Gochis, D., Goswami, B., Guan, B., Harr, P., Heming, J., Hsu, H.-H., et al. (2012). The “year” of tropical convection (May 2008-April 2010): Climate variability and weather highlights. *Bulletin of the American Meteorological Society*, 93(8):1189–1218.
- Xiaopeng, C., Shouting, G., Haixia, Z., and Shifeng, H. (2009). A Diagnostic Analysis of the Simulated Structure of a Meiyu Front System in 1999. *Acta Meteorologica Sinica*, (1):43–52.
- Zhang, C., Nolan, D. S., Thorncroft, C. D., and Nguyen, H. (2008). Shallow meridional circulations in the tropical atmosphere. *Journal of Climate*, 21(14):3453–3470.

Danksagung

Ich möchte mich hier recht herzlich bei meinen beiden Betreuern Peter Knippertz und Andreas Fink bedanken. Das Thema zu bearbeiten war sehr spannend und hat mir wirklich viel Spaß gemacht. Bei Problemen hatten sie immer ein offenes Ohr und halfen mir mit Lösungsvorschlägen weiter. Zusätzlich möchte ich mich für das erste Korrekturlesen dieser Arbeit und die Verbesserungsvorschläge bedanken.

Gregor möchte ich für die Unterstützung beim Herunterladen der Daten danken, was wirklich nicht wenig war. Anke danke ich für das Korrekturlesen meiner Arbeit.

Als nächstes möchte ich mich bei meiner Familie und Freunden bedanken, die mir immer den nötigen Ausgleich geben und immer für mich da sind. Danke für alles!

Zum Schluss möchte ich mich noch bei meinen Zimmerkollegen, Pila, Lukas and Markus bedanken. Es war eine tolle Atmosphäre, obwohl es im Sommer trotz Lüfter echt heiß war im Zimmer. Pila danke ich für das Lesen meiner Arbeit.

Erklärung

Hiermit erkläre ich, dass ich die vorliegende Arbeit selbst verfasst und nur die angegebenen Hilfsmittel verwendet habe.

Ich bin damit einverstanden, dass diese Arbeit in Bibliotheken eingestellt wird und vervielfältigt werden darf.

Karlsruhe, den 29. Juli 2015

Lisa Hannak